E.ON Energy Research Center | RWTH AACHEN UNIVERSITY

Towards Automatization of Distance Protection Coordination and Interoperability Testing for Digital Substations

Thanakorn Penthong
Institute for Automation of Complex Power Systems

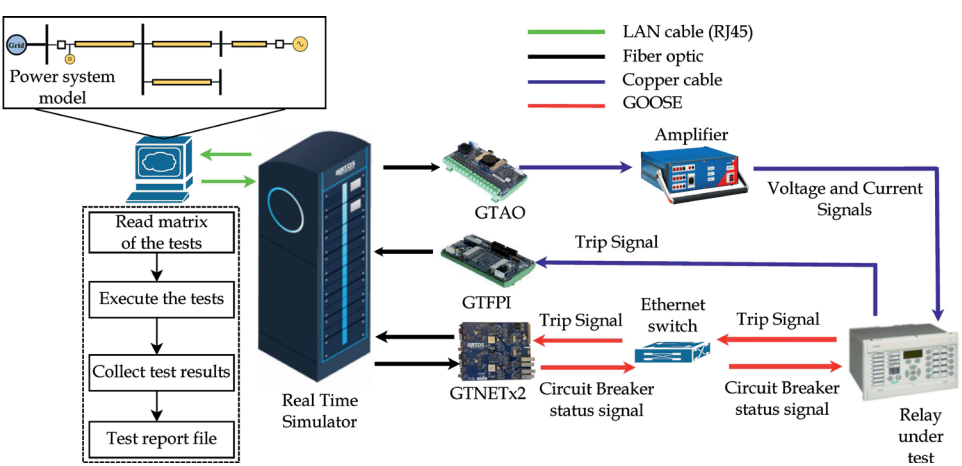

Towards Automatization of Distance Protection Coordination and Interoperability Testing for Digital Substations

Von der Fakultät für Elektrotechnik und Informationstechnik
der Rheinisch-Westfälischen Technischen Hochschule Aachen
zur Erlangung des akademischen Grades eines Doktors
der Ingenieurwissenschaften genehmigte Dissertation

vorgelegt von

Thanakorn Penthong, M. Eng.

aus
Phetchabun, Thailand

Berichter:
Univ.-Prof. Ferdinanda Ponci, Ph. D.
Privatdoz. Dr. techn. Thomas I. Strasser

Tag der mündlichen Prüfung: 12. Dezember 2025

Bibliographische Information der Deutschen Nationalbibliothek
Die Deutsche Nationalbibliothek verzeichnet diese Publikation in der Deutschen Nationalbibliografie; detaillierte bibliografische Daten sind im Internet über https://dnb.dnb.de abrufbar.

D 82 (Diss. RWTH Aachen University, 2025)

Herausgeber:
E.ON Energy Research Center

Institute for Automation of Complex Power Systems (ACS)
E.ON Energy Research Center
Mathieustraße 10
52074 Aachen

E.ON Energy Research Center I 148. Ausgabe der Serie
ACS I Automation of Complex Power Systems

Printed in Germany

ISBN: 978-3-948234-62-1
1. Auflage 2026

Verlag:
E.ON Energy Research Center, RWTH Aachen University
Mathieustraße 10
52074 Aachen
Internet: www.eonerc.rwth-aachen.de
E-Mail: post_erc@eonerc.rwth-aachen.de

Herstellung:
Druckservice Zillekens
Rainweg 19
52224 Stolberg

Kurzfassung

Motivation, Ziel und Aufgabenstellung der Dissertation

Distanzschutz ist eine Schutzfunktion, die in Übertragungssystemen aufgrund ihrer Selektivität und Schnelligkeit weit verbreitet ist. Vor der Feldinbetriebnahme muss das Distanzschutzrelais (DR) eingestellt werden, und seine Einstellung muss mit den anderen DRs im System koordiniert sein. Zur Konfiguration der DR-Einstellungen und zur Überprüfung ihrer Koordination ist grundsätzlich eine Leitungsermittlung erforderlich, um die elektrischen Elemente wie Leitungen, Sammelschienen, Schalter und Leistungsschalter (LS) innerhalb der Schutzzone des zu schützenden DR zu identifizieren. Traditionell ist die Leitungsermittlung ein manueller Prozess, ebenso wie die Einstellung und Koordination der DRs – Verfahren, die fehleranfällig sind, insbesondere bei komplexen Netztopologien (z.B. Schleifen-/Mehrfachschleifennetze) und/oder wenn viele DRs im Netz implementiert sind. Dies gilt umso mehr, wenn DRs von verschiedenen Herstellern verwendet werden, da diese unterschiedliche Parametereinstellungen mit unterschiedlichen Funktionen aufweisen, z.B. Leistungsschwingungen, Lastüberschneidung usw. Nicht-konventionelle Ansätze, wie solche, die auf Graphentheorie und Graphsuchalgorithmen, z.B. Depth-First-Search (DFS), basieren, können die Leitungsermittlung automatisieren; diese Methoden sind jedoch insbesondere bei komplexen Netztopologien immer noch fehleranfällig.

Neben der Einstellung und Koordination von DRs ist DR-Testing eine entscheidende Tätigkeit, um Probleme im DR zu identifizieren, die z.B. durch fehlerhafte Einstellungen oder Firmware-Bugs verursacht werden, sowie um die Wirksamkeit der Fehlererkennungsansätze zu bewerten. Diese Testaktivitäten werden durchgeführt, um letztlich die störenden Auswirkungen von Schutzfehlern zu verhindern. Für das DR-Testing ist die Norm IEC 60255-121:2014 eine wichtige Referenz, die die Mindestanforderungen (Zonencharakteristika, maximale Abweichung der Auslösezeit usw.) für einen begrenzten Funktionsumfang spezifiziert. Aufgrund dieser Einschränkungen bleibt die Leistung des DR bei bestimmten realistischen

Fehlercharakteristika und Systemverhalten unter dynamischen Bedingungen ungetestet und unbeurteilt. Dies kann letztlich dazu führen, dass DRs falsch auslösen, unterreichend arbeiten oder unnötig auslösen, was zu Systeminstabilitäten oder Stromausfällen führen kann. Beispielsweise kann ein DR während stabiler Leistungsschwingungen auslösen (DR darf bei stabilen Schwingungen nicht auslösen und muss zwischen Fehler- und Leistungsschwingungen sowie stabilen und instabilen Schwingungen unterscheiden), oder unterreichend arbeiten aufgrund von Fehlerwiderständen usw. Daher sind die Norm IEC 60255-121:2014 und bestehende Methoden ungeeignet, um zusätzliche Funktionen wie Leistungsschwingung, Sicherungsausfall oder Fehlerortung zu testen; deren Testung wird den Endanwendern überlassen, basierend auf deren spezifischen Anforderungen. Darüber hinaus kann der in früheren Arbeiten vorgestellte One-at-a-Time (OAT)-Ansatz zur Bewertung der DR-Leistung die Wechselwirkungen zwischen Faktoren (z.B. Fehlerwiderstand, Fehlerort, Fehlerbeginnwinkel usw.) nicht erfassen. Neben dem OAT-Ansatz führt eine vollfaktorielle Strategie, wie sie in der Norm IEC 60255-121:2014 zur Testung der Faktoren empfohlen wird, die potenziell die DR-Leistung beeinflussen, schnell zu Hunderten oder Tausenden von Tests; zudem kann sie die Wechselwirkungen und Abhängigkeiten zwischen Faktoren nicht berücksichtigen.

Grundsätzlich besteht eine digitale Umspannstation aus einer Hochspannungsebene als Übertragungssystem und einer Mittelspannungsebene als Verteilungssystem. Die Mittelspannungsebene fungiert als Vermittler zwischen der Übertragungsinfrastruktur und den lokalen Verteilnetzen und ermöglicht die effiziente Versorgung der Endverbraucher in den Bereichen Wohngebäude, Gewerbe und Industrie. In diesem Kontext ist der Schutz der Verteilerspeiseleitungen entscheidend, um die Zuverlässigkeit des Systems zu gewährleisten und großflächige Stromausfälle unter abnormalen Betriebsbedingungen, z.B. Leitungsausfälle oder Mehrfachleitungsfehler (MFFs), zu verhindern. Unter den verfügbaren Schutzstrategien werden Überstromrelais (ORs) am häufigsten als primärer Leitungsschutz eingesetzt. Diese Präferenz beruht auf ihrer einfachen Handhabung, bewährten Zuverlässigkeit und Kosteneffizienz im Vergleich zu komplexeren Alternativen wie Distanz- oder Differenzialschutz. Allerdings ist die bestehende Überstromschutzfunktion anfällig für MFFs, selbst wenn die ORs innerhalb der Umspannstation bei allen Fehlerstromwerten koordiniert arbeiten können. Die MFFs führen dazu, dass das OR am eingehenden Leiter schneller auslöst als die ORs der fehlerhaften Leiter. Dies führt

letztlich dazu, dass alle an den Leistungstransformator angeschlossenen Leiter stromlos geschaltet werden, einschließlich der intakten. Darüber hinaus zeichnen sich digitale Umspannstationen im Gegensatz zu konventionellen Umspannstationen durch die Implementierung standardisierter Kommunikationsframeworks, insbesondere der in IEC 61850 definierten, aus, um die Kommunikation zwischen Geräten verschiedener Hersteller zu erleichtern und letztlich die Interoperabilität (IOP) zu fördern. Die Konformität eines Geräts mit der IEC 61850-Norm garantiert jedoch keine IOP mit Geräten anderer Hersteller. Daher stellt der Einsatz von Relais, die der IEC 61850-Norm von verschiedenen Anbietern entsprechen, innerhalb der digitalen Umspannstation eine Herausforderung für die IOP bei der Durchführung von Schutzschemata auf Feldebene dar. Daher ist IOP-Testing vor der Feldimplementierung entscheidend, um sicherzustellen, dass Relais unterschiedlicher Hersteller nahtlos zusammenarbeiten, basierend auf den Schutzschemata, z.B. zur Erkennung und Identifizierung von Inter-Bay-Fehlern. In diesem Zusammenhang konzentriert sich das IOP-Testing auf die ORs, um das vorgeschlagene Schutzschema im Umgang mit MFFs zu testen und zu validieren. Richtlinien für die IOP-Prüfung wurden in früheren Studien dokumentiert. Allerdings sind diese Referenzen nicht für eine praktische Prüfung auf Systemebene geeignet, insbesondere nicht für die IOP-Prüfung zur Bewertung der Leistungsfähigkeit des Schutzkonzepts von Bay-Level-ORs unterschiedlicher Hersteller, z. B. hinsichtlich Leistungsschalterversagens, Lichtbogenerkennung usw. Daher wird die Entwicklung solcher Methoden den Endanwendern überlassen, die diese auf ihre spezifischen Anforderungen abstimmen.

Insgesamt werden die folgenden drei Hauptprobleme und -ziele identifiziert:

1. Im Kontext der Einstellung und Koordination von DRs erfordern konventionelle Techniken, die von Schutzingenieuren eingesetzt werden, manuelle und fehleranfällige Eingriffe, die selbst bei einer begrenzten Anzahl von Single- oder Multi-Vendor-DRs zeitaufwendig werden. Bei der Anwendung fortschrittlicher Algorithmen wie DFS ist deren Einsatzbereich auf einfache Topologien beschränkt. Daher besteht das Ziel darin, neuartige Algorithmen vorzuschlagen, die die Leitungsermittlung, DR-Einstellung und Koordination automatisieren können, unabhängig von der Netzwerktopologie anwendbar sind, scheinbare Impedanzen mit oder ohne Mehrfachströme von Erzeugungseinheiten handhaben, ohne Unter- oder Überschreitung der

Schutzbereiche, sowie die unterschiedlichen Fehlereinstellungen von Multi-Vendor-DRs mathematisch abbilden und konvertieren, ohne die Selektivität zu verlieren. Außerdem sollen diese Algorithmen höhere Genauigkeit und geringere Rechenzeit bieten als manuelle oder DFS-basierte Techniken.

2. Im Kontext des DR-Testings können die Norm IEC 60255-121:2014 und bestehende Methoden nur für einen begrenzten Satz von impedanzbasierten Funktionen verwendet werden, und der OAT-Ansatz kann die wesentlichen Wechselwirkungen zwischen Faktoren nicht erfassen. Darüber hinaus führt die empfohlene vollfaktorielle Strategie zu einer großen Anzahl von Experimenten und kann die Abhängigkeiten zwischen Faktoren nicht berücksichtigen. Daher besteht das Ziel darin, Testmethoden vorzuschlagen, die ein breiteres Spektrum an Funktionen testen und gleichzeitig die optimale Auswahl der Tests ermöglichen, um die Experimentbelastung zu reduzieren und den experimentellen Aufwand zu begrenzen.

3. Im Kontext von MFFs und IOP-Tests für digitale Umspannstationen verursachen MFFs großflächige Stromausfälle in den Verteilnetzen, und die bestehende Überstromschutzfunktion kann diese Ausfälle nicht verhindern. Darüber hinaus gewährleistet der Standard IEC 61850 keine IOP zwischen ORs unterschiedlicher Hersteller, und die verfügbaren IOP-Testmethodiken sind für eine praktische Prüfung auf Systemebene nicht geeignet. Daher besteht das Ziel darin, ein auf IEC 61850 basierendes Überstromschutzschema vorzuschlagen, das die bestehenden Überstromschutzfunktionen bei der Bewältigung von MFFs unterstützt, sowie eine Methodik, die das IOP von Multi-Vendor-Relais auf Feldebene testbar macht, um die Leistung der Schutzschemata zu bewerten.

Wesentliche wissenschaftliche Beiträge

Zunächst werden neuartige und breiter anwendbare Algorithmen entwickelt, um die Leitungsermittlung, DR-Einstellung und Koordination zu automatisieren, und zwar: (1.1) Eine erweiterte Version des DFS-Algorithmus – Modified Depth-First Search (MDFS) – zur Leitungsermittlung innerhalb der Schutzbereiche von DRs, die unabhängig von der Komplexität

der Netzwerktopologie anwendbar ist. (1.2) Ein MDFS-basierter Algorithmus für die DR-Einstellung, der in der Lage ist, die vom DR gesehene scheinbare Impedanz präziser zu berechnen, für das Mapping von Parametern auf Basis der scheinbaren Fehlerimpedanz bei Multi-Vendor-DRs anwendbar ist und bessere Leistung hinsichtlich Fehler bei der Leitungsermittlung bietet. (1.3) Ein MDFS-basierter Algorithmus zur Validierung der DR-Koordination mit verbesserten Eigenschaften in Bezug auf Rechenzeit, der überlappende Schutzbereiche hervorheben kann, um die intuitive Überprüfung der Koordination zu erleichtern.

Zweitens: (2.1) Es wird eine Testumgebung entwickelt, die auf einem Echtzeit-Digitalsimulator eines Übertragungssystemmodells basiert, sowie Testmethoden, um die Leistung kommerzieller DRs zu bewerten. Dieser Rahmen soll die Einschränkungen der bisherigen Testansätze (einschließlich der Norm IEC 60255-121:2014) überwinden und ermöglicht die Abdeckung eines breiteren Funktionsspektrums, wie z.B. Leistungsschwingungen, Sicherungsausfall und Fehlerortung. (2.2) Das statistische Versuchsdesign wird für das DR-Testing eingeführt, um die optimale Auswahl der Tests zu unterstützen und die experimentelle Effizienz zu steigern, indem der Fokus auf wirkungsträchtige Faktoren gelegt wird, während Wirksamkeit, Objektivität, Reproduzierbarkeit und Generalisierbarkeit der Testaktivität erhalten bleiben.

Drittens: (3.1) Es wird ein auf IEC 61850 basierendes Überstromschutzschema vorgeschlagen, um Mehrfach-Bay-Fehler (multi-bay faults) zu erkennen und zu identifizieren und dadurch die durch MFFs verursachten Ausfallbereiche zu reduzieren. (3.2) Zudem wird die Entwicklung einer Testumgebung vorgestellt, die auf einem Echtzeit-Digitalsimulator eines Verteilungssystemmodells basiert und die Integration dezentraler Erzeugung für das IOP-Testing von Multi-Vendor-Relais auf Feldebene ermöglicht, um die Leistung des Schutzschemas zu bewerten.

Abstract

Motivation, Goal and Task of the Dissertation

Distance protection is a protection function widely used in transmission systems due to its selectivity and speed. Before field deployment, the distance relay (DR) must be set, and its setting must be coordinated with other DRs within the system. For configuring the DR settings and validating their coordination, path determination is fundamentally required to identify the electrical elements, such as lines, buses, switches, and circuit breakers (CBs), within the protection zones of DR to be protected. Conventionally, path determination is a manual process, same for DR settings and DRs coordination validation, error-prone procedures, especially in the case of complex network topologies (e.g., loop/multi-loop networks) and/or when many DRs are implemented in the grid. This is even more so when DRs from different vendors are employed, as they are characterized by different parameter settings with different functions, e.g., power swing, load encroachment, etc. Nonconventional approaches, such as those based on graph theory and graph search algorithms, e.g., Depth-First Search (DFS), can automate path determination; however, these methods are still susceptible to errors, especially in complex network topologies.

Besides DR settings and DRs coordination validation, DR testing is a crucial activity to identify DR issues due to, e.g., setting misconfiguration, and firmware bugs, as well as to evaluate the effectiveness of the fault detection approaches. These test activities are done to ultimately prevent the disruptive effects of protection failures. For DR testing, the IEC 60255-121:2014 standard is an important reference, which specifies the minimum sets of requirements (zone characteristics, maximum deviation of operating time, etc.) for a limited set of functions. With such limitations, the performance of the DR in certain realistic fault characteristics and system behaviors during dynamic conditions remains untested and unevaluated. This ultimately results in DRs may misoperate, underreach, or trip unnecessarily, leading to system instability or blackouts, e.g., DR

may trip during stable power swings (DR must not trip under stable swings and must be differentiate between fault and power swings, as well as stable and unstable swings), underreach due to fault resistances, etc. Therefore, the IEC 60255-121:2014 standard and existing methodologies are inadequate to test additional functions—such as power swing, fuse failure, fault location—, whose testing is left to the final users based on their specific requirements. Moreover, the one-at-a-time (OAT) testing approach for evaluating DR performance presented in the previous works cannot capture the interaction among factors (e.g., fault resistance, fault location, fault inception angle, etc.). Besides the OAT approach, a full factorial strategy recommended by the IEC 60255-121:2014 standard to test the factors potentially affecting the DR performance quickly leads to hundreds or thousands of tests; also, this cannot handle the constraints among factors.

Fundamentally, a digital substation consists of a high voltage level as a transmission system and a medium voltage level as a distribution system. The medium voltage level acts as the intermediary between transmission infrastructure and local distribution networks, enabling the efficient delivery of electrical power to end-users across residential, commercial, and industrial sectors. Within this context, the protection of distribution feeders is therefore essential to maintaining system reliability and preventing wide-area blackout under abnormal operating conditions, e.g., feeder fault, multiple feeder faults (MFFs), etc. Among the available protection strategies, overcurrent relays (ORs) are most widely adopted as a primary feeder protection. This preference arises from their inherent simplicity, proven reliability, and cost-effectiveness compared to more complex alternatives such as distance or differential protection. However, the existing overcurrent protection function is vulnerable to MFFs even if the ORs within the substation can coordinate with each other at all fault current values. The MFFs cause the OR at the incoming feeder to operate faster than the faulted feeder ORs. This ultimately results in all feeders connected to the power transformer being de-energized, including the healthy ones. Furthermore, unlike conventional substations, digital substations are characterized by the deployment of standardized communication frameworks, particularly those defined in IEC 61850 to facilitate communication between devices coming from different manufacturers, and ultimately foster interoperability (IOP). The conformity of a device with the IEC 61850 standard does not guarantee IOP with devices from different

manufacturers. Therefore, the use of relay compliance to the IEC 61850 standard from multiple vendors within the digital substation poses a challenge in IOP to perform protection schemes at the bay level. Hence, IOP testing prior to field implementation is crucial for ensuring that relays from different vendors work seamlessly together based on protection schemes, e.g., detecting and identifying inter-bay faults. Within this context, the IOP testing focuses on the ORs for testing and validating the proposed protection scheme in addressing MFFs. Guidelines for IOP testing have been documented in previous studies. However, these references are not suitable for practical testing at a system level for testing the IOP to assess the performance of the protection scheme of multi-vendor bay-level ORs, e.g., breaker failure, arc detection, etc. Hence, such methodologies are left to the end users, who align them with their specific requirements.

Overall, the following three main challenges and goals are identified:

1. In the context of DR settings and DRs coordination validation, conventional techniques adopted by protection engineers require manual, prone-to-error intervention, which becomes time-consuming even for a limited number of single/multi-vendor DRs. When adopting sophisticated algorithms such as DFS, their applicability boundary is limited to simple topologies. Hence, the goal is to propose novel algorithms for automatizing the path determination, DR settings and DRs coordination validation, which can be applicable regardless of the network topology, can handle apparent impedance with/without multiple currents fed by generation units, without under- and over-reach issues of the protection zones, as well as the different fault detection setting parameters of multi-vendor DRs can be mathematically mapped and converted without losing selectivity, have better accuracy and lesser computational time than manual and DFS-based techniques.

2. In the context of DR testing, the IEC 60255-121:2014 standard and existing methodologies can be used only in a limited set of impedance-based functions, and OAT cannot observe the key interactions among factors. Furthermore, the recommended full factorial strategy results in a large number of experiments, and this cannot handle the constraints between factors. Hence, the goal is to propose testing methodologies that allow testing a broader spectrum of functions

and enable the optimal choice of the tests to reduce the experiment burden while constraining the experimental effort.

3. In the context of MFFs and IOP testing for digital substations, the MFFs cause a wide-area blackout in the distribution systems, and the existing overcurrent protection function cannot prevent blackouts from the MFFs. Furthermore, the IEC 61850 standard does not guarantee IOP of ORs from different vendors, and available IOP testing methodologies are not suitable for practical testing at a system level. Hence, the goal is to propose an IEC 61850-based overcurrent protection scheme to support existing overcurrent protection functions in addressing MFFs, and a methodology that allows testing the IOP of multi-vendor bay-level relays to assess the performance of the protection schemes.

Major Scientific Contributions

First, novel and more broadly applicable algorithms are developed to automatize the path determination, DR settings and DRs coordination validation, namely: (1.1) an extended version of the DFS algorithm—Modified Depth-First Search (MDFS)—for path determination within the DR protection zones which is applicable irrespective of the network topology complexity; (1.2) a MDFS-based algorithm for DR settings that is able to straightforwardly compute the apparent impedance seen by the DR more accurately, it is applicable for mapping parameters based on apparent fault impedance for multi-vendor DRs, and it has better performance in terms of path determination errors; (1.3) a MDFS-based algorithm for validating the DRs coordination with enhanced properties in terms of computational time and can highlight overlapping protection zones to facilitate intuitive verification of coordination.

Second, (2.1) a test environment is developed based on a real-time digital simulator of a transmission system model and testing methodologies to assess the performance of the commercial DRs. This framework aims to overcome the limitations of state-of-the-art testing approaches (including the IEC 60255-121:2014 standard), that allows covering a broader spectrum of functions such as power swing, fuse failure, and fault location, etc.; and (2.2) the statistical design of experiments is introduced for DR testing to aid in the optimal choice of the tests and enhance experimental efficiency

by focusing on impactful factors while retaining the efficacy, objectivity, reproducibility, and generalization of the testing activity.

Third, (3.1) an IEC 61850-based overcurrent protection scheme is proposed for detecting and identifying multi-bay faults to reduce the outage areas caused by MFFs, and (3.2) the development of a test environment based on a real-time digital simulator of a distribution system model with the integration of distributed generation for the IOP testing of multi-vendor relays at the bay level to assess the performance of the protection scheme is presented.

To my family,
and to everyone
whose presence and support have
brought meaning to this journey.

Contents

List of Publications

Journal Articles

[1] Thanakorn Penthong, Antonello Monti, and Ferdinanda Ponci. "Distance Relay Setting and Validating Based on Graph Theory and Modified Depth-First Search". In: *Under review IEEE Transactions on Industrial Informatics* (2025).

[2] Mirko Ginocchi, Thanakorn Penthong, Ferdinanda Ponci, and Antonello Monti. "Statistical Design of Experiments for Power System Protection Testing: A Case Study for Distance Relay Performance Testing". In: *IEEE Access* 12 (2024), pp. 27052–27072. DOI: 10.1109/ACCESS.2024.3367591.

[3] Thanakorn Penthong, Mirko Ginocchi, Amir Ahmadifar, Ferdinanda Ponci, and Antonello Monti. "IEC 61850-Based Protection Scheme for Multiple Feeder Faults and Hardware-in-the-Loop Platform for Interoperability Testing". In: *IEEE Access* 11 (2023), pp. 65181–65196. DOI: 10.1109/ACCESS.2023.3280128.

Conference Articles

[4] Mirko Ginocchi, Thanakorn Penthong, Muhammad Zeeshan Khattak, Alexander Och, Ferdinanda Ponci, and Antonello Monti. "Global sensitivity analysis of distance protection performance for submarine transmission systems". In: *14th Mediterranean Conference on Power Generation Transmission, Distribution and Energy Conversion (MEDPOWER 2024)*. Vol. 2024. 2024, pp. 406–411. DOI: 10.1049/icp.2024.4694.

[5] Thanakorn Penthong, Alberto Dognini, Edoardo De Din, Manuel Pitz, Ferdinanda Ponci, and Antonello Monti. “Hardware-in-the-Loop Validation of AC/DC Service Restoration including industrial IED and Communication Protocols”. In: *2024 Open Source Modelling and Simulation of Energy Systems (OSMSES)*. 2024, pp. 1–6. DOI: 10.1109/OSMSES62085.2024.10668962.

[6] Thanakorn Penthong, Mirko Ginocchi, Ferdinanda Ponci, and Antonello Monti. “Testing Methodology for Performance Evaluation of Distance Protection Relays for Transmission Systems”. In: *2023 IEEE Belgrade PowerTech*. 2023, pp. 1–6. DOI: 10.1109/PowerTech55446.2023.10202837.

[7] Thanakorn Penthong, Erdem Gümrükcü, and Ferdinanda Ponci. “Laboratory of Power System Automation: an example of activity”. In: *2022 IEEE German Education Conference (GeCon)*. 2022, pp. 1–6. DOI: 10.1109/GeCon55699.2022.9942765.

[8] Muhammad Zeeshan Khattak, Thanakorn Penthong, Mirko Ginocchi, Nisai Fuengwarodsakul, Ferdinanda Ponci, and Antonello Monti. “Evaluation of the Impact of the Cable Model on the Distance Protection Performance in a Submarine Transmission System”. In: *PESS 2024; Power and Energy Student Summit*. 2024, pp. 137–142.

[9] Thomas I. Strasser, Edmund Widl, René A. Kuchenbuch, Laura Lázaro-Elorriaga, Borja Tellado Laraudogoitia, Mirko Ginocchi, Thanakorn Penthong, Ferdinanda Ponci, Amelie Gyrard, Antonio Kung, Carlos A. Mac Gregor, Carmen Garcia Montero, and Eduardo Relano Algaba. “Towards interoperability testing of smart energy systems – an overview and discussion of possibilities”. In: *14th Mediterranean Conference on Power Generation Transmission, Distribution and Energy Conversion (MEDPOWER 2024)*. Vol. 2024. 2024, pp. 263–268. DOI: 10.1049/icp.2024.4670.

[10] Cesar Cazal, Su Mon Tun, Irtaza Waheed, Manuel Pitz, Yoga Kannan, Thanakorn Penthong, Ferdinanda Ponci, and Antonello Monti. “Automation Framework for Blockchain-Based Coordination of Distributed Energy Resources”. In: *2024 IEEE 15th International Symposium on Power Electronics for Distributed Generation Systems (PEDG)*. 2024, pp. 1–6. DOI: 10.1109/PEDG61800.2024.10667360.

1

Introduction

Distance protection is a protection function commonly used in transmission systems due to its selectivity, reliability, and speed in safeguarding transmission lines [11, 12, 13]. For modern Distance relay (DR)s, manufacturers incorporate additional functions, e.g., tele-protection, auto-reclose, power swing, etc., to collaborate with the DR zone characteristics to enhance the overall operational performance of the DR [14, 15].

To achieve the goal of selective and secure operation of DRs, the zone characteristics must be set before field deployment, and their settings must be coordinated with the other DRs within the system. In practice, modern DR settings are not limited to the zone characteristics; additional functions must be set. The configuration of DR settings and the validation of their coordination fundamentally rely on accurate path determination, which is essential for the precise identification of electrical components, such as lines and buses, within the DR protection zones targeted for protection. Conventionally, path determination is a manual process, along with DR settings and DRs coordination validation [16, 17, 18]. This approach can be prone to errors, especially in complex network topologies, such as meshed networks, and/or when many DRs are utilized in the power grid. This is even more so when employing DRs from multiple vendors, as each DR manufacturer may have distinct parameter settings and functionalities—such as power swing detection, load encroachment, etc. Nonconventional approaches, such as those based on graph theory and graph search algorithms, e.g., Depth-First Search (DFS), can automatize path determination from the relay location; however, these methods are still susceptible to errors, especially in meshed/loop power systems [19, 20, 21].

So far, various approaches have been presented to address the DR settings and DRs coordination validation. For example, [22] introduces a tool for configuring DR zone characteristics derived from the busbar fault database. Moreover, the DR settings assessment approach is proposed to verify the adequacy of DR settings after changing network topology by performing the fault simulation. However, only zone characteristics of the phase setting are provided; the topology connection is represented based on Ybus/Zbus matrices, and configuring the DR settings based on such matrices may cause under- or over-reach issues due to the infeed effect from generation units. Furthermore, performing fault simulation after network re-configuration to ensure that DRs operate properly based on their settings requires high computational resources and time. In [23] presents a new method for calculating zone-2 setting of DR by fault simulations on the zone-1 reach on the next adjacency line to obtain the fault impedance seen by DRs. Similarly, [24] proposes a zone-2 setting using the apparent fault impedance seen by the relay by considering the infeed effect to mitigate miscoordination issues. However, [23] and [24] focus on specific challenges related to the zone-2 setting, while neglecting a comprehensive perspective on the overall DR settings.

Moreover, in the context of DRs coordination validation, a specific set of relays for initiating the coordination (reference DRs) must be defined. For this purpose, in [25] proposes algorithms for coordinating DRs on transmission networks using Depth-First Search (DFS) and back-tracking (BT) techniques to define a set of reference DRs that are crucial for initiating the coordination process. Similarly, [26] and [27] present graph theory and graph search methods, particularly DFS, which are applied to determine reference DRs. However, since reference DRs are used as technical input data for the specific tools, e.g., Computer-Aided Protection Engineering (CAPE), Digsilent Power Factory, effort and time are still required to perform the DRs coordination validation, particularly path determination.

Since DRs play a crucial role in transmission system protection, additionally, their installation is typically required at the point of interconnection when small power producers—such as converter-based renewable energy resources or synchronous generators—connect to the grid [28, 29]. To identify potential setting flaws or firmware-related anomalies, as well as to assess the performance of the fault detection techniques, comprehensive DR testing is required to ensure that the DR can correctly respond to the

abnormal system conditions both in steady state and transient conditions prior to deployment to prevent unexpected operations of the DR, leading to blackout in the system [30]. For this purpose, testing methodology and testing platform are essential. To perform the test, DR testing can be performed in compliance with the IEC 60255-121:2014 standard [31]. This standard specifies a minimum set of requirements to be tested for both basic zone characteristics accuracy and performance evaluation, for which special testing techniques, such as a real-time digital simulator, are recommended and required.

To this aim, [32] and [33] propose a Hardware-in-the-Loop (HiL) platform to investigate unexpected DR operations due to the high penetration of Photovoltaic (PV) farms and the impact of a Voltage Source Converter (VSC) topology for detecting ground faults. In [34, 35, 36] HiL platform is also proposed to assess the zone characteristics and basic accuracy of DRs based on the testing methodology defined in the standard. Similarly, [37] proposes the modeling of ultra-high voltage (UHV) transmission systems to assess the performance of DRs. However, as mentioned above, modern DRs consist of additional functions to enhance the DR operation performance under different operating conditions of the system; the testing methodology outlined in the standard and approaches proposed in the literature are limited to zone characteristics and are inadequate for the complete DR testing scheme [38].

Furthermore, testing approaches described in the literature align with either one-at-a-time (OAT) or full factorial approaches. When following the guidelines outlined in the IEC 60255-121:2014 standard [31], conducting numerous tests is inevitable. This is particularly true when a broader set of scenarios needs to be investigated to check compliance with utility-specific requirements [39]. The full factorial approach prescribed by the IEC 60255-121:2014 standard cannot accommodate user-specific requirements or physical constraints among factors. Subsequently, the size of experiments determined by factorial designs might not be compatible with the practical tests that are required by the Transmission System Operator (TSO). These aspects pose significant challenges in terms of experiment efficiency and identifying impactful factors while maintaining efficacy, objectivity, and generalization of testing activity. In fact, to reduce the experiment burden, these challenges are often cited to justify selecting tests based on worst-case scenarios or TSO's experiences. Such selections may involve subjectively

limiting the number of factors to perform, avoiding the replication of tests, etc.

In modern grids, the digital substations fundamentally consist of the transmission system and distribution system within the substations. The distribution system acts as the intermediary between transmission infrastructure and local medium voltage networks, enabling the efficient delivery of electric power to end-users, e.g., residential, industrial sectors, etc. Therefore, protecting distribution feeders is important to maintain network reliability and service quality for customers. To protect distribution feeders, an Overcurrent relay (OR) is mostly used as a primary protection due to its simplicity, cost-effectiveness, etc., compared to more complex alternatives such as distance or differential protection [40]. However, the ORs' operation in digital substations is vulnerable to Multi-Feeders Faults (MFFs) [41]. The MFFs cause all feeders to be de-energized, including the healthy ones, due to OR at the low voltage side of the power transformer operating faster than faulted feeder ORs.

The digital substations based on the IEC 61850 standard demonstrate significant construction and operational advantages of IEC 61850 over conventional substations in different aspects, such as reduced costs and wiring complexity associated with connecting equipment within substations, improved interoperability (IOP), etc. [42, 43]. These advantages lead to many electricity utilities and industries implementing digital substation systems based on the IEC 61850 communication standard [44, 45, 46, 47, 48]. By using Ethernet-based communication, protective relays used in digital substations must be interoperated via communication networks using a Generic Object-Oriented Substation Events (GOOSE) to enable the implementation of several applications, e.g., protection, automation, control functions, etc. Therefore, it is common to use multi-vendor relays when replacing life-expired relays, especially when the original manufacturer's relay is unavailable [49, 50, 51]. However, this problem can be solved by using relays that comply with the IEC 61850 standard, and IOP is the key to integrating relays from different vendors with plug-and-play solutions, as well as enabling advanced applications to foster smart grids.

Despite the advantages, when relays from multiple vendors are used within the digital substation, their individual compliance with the IEC 61850 standard does not guarantee IOP between them. Hence, implementing IEC 61850-based systems poses significant challenges in the integration of multi-vendor relays and testing protection schemes at the system level.

Due to the fact that relays at the bay level are employed in different applications, e.g., control and protection. Thus, methodologies for validating control and protection schemes are essential. For this purpose, in [52] specifies the relay testing requirements and procedures in digital substations. Although guidelines for testing, e.g., the signal transmission and reception capabilities of relays from different vendors, are provided, it overlooks methodologies for testing the IOP of multi-vendor bay-level relays in the context of the protection schemes' performance assessment, and such methodologies are left to the end users, who align them with their specific requirements. Moreover, [53] and [54] presents a case study to demonstrate the IOP testing among relays from different manufacturers and emphasizes the critical need for IOP testing as part of site commissioning for IEC 61850-based substation automation systems. However, the works presented in [53] and [54] require predefined analog values to generate initial signals for each testing scenario. As a result, the study cases may be limited to specific conditions, which ultimately may not identify the IOP problem that could arise under different system conditions. In [55] and [56] propose a HiL testing platform to assess the performance of the IEC 61850-based protection scheme in microgrids, but the potential IOP problems of the protection schemes are overlooked.

In fact, IOP issues can arise in both transmission and distribution systems, but the methodology for IOP testing remains consistent. In this work, within this context, the focus of IOP testing is on the distribution system, and the proposed methodologies for IOP testing aim to test and validate the proposed protection scheme in addressing MFFs.

Overall, the above-mentioned literature review underlines the following challenges and goals:

1. In the context of DR settings and DRs coordination validation, conventional techniques adopted by protection engineers require manual, prone-to-error intervention, which becomes time-consuming even for a limited number of single/multi-vendor DRs. To the best of the author's knowledge, previous studies have demonstrated limitations concerning the availability of adequate tools and effective approaches to completely automatize the DR settings and DRs coordination validation; even if sophisticated algorithms such as DFS are deployed, their applicability boundary is limited to identifying reference DRs for DRs coordination and simple topologies for path determination. Hence, the goal is to propose novel algorithms for automatizing

the path determination, DR settings and DRs coordination validation, which can be applicable regardless of the network topology, can handle apparent impedance with/without multiple currents fed by generation units, without under- and over-reach issues of the protection zones, as well as the different fault detection setting parameters of multi-vendor DRs can be mathematically mapped and converted without losing selectivity, have better accuracy and lesser computational time than manual and DFS-based techniques.

2. In the context of DR testing, the IEC 60255-121:2014 standard and the available methodologies proposed in previous studies can be used only in a limited set of impedance-based functions, and the recommended full factorial strategy might not be compatible with the practical tests and TSOs' requirements. Hence, the goal is to propose testing methodologies that allow testing a broader spectrum of functions and enable the optimal choice of the tests while maintaining efficacy, objectivity, and generalization of testing activity.

3. In the context of MFFs and IOP testing for digital substations, the MFFs cause a wide-area blackout in the distribution systems, and the existing overcurrent protection function cannot operate properly when MFFs occur in the system. Moreover, the IEC 61850 standard does not guarantee IOP of relays from different vendors, and existing IOP testing methodologies cannot be applied to validate the protection schemes at a system level. Hence, the goal is to propose an IEC 61850-based overcurrent protection scheme to support existing overcurrent protection functions in addressing MFFs, and a methodology that allows testing the IOP of multi-vendor bay-level relays to assess the performance of the protection scheme.

Up to now, new research challenges and questions revolve around developing DR-setting techniques and identifying reference DRs for coordination that can be integrated and deployed in the planning and operational context. Besides DR settings and DRs coordination validation, approaches for DR and IOP testing in the context of assessing the performance of the protection schemes, which reveal common challenges for TSO and Distribution System Operator (DSO). Consequently, the goal of this work does not merely focus on identifying recent methodologies that provide

better performance for DR settings and DRs coordination validation, DR and IOP testing methodologies; it also seeks to address the following three research questions:

1^{st} **research question** Which techniques are applicable to completely automatize the DR settings regardless of network topologies, and which methodologies are applicable to identify miscoordination problems for multiple relays in series?

2^{nd} **research question** How can the gaps between TSOs and manufacturers be bridged in terms of DR testing for acceptance tests? Which approaches are applicable to enable the optimal choice of DR testing while maintaining efficacy and generalization of testing activity?

3^{rd} **research question** Which approaches are applicable to enhance the operation performance of the existing OR in addressing MFFs? How can TSOs and DSOs ensure that the relays in digital substations from different manufacturers interoperate based on protection and control designed schemes when relays are integrated into the system through a communication network?

1.1 Contributions of this dissertation

This dissertation proposes to solve problems of DR settings and DRs coordination validation, methodologies for DR testing, and IOP testing to cover complete DR schemes and to test and validate the IOP of multi-vendor relays in the context of the protection schemes' performance assessment in the digital substations. These steps comprise problem formulation, algorithm development for protection system design for operational planning, methodology development, and deployment for acceptance and commissioning tests.

To address research question 1, it is important first to examine existing approaches. This first step is indispensable for later algorithm development, especially now that, after many years of setting techniques and identifying reference DRs for coordination research, the focus has moved to automatically both DR settings and DRs coordination validation. This raises related questions about how to automatize DR settings and DRs coordination validation strategies that are generalizable for both simple and complex network topologies, straightforwardly computing the apparent impedance seen by the DR more efficiently, automatically mapping the fault detection setting parameters of multi-vendor DRs, as well as

identifying the miscoordination problem among primary and backup DRs, particularly after network reconfiguration and planning, in order to reduce computational resources, errors, and time. Here, this work presents: (i) an extended version of the DFS algorithm, (Modified Depth-First Search (MDFS)), for path determination within the DR protection zones, which is applicable irrespective of the network topology complexity, (ii) a MDFS-based algorithm for DRs setting that is able to straightforwardly compute the apparent impedance seen by the DR more accurately, it is applicable for mapping parameters based on apparent fault impedance for multi-vendor DRs, and it has better performance in terms of path determination errors, and (iii) a MDFS-based algorithm for validating the DRs coordination with enhanced properties in terms of computational time and can highlight overlapping protection zones to facilitate intuitive verification of coordination.

In addressing research question 2, (i) a test environment is developed based on a real-time digital simulator of a transmission system model and testing methodologies to assess the performance of the commercial DRs. This framework aims to overcome the limitations of state-of-the-art testing approaches (including the IEC 60255-121:2014 standard), that allows covering a broader spectrum of functions such as power swing, fuse failure, and fault location, etc., and (ii) the Statistical Design of Experiments (stat-DOE) is introduced for DR testing to aid in the optimal choice of the tests and enhance experimental efficiency by focusing on impactful factors while retaining the efficacy, objectivity, reproducibility, and generalization of the testing activity.

To comprehensively answer research question 3, (i) an IEC 61850-based overcurrent protection scheme is proposed for detecting and identifying multi-bay faults to reduce the outage areas caused by MFFs, and (ii) the development of a test environment based on a real-time digital simulator of a distribution system model with the integration of distributed generation for the IOP testing of multi-vendor relays at the bay level to assess the performance of the protection scheme is presented.

Collectively, these contributions address current gaps in DR settings and DRs coordination validation, DR performance testing, IOP testing, and the operational performance of ORs in digital substations. The contributions of the present work lay the foundation for translating the latest advanced research approaches into practical applications for TSOs and DSOs. In light of the preceding analysis, the contributions are summarized as follows:

1^{st} **contribution** Algorithms for automatizing DR settings based on MDFS,

2^{nd} **contribution** An MDFS-based algorithm and methodology to identify the miscoordination problems between primary and backup DRs,

3^{rd} **contribution** A methodology for DR performance testing beyond existing testing approaches to comply with both TSO and manufacturer requirements,

4^{th} **contribution** The integration of the stat-DOE in DR performance testing to minimize the set of scenarios and number of tests without harming or limiting the efficacy and generalization of the testing procedure,

5^{th} **contribution** An IEC 61850-based overcurrent protection scheme for detecting and identifying MFFs to prevent healthy feeders from de-energizing due to MFFs, and

6^{th} **contribution** A methodology and approach for testing IOP in digital substations of multi-vendor relays.

1.2 Outline

The outline of this dissertation is described in Figure 1.1 and Figure 1.2. Following this introduction, this work first introduces the theoretical background and methodologies review on DR setting and coordination, DR testing methodologies, and protection scheme and methodologies for IOP testing and validation to assess the performance of the protection scheme at the bay level within digital substations. Subsequently, the challenges and research gaps identified in previous studies are systematically highlighted and discussed in chapter 2. Having established this theoretical basis, Chapter 2 facilitates the identification of potential techniques for DR setting and coordination, further described in Chapter 3, which suit the earlier defined setting and coordination issues. In Chapter 4, methodology and the developed test environment are detailed for complete DR scheme testing. The three DRs from different manufacturers are tested and evaluated the performance based on the proposed methods. The proposed protection scheme to address MFFs is elaborated in Chapter 5, and its performance will be tested and evaluated according to the established requirements. Furthermore, a methodology and the developed test environment for IOP testing of multi-vendor bay-level relays in digital substations are presented. Finally, Chapter 6 summarizes the dissertation and highlights potential areas for further research and investigation.

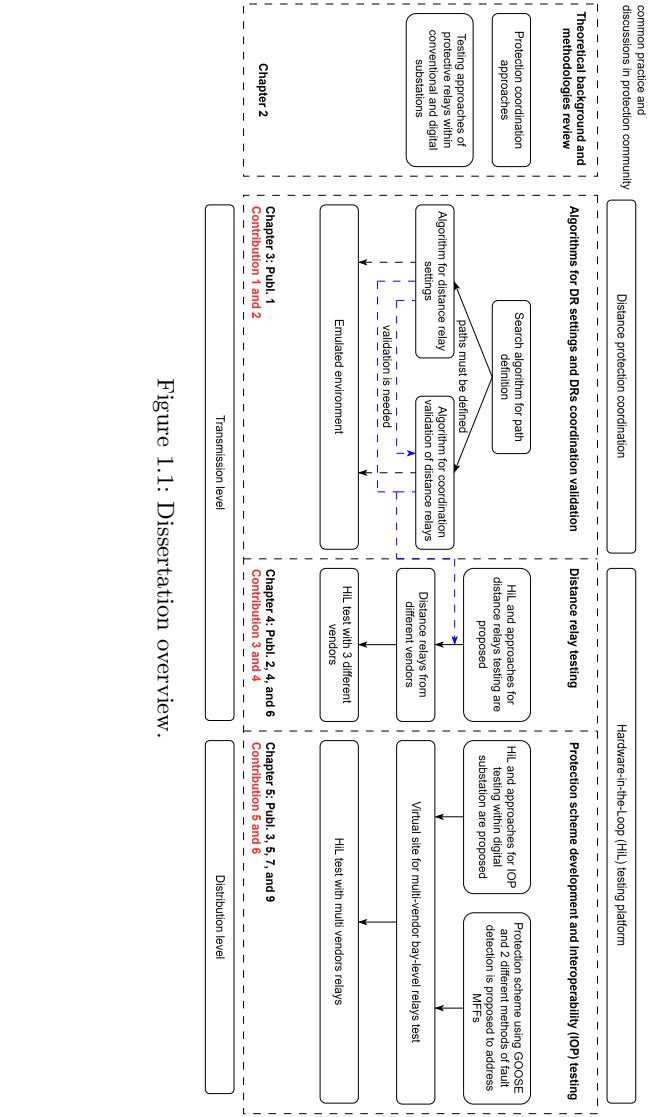

Figure 1.1: Dissertation overview.

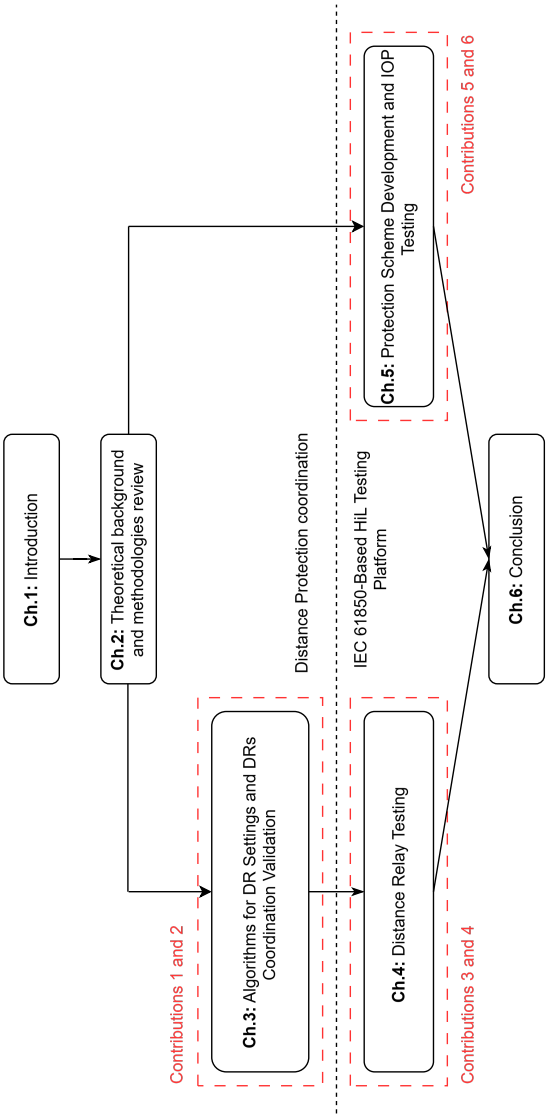

Figure 1.2: Dissertation workflow.

2

Theoretical Background and Methodologies Review

This chapter is organized as follows. Sections 2.1, 2.2, 2.3, and 2.4 provide the fundamental principles and essential terminology associated with distance protection functions, methodologies for DR settings and DRs coordination validation are reviewed, as well as challenges from the previous studies are identified for further improvement. In addition to DR settings and DRs coordination validation strategies, the methodologies and approaches employed for DR testing are critically examined in Section 2.5. Furthermore, protection schemes and approaches employed at the bay level of the digital substations in protecting feeders from faults in the distribution systems, as well as the methodologies for performance assessment of the protection schemes of multi-vendor relays, so-called IOP testing and validation, are discussed in Section 2.6. Subsequently, the challenges and research gaps identified in previous studies are systematically highlighted and discussed.

2.1 Distance protection in transmission system

The distance protection function operates and detects faults based on the impedance between the relay location and the fault point. In doing so, the DR calculates the apparent impedance (Z_{app}) using the current and voltage signals received from the instrument transformers (e.g., current and voltage transformers) at the relay location and compares it with the setting values. If Z_{app} is smaller than the setting values, the DR releases the trip signal to open the appropriate Circuit Breaker (CB) to separate the faulted line section. The measured values based on time series used by

the DR to compute the Z_{app} to determine whether the fault location is located in the protection zones of the DR are shown in Table 2.1, where I_0 is the zero-sequence current and k is the ground compensation factor:

$$k = \frac{(Z_{l0} - Z_{l1})}{Z_{l1}} \tag{2.1}$$

with Z_{l0} and Z_{l1} being the zero-sequence and positive-sequence impedances of the transmission line, respectively.

Table 2.1: Impedance calculation of distance protection function [57].

Fault type	**Impedance calculation**	**Fault type**	**Impedance calculation**
AG	$\frac{V_A}{I_A + 3kI_0}$	AB	$\frac{V_A - V_B}{I_A - I_B}$
BG	$\frac{V_B}{I_B + 3kI_0}$	BC	$\frac{V_B - V_C}{I_B - I_C}$
CG	$\frac{V_C}{I_C + 3kI_0}$	CA	$\frac{V_C - V_A}{I_C - I_A}$

Fundamentally, four protection zones can be set within the DR, as expressed in Figure 2.1, where mho and quadrilateral characteristics are deployed by the DR to detect phase and ground faults, respectively.

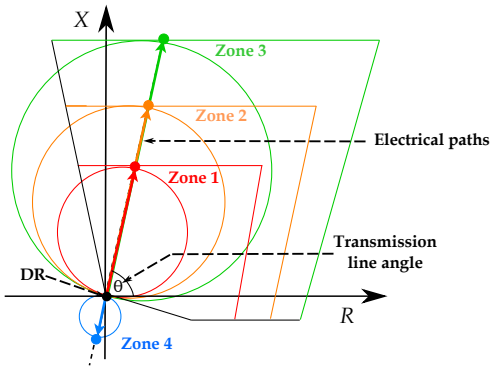

Figure 2.1: Zone characteristics of DR.

2.2 Distance relay settings

Before deploying the DR in the transmission systems, the protection zones of the DR must be set and its setting must correspond to the network topologies. Initially, the electrical components, e.g., transmission lines, buses, etc., within the protection zones, so-called "*path*", must be determined to identify all possible components to be protected [58, 17]. Conventionally, *DR setting refers to a manual process of determining the electrical components within the protection zones, calculating the initial settings, executing short circuit simulations one by one, obtaining the operation times and the impedances of the relays by graphics and tables* [16]. There are two main options to compute the protection zone settings: (i) the protection zone settings are only computed based on transmission line impedance [59, 60], and (ii) the zone settings are computed by considering both transmission line impedance and the apparent fault impedance seen by the DR based on the bus fault studies [22]. Besides these approaches, a method for calculating zone-2 setting by fault studies on the zone-1 reach on the next adjacency line is proposed in [23]. Similarly, a method for calculating zone-2 setting by fault studies and considering the infeed effect is proposed in [24].

In practice, to configure the protection zone settings of the DR, different criteria are used based on TSOs' requirements, i.e., different TSOs have their own criteria depending on network topologies and transmission line configurations. The setting criteria implemented by TSOs are synthetically summarized next [61, 62].

Criteria I

Considering the DR at substation A depicted in Figure 2.2, the criteria setting of DR_A can be expressed as follows:

$\mathrm{Z}_1 = 85\% \cdot \mathrm{Z}l_{AB}$

$\mathrm{Z}_2 = 100\% \cdot \mathrm{Z}l_{AB} + 50\% \cdot \mathrm{Z}l_{BD}$ (shortest line)

$\mathrm{Z}_{3a} = 100\% \cdot \mathrm{Z}l_{AB} + 125\% \cdot \mathrm{Z}l_{BC}$ (longest line)

$\mathrm{Z}_{3b} = 100\% \cdot \mathrm{Z}l_{AB} + 100\% \cdot \mathrm{Z}l_{BC} + 25\% \cdot \mathrm{Z}l_{CE}$

$\mathrm{Z}_4 = 15\% \cdot \mathrm{Z}_1$

Where Z_1 to Z_4 are the phase and ground settings of zone-1 to zone-4 of the DR, $\mathrm{Z}l$ is the impedance of the transmission line between substations, and TX is represented as the power transformer.

Generally, the zone-2 reach is set to cover 50% of the next adjacent line with the minimum positive sequence impedance and the zone-3 reach is set to cover more than the next adjacent line with the highest positive sequence impedance by about 25% [23, 59]. Meanwhile, zone-4 reach is set at 15% of the zone-1 reach with the direction toward substation A (the reverse direction) [61, 62].

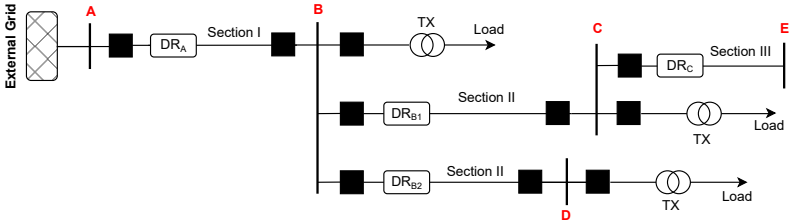

Figure 2.2: Network topology with multi-adjacent lines connected to the remote substation.

Criteria II

When DG is connected to the remote substation, as illustrated in Figure 2.3, the infeed current fed by the DG affecting the protection zones of the DR$_A$ at substation A must be considered. This effect is represented by the current ratios—the so-called K factor—between the current fed by the DG and the current passed through the DR$_A$, as shown in (2.2). This criterion can be expressed as follows:

$$K = 1 + \frac{I_{DRG}}{I_{DRA}} \tag{2.2}$$

$\mathrm{Z}_1 = 85\% \cdot \mathrm{Z}l_{AB}$
$\mathrm{Z}_2 = 100\% \cdot \mathrm{Z}l_{AB} + 50\% \cdot \mathrm{Z}l_{BD} \cdot K$ (shortest line)
$\mathrm{Z}_{3a} = 100\% \cdot \mathrm{Z}l_{AB} + 125\% \cdot \mathrm{Z}l_{BC} \cdot K$ (longest line)
$\mathrm{Z}_{3b} = 100\% \cdot \mathrm{Z}l_{AB} + [100\% \cdot \mathrm{Z}l_{BC} + 25\% \cdot \mathrm{Z}l_{CE}] \cdot K$
$\mathrm{Z}_4 = 15\% \cdot \mathrm{Z}_1$

It is noticeable that the effect of the infeed current fed by the DG directly affects zone-2 and zone-3 reaches of the DR$_A$. Based on this topology, Z_4 can detect the current fed by the DG in a reverse direction.

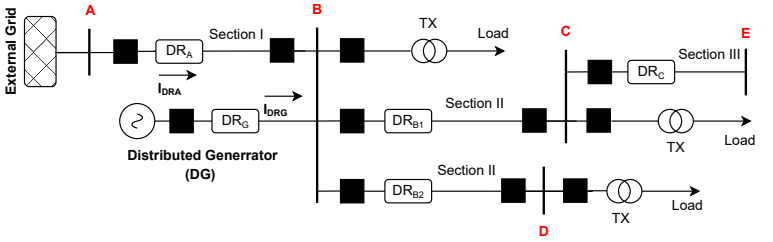

Figure 2.3: Network topology with multi-adjacent lines and DG connected to the remote substation.

Hence, in practice, Z_4 is used as a backup protection for the bus bar differential protection when the fault occurs at the bus bar at substation A. Furthermore, in the case of complex networks/meshed topologies, as shown in Figure 2.4, fault currents can be fed by all generation units in the system to the fault point. As such, the K factor of the DR_A must consider the infeed effect under this circumstance. Consequently, the infeed effect can be reformulated and expressed as follows [63]:

$$K = 1 + \frac{I_{G2} + I_{G3} + I_{G5}}{I_{G1}} \tag{2.3}$$

Criteria III

This criterion is usually applied in rural areas because the remote substation is the end substation (only a transformer bay connected to the substation), as shown in Figure 2.5. Since only the power transformer bay is connected to the remote substation, zone-2 and zone-3 settings of the DR_A are computed by combining with the transformer impedance and are also used as backup protection for the transformer differential relay at the remote substation. The setting for each protection zone of this criterion can be expressed as follows.

$Z_1 = 85\% \cdot Zl_{AB}$

$Z_2 = 100\% \cdot Zl_{AB} + 20\% \cdot Z_{TX}$ at the remote substation

$Z_3 = 100\% \cdot Zl_{AB} + 60\% \cdot Z_{TX}$ at the remote substation

Where Z_{TX} is the impedance of the power transformer at the remote substation.

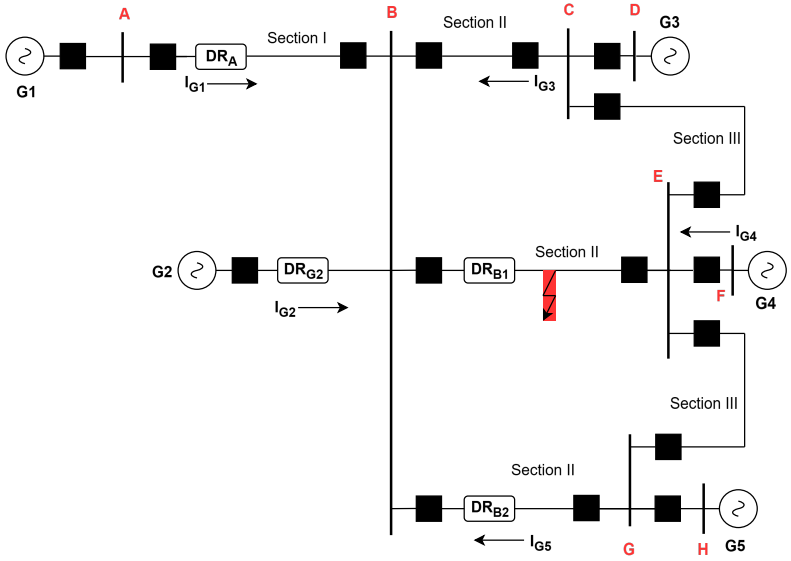

Figure 2.4: Infeed effect on the protection zones.

Besides the protection zone settings of the DR, in practice implementations, some specific parameters for each protection zone—e.g., Fault resistance reach, Phase-Phase (RFPP) and Phase-Earth (RFPE)—and additional functions, such as power swing, phase selection, etc., must be set to improve the overall operation performance of the DR, aiming to avoid unexpected operation under different operating conditions of the system. Hence, some guidelines and instructions for DR settings with specific parameters and additional functions are expressed here, and more details on additional functions can be found in [64, 65, 66, 67].

To avoid load encroachment for phase-to-earth and phase-to-phase measuring elements, the resistive reach of any protection zone of ground and phase protections must be set less than 80% and 160% of the minimum load impedance (Z_{Lmin}), respectively. The instructions to determine such resistive reaches can be expressed as follows.

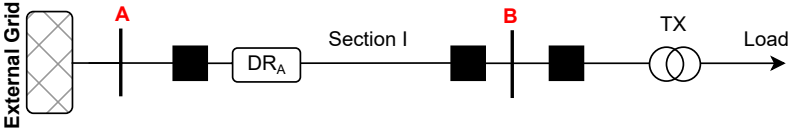

Figure 2.5: Radial system connected to the end substation.

$$\left|\overline{Z}_{L_{\min}}\right| = \frac{U_{\min}^2}{S_{\max}} \tag{2.4}$$

$$\text{RFPE} \leq 0.8\, Z_{L_{min}} \cdot \left[\cos\delta - \frac{2R_{l1} + R_{l0}}{2X_{l1} + X_{l0}} \sin\delta\right] \tag{2.5}$$

$$\text{RFPP} \leq 1.6\, Z_{L_{min}} \cdot \left[\cos\delta - \frac{R_{l1}}{X_{l1}} \sin\delta\right] \tag{2.6}$$

where:

- δ is a maximum load-impedance angle, related to the maximum load power.
- U_{min} is a minimum expected system voltage under critical system conditions.
- S_{max} is a maximum expected load in the direction of substations A to B (with minimum operating voltage of the system U_{min}).
- R_{l1} is a line positive sequence resistance.
- X_{l1} is a line positive sequence reactance.
- R_{l0} is a line zero sequence resistance.
- X_{l0} is a line zero sequence reactance.

Similarly, the guidelines to determine the parameter settings of the detection zones of power swing and phase selection for fault detections with respect to the distance protection function can be computed based on the recommendations in [66, 67] and can be expressed as follows.

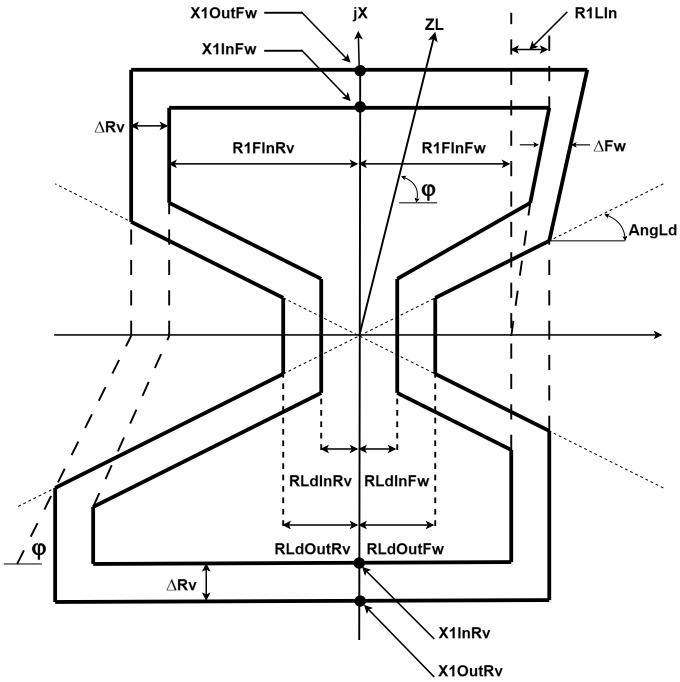

Figure 2.6: Power swing setting with respect to the distance protection function [67].

The outer boundary of power swing detection characteristic in forward and reverse directions, so-called "$RLdOutFw$" and "$RLdOutRv$", should be set with certain safety margin K_L compared to the minimum expected load resistance R_{Lmin}. A safety margin K_L can be classified and approximated based on the length of the protected line as:

- 0.9 for the protected line longer than 150 km.
- 0.85 for the protected line between 80 and 150 km.
- 0.8 for the protected line shorter than 150 km.

$$R_{L_{\min}} = \left|\overline{Z}_{L_{\min}}\right| \cdot \cos\left(\varphi_{\max}\right) \tag{2.7}$$

$$RLdOutFw, RLdOutRv = K_L \cdot R_{L_{\min}} \tag{2.8}$$

where:

- $R_{L_{min}}$ is a minimum load resistance at maximum load and minimum system voltage.
- $\varphi_{\max}$ is a maximum expected load angle.

For the inner boundary of power swing detection characteristic in forward and reverse directions, "$RLdInFw$" and "$RLdInRv$", these settings are recommended to be set to 80% or less of their outer boundary, as expressed in (2.9). For the remaining parameter settings of the power swing element, details can be found in [66, 67].

$$RLdInFw, RLdInRv = 0.8 \cdot (RLdOutFw, RLdOutRv) \tag{2.9}$$

For the phase selection element (or faulted-phase selection/loop selection), this element is used to ensure that the distance protection function evaluates impedance only on the correct fault loop (phase-phase or phase-earth). This avoids false tripping on non-fault loops, *i.e, "the phase selection function is designed to accurately select the proper fault loop(s) in the distance function dependent on the fault type"* [66].

The phase selection element is classified into different categories, depending on the fault types. The parameters to be set for this element are shown in *italic*, as illustrated in Figures 2.7 to 2.9, for each fault type. The details and recommendations to set such parameters can be found in [66, 67].

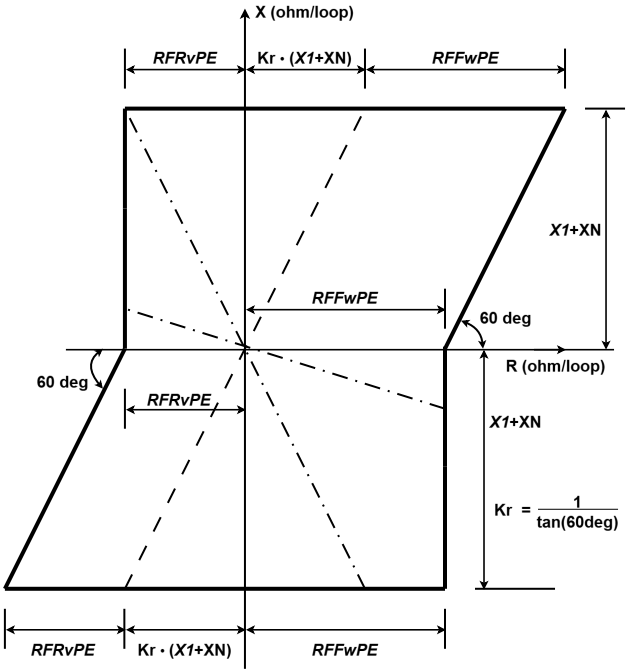

Figure 2.7: Parameters to be set of the phase selection element for phase-to-ground fault with respect to the distance protection function [67].

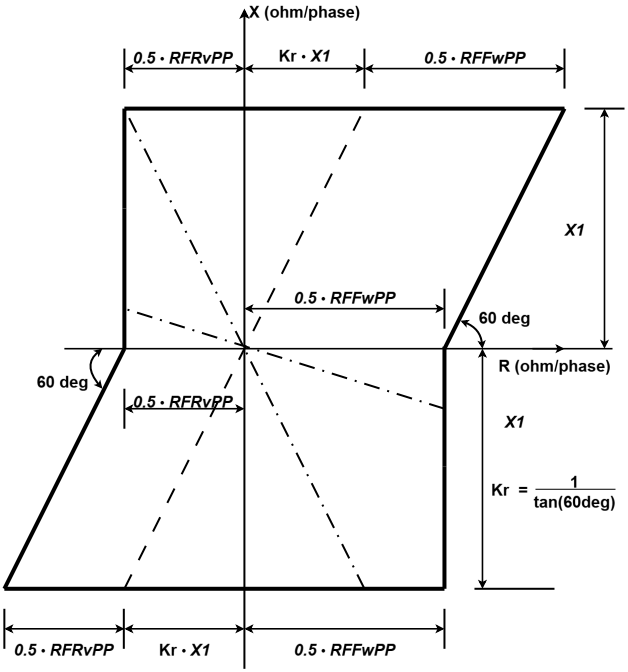

Figure 2.8: Parameters to be set of the phase selection element for phase-to-phase fault with respect to the distance protection function [67].

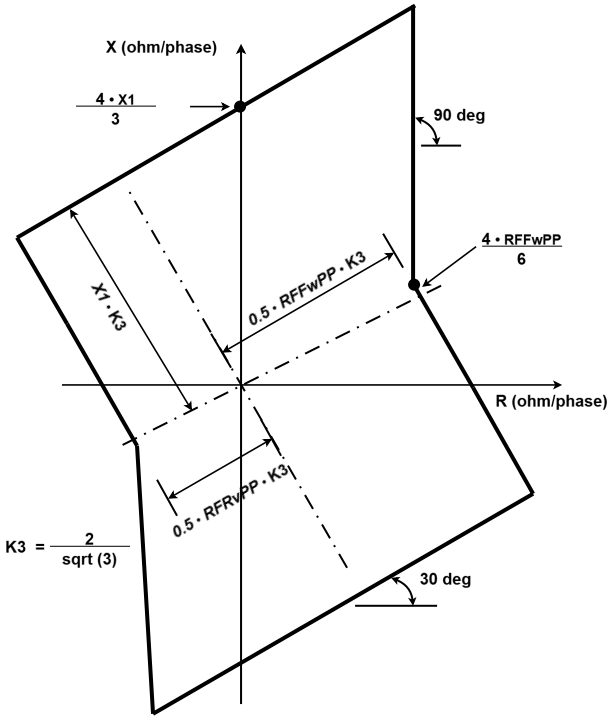

Figure 2.9: Parameters to be set of the phase selection element for three-phase fault with respect to the distance protection function [67].

Within this context, the following drawbacks are observed and listed:

- Path determination remains a manual process, resulting in increased operational time and overhead, particularly in cases of complex network topologies or large-scale networks. This is even worse when many DRs need to be set.
- The DR settings based on the transmission impedance may encounter under- and over-reach problems when DGs connect to the transmission systems. Furthermore, DR settings derived from bus

fault studies may be affected by inaccuracies arising from the infeed effect, especially in Zone 2, which is generally set at the middle of the shortest adjacency section.

- So far, the DR settings approaches have been focused on the zone characteristics and the Zone 2 setting. However, in practice, not only do zone characteristics need to be set, but additional functions also need to be set. Fundamentally, additional functions are set according to the zone characteristic settings and different DR manufactures have different parameter settings. Hence, when DRs from different manufacturers are deployed in the system, the parameters of the additional functions need to be mapped and converted with respect to the specific parameter settings for each DR manufacturer. This also leads to time-consuming and prone to errors.
- Lack of tools/approaches to automatize the entire process of the DR setting.

2.3 Distance relay setting validation

High-quality distance protection studies, *so-called "distance protection coordination study"*, aim to validate the operation of DRs in the systems based on their available settings by performing a fault study. This study has been done to ensure that DRs in the system can coordinate with each other as primary and backup relays to correctly respond to the fault in the system according to the network topologies and relay locations without any miscoordination problems [16, 18, 68, 69]. To achieve the goal of this study, in the initial step, a set of reference DRs must be determined as starting points for the coordination study. For this purpose, in [25] presents algorithms to define a set of references DRs using DFS and back-tracking (BT) techniques. Similarly, [26] and [27] graph theory and graph search methods, particularly DFS, are proposed to determine a set of references DRs.

Following the identification of reference DRs, possible paths must be determined and identified for the fault studies, and this step remains a manual process [17, 58, 69].

In fact, the DRs' coordination study has been performed and validated according to the common practices of each TSO and will be considered and carried out when (but not limited to) [62]:

- Addition of the new DRs or replacement DRs in the system
- Settings and network topologies are changed
- Changes in protection schemes
- Maloperations of the DRs after post-fault analysis, e.g., underreach or overreach issues
- Verify the DR settings and coordination periodically and recurrently in wide area network; a regular practice of TSO

Within this context, the following challenges are observed and listed:

- So far, the DRs coordination validation relies on the fault studies. In doing so, computational resources and time are required, particularly in the case of large-scale power systems.
- Although reference DRs can be automatically determined as starting points, an approach to automatize the entire DRs coordination validation is missing.
- Path determination remains a manual process. This also ultimately results in time-consuming and errors due to the same reasons for DR setting.

2.4 Graph theory and graph search method

In graph theory a graph G is defined as $G(V, E)$ and composed of a set of vertices and a set of edges, each of which connects to two vertices at both ends [19, 20]. In graphs that model power system networks, the vertex represents both a busbar and a node. Meanwhile, the edge represents the transmission line, power transformer, or equipment that connects to two vertices. In fact, an adjacency matrix (A) is used to demonstrate the connection of each edge with the two corresponding vertices to represent the topological connection between elements in the graph and can be determined by equations (2.10) and (2.11).

$$A = [a_{ij}] \in \Re^{nxn} \tag{2.10}$$

$$\mathbf{a}_{ij}, \mathbf{a}_{ji} = \begin{cases} 1, & \text{if } \vartheta_i \text{ connects to } \vartheta_j \\ 0, & \text{otherwise.} \end{cases} \tag{2.11}$$

where, A indicates the set of all n-by-n real matrices, and n indicates the total number of vertices in the graph. ϑ_i and ϑ_j represent vertices connected to both ends of the edge.

To traverse such a matrix A to explore vertices and edges, the DFS and breadth-first search (BFS) methods can be applied to find a target vertex by path analysis from a staring vertex [70, 71, 72]. However, DFS is more efficient than BFS when a full one path must be explored before backtracking, and path analysis is more critical than finding the shortest one [20]. The DFS operates using a last-in, first-out (LIFO) stack, implemented to add (push) and remove (pop) vertices during searching and backtracking. It can be described as follows.

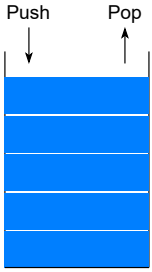

Figure 2.10: Stack structure.

1. Start traversing the matrix A from the starting vertex (ϑ_i)
2. Add ϑ_i to Stack
3. Find the adjacency vertex (ϑ_j)
4. Add ϑ_j to Stack
5. Update $n_s = n_s + 1$ by adding the new vertex to Stack (Push)
6. Repeat steps (3)-(5) until the farthest vertex on the path is explored

7. Start backtracking
8. Update $n_s = n_s - 1$ by removing the latest vertex from Stack (Pop)
9. Find another adjacency vertex ($i = i + 1$)
10. Repeat steps (3)-(8) until all vertices have been visited and explored

The pseudocode of the DFS method is shown in algorithm (1).

Algorithm 1 Pseudocode of the DFS method.

Randomly pick the reference vertex (ϑ_0) // n is the total number of vertices
Identify the starting vertex (ϑ_i) from ϑ_0 and $LastStackBus_i$ is used to indicate the row of ϑ_i on the matrix A
Stack = $[\vartheta_i]$ // n_s is the total number of vertices in the Stack
while $n_s > 0$ and $i < MaxLoop$ **do**
    while $j \leq n$ **do**
        Update $iM = A[LastStackBus_i, j]$ and ϑ_j.visited
        if $iM > 0$ and visited $= 0$ **then**
            ϑ_j.visited $= 1$
            Stack = $[\vartheta_{j^{th}}]$ (Push)
            $n_s \leftarrow n_s + 1$
            Update $LastStackBus_i = j$
        end if
        j=j+1
    end while
    Backtracking process starts
    Pop $[\vartheta_{j^{th}}]$
    $n_s \leftarrow n_s - 1$
    Update $LastStackBus_i$ = the latest vertex in the Stack
    i=i+1
end while

So far, graph theory and graph search approaches have been deployed for various applications in power engineering. For example, [73] presents graph theory to represent the connection among electrical components of the network model, and DFS is used to identify the paths from the

electrical sources to the fault point based on the network graph model in a radial system. Similarly, [74] and [21] present the methods using graph theory and DFS in a radial system to detect an islanding condition for renewable energy resources, and identify the cascading outage paths under different system operating scenarios. Moreover, graph theory and path analysis are presented to design the bus bar protection for any bus bar configuration, considering the status of the switching devices [75].

In the context of relay coordination, [25, 26, 27] propose graph theory and DFS to identify the paths in determining the reference DRs as starting points for DR setting and coordination.

To be more specific details and demonstrate how graph theory and DFS works based on previous studies, the multi-loops graph consisting of 8 vertices: A, B, C, D, E, F, G, and H, and 9 edges: e_{AB}, e_{BC}, e_{BE}, e_{BG}, e_{CD}, e_{CE}, e_{EF}, e_{EG}, and e_{GH}, as shown in Figure 2.4 is used as an example. Before graph traversal by DFS, the adjacency matrix needs to be built to demonstrate the topology connection between vertices in the system; this matrix can be built using equations (2.10) and (2.11). Hence, the topology connection of the multi-loop system, as illustrated in Figure 2.4, in the form of the matrix A, can be expressed as follows.

	A	B	C	D	E	F	G	H
A	0	1	0	0	0	0	0	0
B	1	0	1	0	1	0	1	0
C	0	1	0	1	1	0	0	0
D	0	0	1	0	0	0	0	0
E	0	1	1	0	0	1	1	0
F	0	0	0	0	1	0	0	0
G	0	1	0	0	1	0	0	1
H	0	0	0	0	0	0	1	0

Figure 2.11: Adjacency matrix represents a topology connection of the multi-loops system illustrated in Figure 2.4

Following the creation of the matrix A, in this example, the vertex A is considered as a reference vertex, and the vertex B is considered as

a starting vertex. Hence, the DFS can explore the connectivity among vertices, and paths can be identified, as illustrated in Figure 2.12.

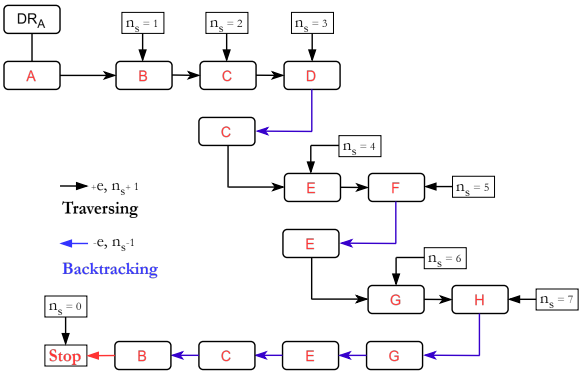

Figure 2.12: Connectivity among vertices and paths identification determined by DFS.

With respect to the context of DR setting and coordination, the following challenges are observed and listed:

- The adjacency matrices of large graphs are often sparse. This can lead to extensive computational burden due to the DFS's search characteristic.
- Conventional graph theory and DFS only gives connectivity, not weighted paths by impedance or protection zones, i.e., this approach, cumulative impedance and length of the transmission line along paths cannot be tracked.
- In general, network models consist of different types of vertices; also, vertices are used in different voltage levels both as substations and connection points (e.g., tap lines and load points). In this regard, Conventional graph theory and DFS cannot classify the type of vertex and cannot identify the voltage level of the vertex. Besides the vertex and voltage level, this approach cannot classify the types of edges in the system, e.g., transmission line, power transformer, etc.

This ultimately may encounter errors during graph traversal and backtracking processes to determine a set of paths for fault studies and setting verifications, especially in the previous studies that rely on the bus representing the substation for fault studies to derive the DR settings.

- Although DFS can keep track of visited vertices to avoid loops, path determination within the protection zones of the DR is incorrect, especially in multi-loop systems. For example, the vertex E must be located within Zone 2 ($n_s = 2$) of the DR_A, but in this case, it is located in Zone 4.

2.5 Methodologies for the performance assessment of distance relay

Following the DR setting and coordination, before deploying DRs in the field, DR testing is required to validate the possible issues that might happen, such as setting misconfiguration and firmware bugs, etc. Besides issues related to configuration and firmware, the performance of the DR needs to be tested and validated to quantitatively assess how well it will perform under different system conditions, as each TSO has different applications in deploying DR in protecting equipment in the transmission system. These test activities are done to prevent the disruptive effects of protection failures ultimately.

To conduct the test, utilities can perform the test based on the methodology defined in the IEC 60255-121:2014 standard [31]. The IEC 60255-121:2014 standard, "Functional requirements for distance protection," is the standard that specifies the minimum sets of requirements for the functional and performance assessment of DR, as well as outlines the test to be conducted [38]. This standard is deployed by different TSOs and aims to assess the performance of the DR that the manufacturers claim their DR performance complies with the IEC 60255-121:2014. Such a test is the so-called acceptance test [39]. In practice, DR is required as a primary protection at the interconnection point when converter-based renewable energy resources or synchronous generators connect to the grid [28, 29]. For this purpose, comprehensive DR testing and validation are essential to ensure the DR can properly respond to the abnormal system conditions under both steady state and transient conditions prior to deployment

to prevent unintended operations of the DR, leading to blackout in the system [30].

To this end, [32] and [33] propose a HiL platform to systematically investigate the occurrence of unexpected DR operations arising from the high penetration of Photovoltaic (PV) farms, as well as to evaluate the influence of a Voltage Source Converter (VSC) topologies on ground faults detection performance. In [34, 35, 36] HiL platform is also proposed to evaluate the zone characteristics and fundamental accuracy of DRs in accordance with the testing methodology prescribed by the standard. Similarly, [37] proposes a comprehensive modeling of ultra-high voltage (UHV) transmission systems to evaluate the performance of DRs under realistic operating conditions. Furthermore, to assess the performance of DRs under transient conditions, [31] outlines a methodology for testing and reporting the relay operating time as a function of fault location, fault type, and the Source Impedance Ratio (SIR), which is the ratio of source impedance to the line impedance. This methodology is implemented using a specific test system, as illustrated in Figure 2.13 [31, 38]. Moreover, the standard recommends performing the test with real-time power system simulations to observe and capture possible unexpected operations under real-world disturbances and different operating conditions.

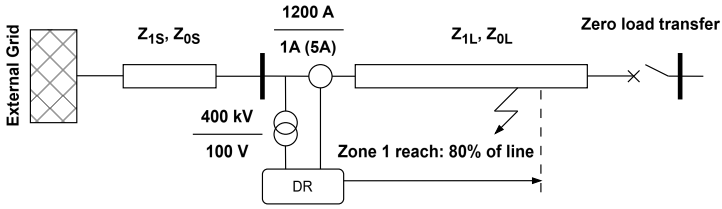

Figure 2.13: Network model to be simulated for evaluating the SIR diagram [31].

Since unexpected operations of DRs are not only caused by fault-related issues in the systems, there are several issues that cause the DR to operate incorrectly, and common causes of unexpected operations of the DR are outlined in Table 2.2 [57].

As reported in Table 2.2, functional or setting-based DR testing is able to verify only individual parameters of the DR, i.e., zone characteristics.

Table 2.2: Summary of transmission line protection challenges causing unexpected operation of DRs.

Fault-related	**Power System-related**	**CT and VT-related**	**Application-related**
1. Infeed effect	1. Load encroachment	1. CT saturation	1. Single pole tripping
2. Fault resistance	2. Unbalance condition	2. Open or shorted CT	2. Short lines
3. Mutual coupling	3. Power swing	3. Loss of potential	3. Long lines
4. Evolving faults	4. Weak sources	4. Transient effect on coupling-capacitor voltage transformer	4. Parallel lines
5. Intercircuit faults	5. Effect of unfaulted phases		5. Three terminal
6. Simultaneous faults			6. Tapped line
7. Close-in zero-voltage faults			
8. SOTF			

Hence, the methodology and special testing techniques, such as HiL, are required to cover complete DR scheme testing.

Furthermore, the DR testing approaches in the literature aligned with OAT and full factorial designs (2^K) [31, 76, 77, 78, 79]. Therefore, in general terms, the performance of the DR can be expressed as a process f, which takes as input a set of factors $\mathbf{U} = \{U_i\}_{i\in\{1,\dots,K\}}$ (e.g., fault location, fault resistance) and outputs a set of measurable response variable(s) $\mathbf{Y}$ (e.g., the operating time of the DR) [2].

$$\mathbf{Y} = f(\mathbf{U}) \tag{2.12}$$

To evaluate the performance of the DR and investigate which factors most significantly affect this, one or more *experiments* (defined as a sequence of N_T tests) are carried out by intentionally changing the factors $\mathbf{U}$ to various levels (e.g., applying faults at different locations with different

fault resistances) and recording the response(s) of interest. Furthermore, to differentiate the OAT and full factorial approaches, consider the model $Y = f(U_1, U_2)$ with two quantitative factors U_1 and U_2, whose variation range is between -1 and $+1$, and the numbers of tests (N_T) is considered $= 8$ tests, this ultimately leads to a squared design space of area equal to 4, as depicted in Figure 2.14.

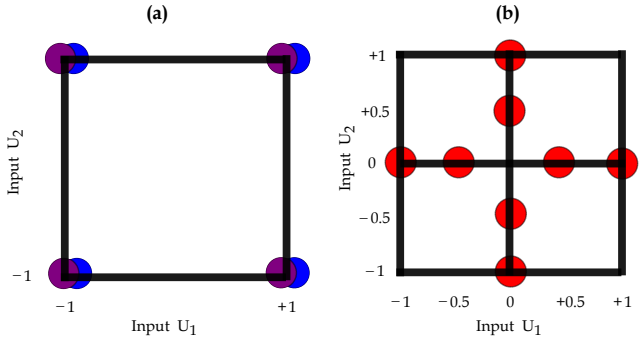

Figure 2.14: (a) Full factorial (2^2). (b) OAT design [© 2024 IEEE].

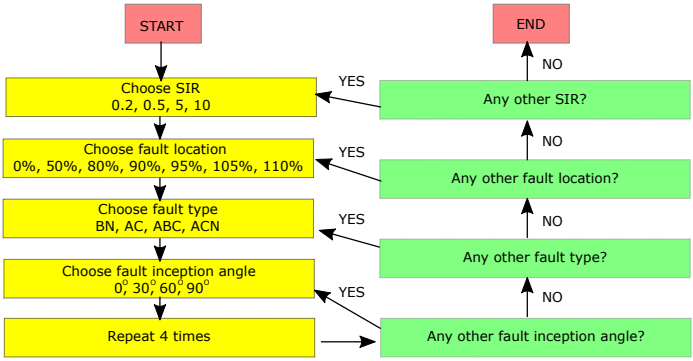

Figure 2.15: Flowchart of the sequence of tests recommended by the IEC 60255-121:2014 standard [© 2024 IEEE].

As depicted in Figure 2.14a, a full factorial approach systematically evaluates the influence of K factors $\{U_1, ..., U_K\}$ on a process response. Each factor's range of variability is discretized into a specific number of values $\{L_1, ..., L_K\}$, referred to as 'levels'. [80]. Experiments are then conducted for every possible combination of these levels—referred to as 'runs'—with each combination potentially replicated R times. On the other hand, Figure 2.14b illustrates a standard OAT approach: beginning at the nominal point $\{0, 0\}$, the factor U_1 is initially varied four times over its variation range while keeping $U_2 = 0$, and afterward, U_2 is varied in the same manner with $U_1 = 0$. Hence, it is noticeable that the OAT approach is not possible to capture two-factor interactions [2].

In fact, manufacturers and utilities perform the DR testing based on the full factorial approach and methodology outlined in [31]. The sequence of test guidelines by the [31] is illustrated in the flowchart of Figure 2.15. As indicated in the flowchart, four factors are considered, consisting of SIR, fault location, fault type, and fault inception angle, as well as the total number of tests conducted is given by $N_T = L_1 \times ... \times L_K \times R$. Hence, to perform the test based on the test methodology defined in [31], each factor is studied at specific levels (4, 7, 4 and 4, respectively) and other factors such as fault resistance, DR settings, remain constant at the nominal values, resulting in $N_T = 1792$ since each fault is injected by 4 times.

With respect to the context of DR testing, the following challenges are observed and listed:

- The available testing methodologies are limited to impedance-based functions and basic accuracy, e.g., zone characteristics and operating times; also, the previous studies are insufficient to test and validate the complete DR functions, including additional functions, e.g., power swing, fault locator, etc. This results in unintended operations of the DR that can possibly happen when the DR is deployed in the system.

- The OAT method is unable to adequately capture the critical interactions among multiple influencing factors.

- The full factorial method significantly leads to a large number of experiments when additional or specific requirements need to be tested and validated, beyond the minimum requirements defined in

the standard and available methodologies. Moreover, this method is incapable of addressing the constraints between factors. This ultimately results in unnecessary experiments, which do not give any advantage to the interpretation of the results and common practice in the testing activity.

2.6 Protection scheme and methodologies for IOP validation

In modern power systems, the digital substations based on the IEC 61850 standard offer significant construction and operational advantages compared to conventional substations [42, 43]. Within such substations, OR plays a crucial role in protecting distributed feeders due to its simplicity, cost-effectiveness, etc., unlike more complex alternatives, such as distance or differential protection [40].

So far, several overcurrent protection schemes within digital substations have been developed. For example, [81] proposes the overcurrent protection scheme using GOOSE to protect cable compartments within switchgear from arc flash with high-speed tripping. Meanwhile, the GOOSE-based overcurrent protection scheme is proposed in [82] to exchange blocking signals between ORs located in upstream and downstream substations to avoid miscoordination issues. Similarly, [55] proposes the GOOSE-based overcurrent protection scheme to identify the fault location in the distribution system. Moreover, there are also studies of the overcurrent protection scheme for adaptive setting after network re-configurations using GOOSE signal to change the setting groups of the ORs [83, 84].

In practice, largely due to economic considerations and the constraints imposed by right-of-way limitations, many distribution systems—particularly in North and South America as well as Southeast Asia—are designed with multiple feeders sharing a common overhead line corridor on the same structure [3]. In such configurations, the inherent characteristics of overhead lines render them susceptible to external disturbances, including those caused by thunderstorms, fallen trees, and vehicular collisions. Besides external disturbances, switching operations within distribution systems—often performed to mitigate congestion by transferring loads between adjacent feeders—can potentially lead to operational disturbances, particularly when the switching actions involve high arc currents. Both the aforementioned external and operational disturbances are the main causes

of multi-feeder faults (MFFs), which are defined as faults affecting more than one feeder simultaneously. Such faults result in a wide area outage in the distribution system, as the OR at the low voltage side of the power transformer operates faster than ORs of the faulted feeders. Consequently, feeders that remain unaffected but are connected to the same transformer are inadvertently de-energized. As such faults are inevitable in distribution systems predominantly comprising overhead lines, it is crucial to investigate and account for them when designing protection schemes for these systems.

In fact, ORs at the bay level within digital substations are used to perform in many protection schemes, such as arc protection, breaker failure, etc. As mentioned before in Chapter 1, it is a common practice to deploy relays from multiple manufacturers within digital substations when replacing obsolete units, particularly in cases where the original manufacturer's relay is no longer available [49, 50, 51]. In such a case, IOP testing is essential before deployment.

For this purpose, [52] outlines the testing requirements and procedures for interoperability testing within the digital substations. Furthermore, [53] and [54] present a case study illustrating IOP testing among relays from different manufacturers and focus on the critical need for IOP testing as part of site commissioning for IEC 61850-based substation automation systems. There are also studies of the performance assessment of the IEC61850-based protection scheme using HiL testing platform [55, 56], as illustrated in Figure 2.16.

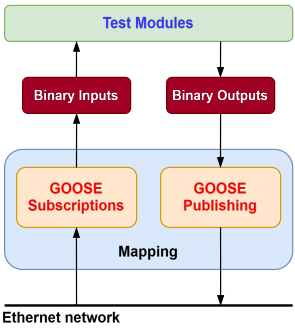

Figure 2.16: IEC 61850 test setup.

In this context, the IOP testing aims to guarantee the IOP of relays from different manufacturers in terms of the operation of the protection schemes when relays are integrated into the system at the bay level. This can help identify possible IOP problems that may arise and result in the incorrect operation of relays. This type of test fosters pre-commission and acceptance tests in assessing the performance of the protection schemes before deployment.

With respect to the context of the overcurrent protection scheme and methodologies for IOP testing, the following challenges are observed and listed:

- The available GOOSE-based overcurrent protection schemes are not able to deal with MFFs, and they are designed to deal with only a single-feeder fault.
- The IOP testing methodologies proposed in previous studies are insufficient for assessing and validating the performance of the protection scheme of multi-vendor bay-level relays under different operating conditions. This may lead to undesired operations of the protection schemes at the bay level, consequently resulting in a wide area blackout in the distribution systems.

3

Algorithms for DR Settings and DRs Coordination Validation

In order to overcome the challenges and drawbacks in the context of DR settings and DRs coordination validation listed in Chapter 2, Sections 2.2, 2.3, and 2.4, this chapter presents:

(i) the topology connection identifier and MDFS algorithm for DR settings and DRs coordination validation to: reduce the computational burden and time due to the sparse matrix by limiting the search space with respect to the protection zones of the DRs; identify the types of the vertices, edges, voltage levels of the vertices during graph traversal and backtracking processes to avoid errors in determining a set of paths within protection zones for fault studies (edges and vertices are stored in the arrays), regardless the network topology; and keep track cumulative length of the transmission lines along paths,

(ii) algorithm to automatize the DR settings based on the proposed MDFS to: automatize the entire process of DR settings, including mapping and converting parameter settings, e.g., zone characteristics, power swing, phase selection, etc, of the DRs from different manufacturers; compute the DR settings, considering both line impedance and the apparent impedance seen by the DR, and reduce errors (under-, over-reach problems) due to the infeed effect of the Zone-2 setting by proposing the fault studies at the boundary instead of simulating at the bus,

(iii) algorithm to automatize the DRs coordination validation based on the proposed MDFS to: verify multiple settings of DRs from different manufacturers to reduce the computational burden and time based on a time-step distance diagram; identify the miscoordination

problems between primary and backup DRs in the system; and automatize the entire process of DRs coordination validation.

The architectures of the proposed algorithms for DR settings and DRs coordination validation presented in this chapter are expressed in Figures 3.1 and 3.2, respectively.

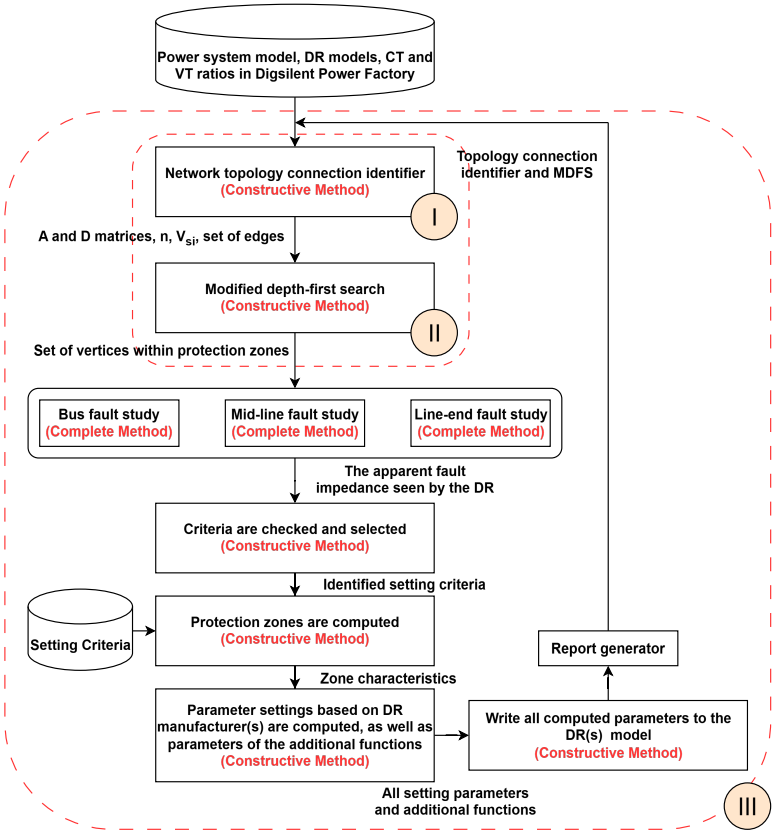

Figure 3.1: Algorithm architecture of the DR settings approach.

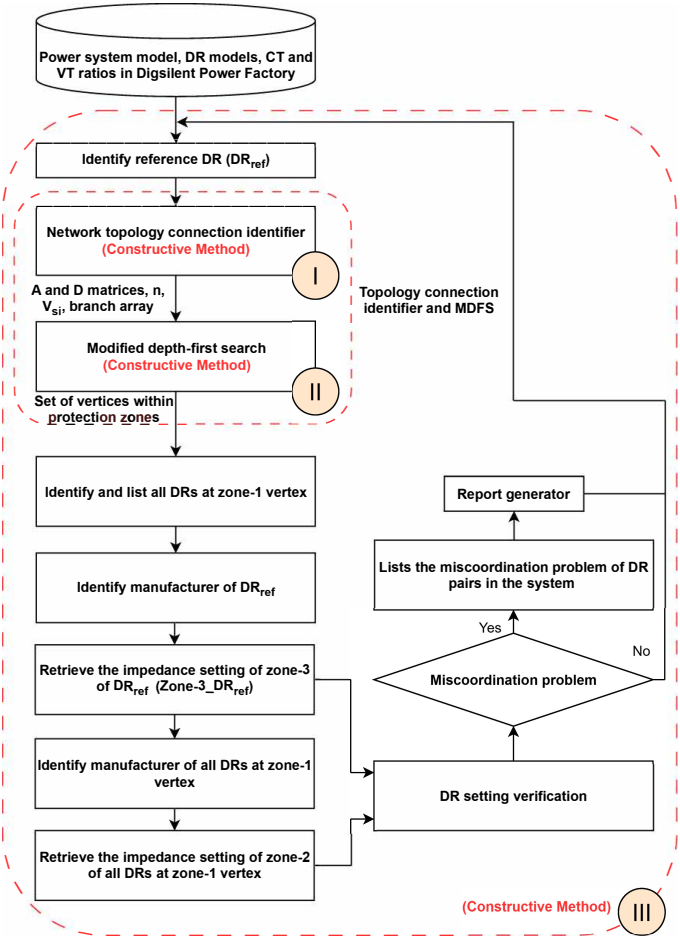

Figure 3.2: Algorithm architecture of the DRs coordination validation.

Each algorithm addresses the identified gaps and the 1^{st} research question. A major part of this chapter is based on the work published in [1], which contributes to the first and second research contributions, as formu-

lated in Chapter 1. The proposed methods are based on object-oriented programming and developed using Digsilent Programming Language (DPL Script) [85], and this chapter can be organized as follows. Section 3.1 elaborates on the topology connection identifier and the graph search method based on the proposed MDFS for path determination within protection zones of DRs. Similarly, algorithms for DR settings and DRs coordination validation are expressed in Sections 3.2 and 3.3, respectively. Finally, in Section 3.4, the proposed algorithms are tested and validated using the TSO's network, and Section 3.5 summarizes the outcomes of the chapter.

3.1 Topology connection identifier and modified depth-first search

This section provides more details on the proposed algorithm related to the topology connection identifier (I) and MDFS (II), as illustrated in Figures 3.1 and 3.2, respectively.

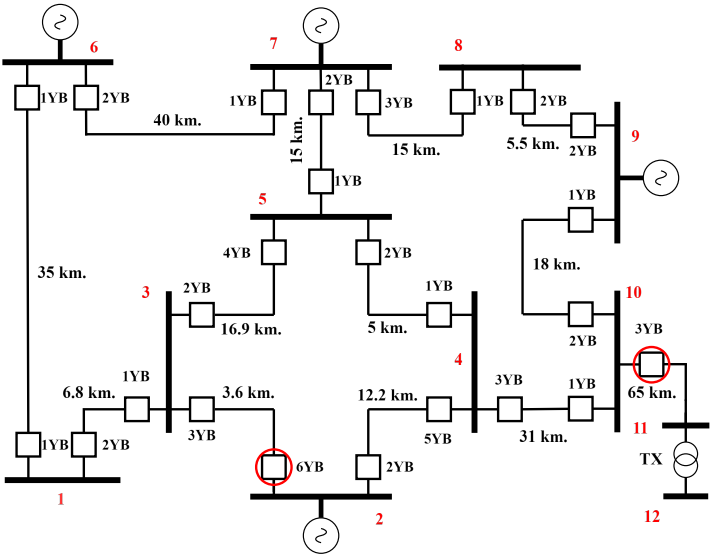

Figure 3.3: Test system.

Topology connection identifier

An algorithm to automatically form the adjacency matrix to demonstrate the connection between elements within the network topology will be thoroughly described, and the DR at the ϑ_2 indicated in Figure 3.3 will be used as a showcase when the proposed method is applied to the test system. This algorithm gives the topology connection of the grid by checking both statuses CBs and the voltage level of the vertices at both ends of the edge to ensure that the connection is correct—e.g., no CB open—, and all vertices are at the same voltage level. The operation of this algorithm can be elaborated as follows:

1. Read ϑ_{si0}, ϑ_{si}, and e_{si0} from the main program. The ϑ_{si0} indicates the vertex at the DR location, ϑ_{si} is the adjacency vertex connected to ϑ_{si0}, and e_{si0} is the starting edge connected to ϑ_{si0} and ϑ_{si}.

2. Read all vertices from the test system and check number of vertices (n).

3. Initialize adjacency (A) and D matrices as well as $Branch$ array. The size of the A and D matrices are nxn and nx2, respectively.

   The D matrix is used to track visited and unvisited vertices during graph traversal (adjacency matrix). This helps avoid cycles in an undirected graph by indicating the status of each vertex within the matrix: a value of 1 represents a visited vertex, while a value of 0 indicates an unvisited vertex. Additionally, the matrix keeps track of the degree of each vertex from vertex ϑ_{si0} by checking row and column indexes of each vertex in the A matrix, which indicates its numbering (degree from vertex ϑ_{si0}).

4. Name columns and rows of the A matrix by sorting the discovered vertex in order of traversal for all i, and $i \in \{1, \ldots, n\}$. During the graph traversal step for naming, if the order/position of the ϑ_{si} on the A and D matrices is discovered at the i^{th} iteration, $D[i^{th}, 1]$ and $D[i^{th}, 2]$ are set $= 1$. Then, the Start-ϑ_{si} variable is used and set equal to i^{th} in order to identify as a starting vertex for traversing the A matrix.

5. Read all edges from the test system and check number of edges (m).

6. Initialize "Row" and "Col" variables and set them equal to 0. Then, start traversing to explore the edge within the array for all j, and $j \in \{1, \ldots, m\}$.

7. Get the connected vertices $(\vartheta_{ai}, \vartheta_{aj})$ at both ends of e_j. Before start traversing the A matrix, the CB statuses at both ends of e_j are checked to see whether CBs are closed. If this condition is true, "$idk1$" index is set = 1; otherwise, 0.

8. Subsequently, start traversing the A matrix for all $i1$, and $i1 \in \{1, \ldots, n\}$ to identify the row label for comparison with ϑ_{ai}. If any element of $A[i1] = \vartheta_{ai}$, set the variable "Row" to $i1^{th}$ and stop the traversal. Next, apply the same process to identify the column label for comparison with ϑ_{aj}. If any element of $A[i2] = \vartheta_{aj}$, set the variable "Col" to $i2^{th}$.

9. Next, ϑ_{ai} and ϑ_{aj} are validated to determine whether both are ϑ_{si0}; if they are not, the "$idk2$" index is set to 1; otherwise, it is set to 0. This index is used to check and set the connection index for ϑ_{si0} in the A matrix to prevent the cycles during the graph traversal. Furthermore, if the voltage level of ϑ_{ai} and ϑ_{aj} differs from the ϑ_{si0}, the "$idk3$" index is set to 0; otherwise, it is set to 1.

10. Set the connection index to indicate the connection between ϑ_{ai} and ϑ_{aj} in the A matrix by checking these conditions:

    - $Row > 0$; to indicate that the target vertex is discovered on a row of the A matrix.
    - $Col > 0$; to indicate that the target vertex is discovered on a column of the A matrix.
    - $idk1 = 1$; to indicate the CB statuses at both ends of e_j.
    - $idk2 = 1$; to indicate that discovered vertices at both ends of e_j are not ϑ_{si0}.
    - $idk3 = 1$; to indicate that the discovered vertices at both ends of e_j have the same voltage level as ϑ_{ai}.

    If all of these conditions are met, check whether e_j is e_{si0}; if this is true, set both $a[Row, Col]$ and $a[Col, Row]$ to 0. On the other

hand, if e_j is not e_{si0}, assign values to $a[Row, Col]$ and $a[Col, Row]$ according to equation (2.11).

In addition, e_j is added to the array $Branch$. The size of the array $Branch$ is determined by $m_{eb} - by - 1$, where m_{eb} indicates the total number of edges in the array $Branch$.

11. Repeat steps 6 to 10 to determine the connection indices on the A matrix of the remaining edges in the graph.

When all the connection indices in the A matrix are established, the matrices A and D, along with the arrays $Branch$ and n, as well as the Start-ϑ_{si} variable, are passed to the MDFS to be used as input information for the process "P1", as illustrated in Figure 3.4. Additionally, all discovered edges are stored in the array $Branch$, except for e_{si0}.

The initialized matrix D and the complete matrix A demonstrate the topological connections of the graph presented in Figure 3.3, corresponding to the DR located at ϑ_2, and can be represented by (3.1). However, although the topology of the power system remains the same, the A and D matrices of each DR are slightly different depending on DR's location.

$$A = \begin{array}{c} \\ 7 \\ 1 \\ 2 \\ 3 \\ 8 \\ 9 \\ 10 \\ 11 \\ 12 \\ 6 \\ 4 \\ 5 \end{array} \begin{array}{c} \begin{array}{cccccccccccc} 7 & 1 & 2 & 3 & 8 & 9 & 10 & 11 & 12 & 6 & 4 & 5 \end{array} \\ \begin{pmatrix} 0 & 0 & 0 & 0 & 1 & 0 & 0 & 0 & 0 & 1 & 0 & 1 \\ 0 & 0 & 0 & 1 & 0 & 0 & 0 & 0 & 0 & 1 & 0 & 0 \\ 0 & 0 & 0 & 0 & 0 & 0 & 0 & 0 & 0 & 0 & 0 & 0 \\ 0 & 1 & 0 & 0 & 0 & 0 & 0 & 0 & 0 & 0 & 0 & 1 \\ 1 & 0 & 0 & 0 & 0 & 1 & 0 & 0 & 0 & 0 & 0 & 0 \\ 0 & 0 & 0 & 0 & 1 & 0 & 1 & 0 & 0 & 0 & 0 & 0 \\ 0 & 0 & 0 & 0 & 0 & 1 & 0 & 1 & 0 & 0 & 1 & 0 \\ 0 & 0 & 0 & 0 & 0 & 0 & 1 & 0 & 1 & 0 & 0 & 0 \\ 0 & 0 & 0 & 0 & 0 & 0 & 0 & 1 & 0 & 0 & 0 & 0 \\ 1 & 1 & 0 & 0 & 0 & 0 & 0 & 0 & 0 & 0 & 0 & 0 \\ 0 & 0 & 0 & 0 & 0 & 0 & 1 & 0 & 0 & 0 & 0 & 1 \\ 1 & 0 & 0 & 1 & 0 & 0 & 0 & 0 & 0 & 0 & 1 & 0 \end{pmatrix} \end{array} \quad D = \begin{array}{c} \\ 7 \\ 1 \\ 2 \\ 3 \\ 8 \\ 9 \\ 10 \\ 11 \\ 12 \\ 6 \\ 4 \\ 5 \end{array} \begin{array}{c} \begin{array}{cc} & \end{array} \\ \begin{pmatrix} 0 & 0 \\ 0 & 0 \\ 0 & 0 \\ 1 & 1 \\ 0 & 0 \\ 0 & 0 \\ 0 & 0 \\ 0 & 0 \\ 0 & 0 \\ 0 & 0 \\ 0 & 0 \\ 0 & 0 \end{pmatrix} \end{array} \quad (3.1)$$

The pseudocode of the topology connection identifier is shown in algorithm (2).

Algorithm 2 Pseudocode of the topology connection identifier.

Read the starting terminal (ϑ_{si0}), starting edge (e_{si0}), and starting vertex (ϑ_{si})
Read all vertices and check number of vertices (n)
Initialize A by (2.10), $D[0]_{nx2}$, $i = 1$ and Start-$\vartheta_{si} = 0$
while $i \leq n$ **do**
    Set Row and Column Label of the matrices $A[\vartheta_{name}, i]$, $A[i, \vartheta_{name}]$, and $D[\vartheta_{name}, i]$
    if $\vartheta_i = \vartheta_{si}$ **then** $D[i, 1] = 1$, $D[i, 2] = 1$, Start-$\vartheta_{si} = i$
    end if
    $i = i + 1$
end while
Read all edges (m); $j = 1$
while $j \leq m$ **do**
    Get the connected vertices ($\vartheta_{ai}, \vartheta_{aj}$) at both ends of e_j
    Set $Row = 0$, $Col = 0$, $i1 = 1$
    while $i1 \leq n$ **do**
        Get Row Label from $A[i1]$
        if $A[i1] = \vartheta_{ai}$ **then** Set $Row = i1$ Break;
        end if
    end while
    $i2 = 1$
    while $i2 \leq n$ **do**
        Get Column Label from $A[i2]$
        if $A[i2] = \vartheta_{aj}$ **then** Set $Col = i2$ Break;
        end if
    end while
    if The CB statuses at the both ends of e_j are closed **then** Set $idk1 = 1$
    end if
    if ϑ_{ai} and $\vartheta_{aj} \neq \vartheta_{si0}$ **then** Set $idk2 = 1$
    end if
    if ϑ_{ai} and ϑ_{aj} are the same voltage level as ϑ_{si0} **then** Set $idk3 = 1$
    end if
    if $Row > 0$ and $Col > 0$ and $idk1 = 1$ and $idk2 = 1$ and $idk3 = 1$ **then**
        if $e_j \neq e_{si}$ **then**
            $a_{Row,Col}$ and $a_{Col,Row}$ are set by (2.11)
        else
            $a_{Row,Col}$ and $a_{Col,Row}$ are set = 0
        end if
    end if
    e_j is added to *Branch* array
end while

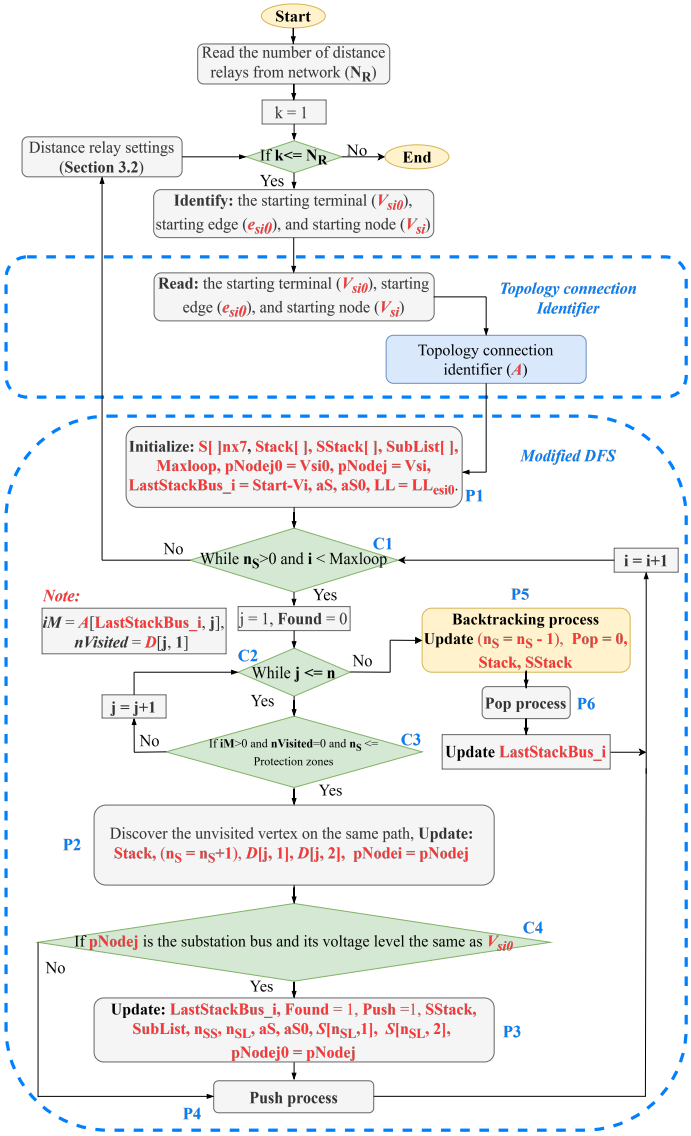

Figure 3.4: Flowchart of the proposed MDFS.

Modified depth-first search

To enhance the performance of the conventional DFS in reducing the computational burden and time by limiting the search space to the protection zones of the DR, provide the correct set of paths for fault studies, regardless of the network topology, and keep track cumulative length of the transmission lines along paths, the MDFS is presented to address these challenges and its operation will be described in the following section.

Once the A matrix is completely formed and the D matrix is initialized, as expressed in 3.1, the traversal of the A matrix for the path determination to determine the edges and vertices within the protection zones of the DR(s) is started according to the flowchart illustrated in Figure 3.4. In doing so, MDFS (an extended version of the DFS algorithm) is built on top of the methodological techniques expressed by an algorithm (1) in Chapter 2, Section 2.4, to avoid errors in determining edges and vertices within protection zones of DR(s). To identify only the vertices and edges within the protection zones and the vertices that represent the substations, the real matrix S is used. This matrix stores the degrees of the vertices and distance in kilometers from the ϑ_{si0}, as well as the types of vertices for any DR during the graph traversal and backtracking processes. Additionally, during the path determination process, a stack structure (LIFO) is deployed to sort the order of the vertices. Since the matrix S is initialized by $n{-}by{-}7$, only the first three columns used to store the discovered vertices, type of vertex, and cumulative length in km are discussed in this section, and the other columns will be discussed in more detail later in Section 3.2. According to Figure 3.4, the proposed MDFS can be described by breaking it down into steps as follows.

1. Process P1: Initialize arrays ($Stack$, $SStack$, $SubList$, aS, and $aS0$), object variables ($pNodej$ and $pNodej0$), integer variables ($Maxloop$ and $LastStackBus_i$), double variable (LL), and the S matrix for the main MDFS. At this process, $pNodej0$ and $pNodej$ are set to store ϑ_{si0} and ϑ_{si}, respectively. Meanwhile, LL is used to store the length of the e_{si0} in kilometers.

   Since the A and D matrices expressed in 3.1 are used as an example, the variables $pNodej0$ is used to store ϑ_2, while $pNodej$ is used to store ϑ_3. Additionally, the value of $LastStackBus_i$ is set to 3 at the beginning of the process.

2. Add the current vertex stored in $pNodej$ to the $Stack$. The size of the $Stack$ is represented by $n_s - by - 1$ and defined by equation 3.2; where n_s is the cardinality of vertices in the $Stack$.

$$n_s = \begin{cases} 1, \text{ If } \vartheta_{si} \text{ is visited} \\ n_s \leftarrow n_s + 1, \text{ If } \vartheta \text{ is the unvisited vertex} \\ n_s \leftarrow n_s - 1, \text{ If Pop} \\ 0, \text{ If all vertices within protection zones} \\ \text{of DR are explored and visited} \end{cases} \tag{3.2}$$

3. Check the current vertex stored in $pNodej$ whether it is a vertex that represents the substation. If true, the $Status$ variable is set to 1 and the vertex is added to the $SStack$ and $SubList$; otherwise, it is set to 2. The cardinality of the vertices in $SStack$ and $SubList$ depends on n_{SS} and n_{SL}, respectively.

   The n_{SS} indicates the degree of each visited vertex from ϑ_{si0}, as expressed in equation 3.3, while the n_{SL} indicates the order of any visited vertex within the protection zones of the DR in the matrix S, as expressed in the equation 3.4.

   In addition, vertices stored in $pNodej0$ and $pNodej$ are added to the arrays $aS0$ [2] and aS [3], respectively. The arrays aS and $aS0$ store pairs of vertices that are connected to each other according to the matrix A. These pairs are sorted in the order they are added to the arrays, and further details on how these arrays are used will be provided in Section 3.2.

4. Update $pNodej0$ to store the latest vertex in aS. Subsequently, $S[n_{SL}, 1]$, $S[n_{SL}, 2]$, and $S[n_{SL}, 3]$ are defined by equations (3.3)-(3.6).

$$n_{SS} = \begin{cases} 1, \text{ If } n_s = 1 \\ n_{SS} \leftarrow n_{SS} + 1, \text{ If Push} \\ n_{SS} \leftarrow n_{SS} - 1, \text{ If Pop} \end{cases} \tag{3.3}$$

$$n_{SL} = \begin{cases} 1, \text{ If } n_s = 1 \\ n_{SL} \leftarrow n_{SL} + 1, \text{ If Push} \end{cases} \tag{3.4}$$

$$LL = \begin{cases} LL_{esi0}, \text{ If } n_s = 1 \\ LL = LL + LL_{e_i}, \text{ If Push} = 1 \\ LL = LL - LL_{e_i}, \text{ If Pop} = 0 \end{cases} \tag{3.5}$$

$$\begin{aligned} S_{n_{SL},1} &= n_{SS} \in \mathbf{S}^{nx7} \\ S_{n_{SL},2} &= Status \in \mathbf{S}^{nx7} \\ S_{n_{SL},3} &= LL \in \mathbf{S}^{nx7} \end{aligned} \tag{3.6}$$

5. Condition C1: Check condition $C1$; if the condition is true, the index $Found$ is set $= 0$, and the control loop variable j is set $= 1$. On the other hand, if condition $C1$ is false, the MDFS subroutine of the current DR will stop the process, and the DR setting process will start.

6. Condition C2: Check condition $C2$; if $j \leq n$, start traversing A and D matrices to obtain the connection index ($iM = A[LastStackBus_i, j]$) and the visited/unvisited status of the current vertex ($nVisited = D[j, 1]$). On the contrary, if $j \geq n$, the backtracking process is executed.

7. Condition C3: Check condition $C3$; if $iM = 1$, $nVisited = 0$, and $n_S \leq$ protection zones of DR, the adjacency vertex on the same path is discovered. On the other hand, if the condition $C3$ is false, the process returns to condition $C2$ with the updated j ($j = j + 1$).

8. Process P2: The n_S is updated by equation 3.2. Additionally, $D[j, 1]$ and $D[j, 2]$ are updated and set by equation 3.7- 3.9. For example, at $j = 1$, ϑ_1 is added to $Stack$ and the vertices in the $Stack$ are expressed as $[\,^1_3]$. At this point, $pNodej$ is updated to store the latest vertex in the $Stack$, while $pNodei$ is updated to store the vertex that has the order in the $Stack$ next to the latest vertex.

$$\begin{aligned} &D[j, 1] = d_j \in \mathbf{D}^{nx2} \\ &D[j, 2] = n_s \in \mathbf{D}^{nx2} \\ &d_j = \vartheta_j; j = 1, ..., n \\ &\text{where } n \leq \text{Protection zones of } DR \end{aligned} \tag{3.7}$$

$$D[j,1] = \begin{cases} 1, \text{ if } d_j \text{ is unvisited vertex} \\ 0, \text{ if } d_j = \vartheta_{si0} \text{ and out of protection zones} \end{cases} \tag{3.8}$$

$$D[j,2] = \begin{cases} n_s \leftarrow n_s + 1, \text{ If Push} \\ 0, \text{ if } d_j = \vartheta_{si0} \text{ and out of protection zones} \end{cases} \tag{3.9}$$

9. Condition C4: Check the current vertex stored in $pNodej$ whether it is the vertex that represents the substation; also, the voltage level of $pNodej$ must be the same level as ϑ_{si0}. If true, the $Status$ variable is set to 1 and the vertex is added to the $SStack$ and $SubList$ by equation 3.3 and 3.4. Otherwise, jump to the push process.

10. Process P3: Update $LastStackBus_i$ and set it equal to j^{th}. Also, the $Found$ and $Push$ indices are set to 1.

    Similarly, n_{SS} and n_{SL} are updated. Subsequently, the values of $S[n_{SL}, 1]$ and $S[n_{SL}, 2]$ are also set and updated. In addition, vertices stored in $pNodej0$ and $pNodej$ are added to $aS0$ and aS, respectively. At this point, arrays $aS0$ and aS can be expressed: $aS0 = [\begin{smallmatrix} 3 \\ 2 \end{smallmatrix}]$, whereas $aS = [\begin{smallmatrix} 1 \\ 3 \end{smallmatrix}]$. In the final step of the process P3, $pNodej0$ is updated and set to store the current vertex stored in $pNodej$.

11. Process P4: Since the push process is a subroutine, this process is then executed by retrieving the input information from the MDFS subroutine, such as $pNodei$, $pNodej$, LL, $Branch$, $Push$ variable, etc.

    Next, due to the fact that the edge (denoted as e) represents the element, which is connected to vertices stored in $pNodei$ and $pNodej$. Hence, it can be identified by examining the edges within $Branch$ for all ii and $ii = 1....mk$; where mk represents the total number of edges within $Branch$. During this process, if any e_{ii}^{th} is discovered as a transmission line and both vertices stored in $pNodei$ and $pNodej$ are part of e_{ii}^{th}, then the total length LL is updated. This update is achieved by adding the length of the respective edge LL_{e_i}, as outlined in equation (3.5). Then, the updated value of LL is forwarded to the main MDFS, allowing the process to proceed to the next step by incrementing the index $i = i + 1$.

12. Proceed to execute steps 5 through 11 for the remaining unvisited vertices and edges within the protection zones that have not yet been explored. For example, $2 \rightarrow 3_{n_s=1} \rightarrow 1_{n_s=2} \rightarrow 6_{n_s=3} \rightarrow 1_{n_s=2}$. In this scenario, the proposed algorithm stops its searching process at vertex ϑ_6, as ϑ_6 represents the final vertex on this path within the protection zones of DR. Subsequently, the backtracking process (P5) is executed.

13. Process P5: The backtracking process is executed when the condition $C2$ is false. At this point, the variables $Found$ and Pop are initialized to 0, and $pNodei$ is updated to store the latest vertex stored by $pNodej$. Following this update, the current vertex stored in $pNodej$ is taken out of the $Stack$, and n_s is updated accordingly. Furthermore, the current vertex stored in $pNodej$ is checked whether it is the vertex that represents substation. If true, the vertex is taken out of the $SStack$, and n_{ss} is updated.

14. Search for the latest vertex in the array $Stack$. When the latest vertex is discovered, $pNodej$ is updated to store the latest vertex.

15. Process P6: Input information is obtained from the main MDFS subroutine: Pop, LL, $pNodei$, $pNodej$, and $Branch$; subsequently, the pop process is executed. The edge e, which connects to the vertices stored in $pNodei$ and $pNodej$, is identified by exploring the edges within $Branch$ for all values of ii from 1 to mk. If any e_{ii}^{th} is discovered and identified as a transmission line and both vertices stored in $pNodei$ and $pNodej$ are part of it, then the total length LL is updated by decrementing its value. This adjustment is made by subtracting the length of the corresponding edge $LL_{e_{ii}}$, as defined in equation (3.5).

16. Step back to the previous vertex before the backtracking process to find any other possible paths from its position (if unvisited vertices and edges within the protection zones of DR have not yet been explored). To do this, the row index of the previous vertex on A and D matrices must be identified by updating $LastStackBus_i$. The $LastStackBus_i$ is updated and identified by exploring the vertices in the matrix D for all jj and checking with the current vertex stored in $pNodej$, where jj ranges from 1 to n. During this process, if any

vertex is discovered as the currrent vertex stored in $pNodej$, then the $LastStackBus_i$ is set and updated equal to jj^{th}.

17. After steps 16, start traversing the A matrix by taking an alternative path from the current vertex stored in $pNodej$ to discover other unvisited vertices by stepping back to step 5 (Condition C1).

The proposed MDFS will stop the process when all edges and vertices within the DR's protection zones are identified and determined. Consequently, the paths during the graph traversal based on the exemplary A and D matrices expressed in (3.1) of the DR at the vertex ϑ_2 (6YB) obtained through the proposed MDFS are $2 \rightarrow 3_{n_s=1} \rightarrow 1_{n_s=2} \rightarrow 6_{n_s=3} \rightarrow 1_{n_s=2} \rightarrow 3_{n_s=1} \rightarrow 5_{n_s=2} \rightarrow 4_{n_s=3} \rightarrow 5_{n_s=2} \rightarrow 7_{n_s=3} \rightarrow 5_{n_s=2} \rightarrow 3_{n_s=1} \rightarrow 2_{n_s=0}$. The identified paths for the setting and coordination processes are: i) $3 \rightarrow 1 \rightarrow 6$, ii) $3 \rightarrow 5 \rightarrow 4$, and iii) $3 \rightarrow 5 \rightarrow 7$. Furthermore, S and D matrices, along with the aS and $aS0$ arrays, are represented by (3.10) and (3.11), respectively.

$$S = \begin{bmatrix} 1^{(3)} & 1 & 3.6 \\ 2^{(1)} & 1 & 10.4 \\ 3^{(6)} & 1 & 45.4 \\ 2^{(5)} & 1 & 20.5 \\ 3^{(4)} & 1 & 25.5 \\ 3^{(7)} & 1 & 35.5 \end{bmatrix} \quad D = \begin{bmatrix} 1^{(7)} & 3 \\ 1^{(1)} & 2 \\ 0^{(2)} & 0 \\ 1^{(3)} & 1 \\ 0^{(8)} & 0 \\ 0^{(9)} & 0 \\ 0^{(10)} & 0 \\ 0^{(11)} & 0 \\ 0^{(12)} & 0 \\ 1^{(6)} & 3 \\ 1^{(4)} & 3 \\ 1^{(5)} & 2 \end{bmatrix} \tag{3.10}$$

$$aS0 = \begin{bmatrix} 5 \\ 5 \\ 3 \\ 1 \\ 3 \\ 2 \end{bmatrix} \quad aS = \begin{bmatrix} 7 \\ 4 \\ 5 \\ 6 \\ 1 \\ 3 \end{bmatrix} \tag{3.11}$$

The pseudocode of the proposed MDFS is shown in algorithms (3)-(5).

Algorithm 3 Pseudocode of the MDFS.

Read A and D matrices, $Start - \vartheta_i$, n, and set of edges (Branch array) from the topology connection identifier
Initialize associated variables and arrays, as indicated in Fig. 3.4, process $P1$
Count the number of vertices within Stack (n_s)
Set $LL = LLe_{si0}$
if $pNodej$ is the substation bus; $status = 1$ **then**
    Add the current vertex stored in $pNodej$ to $SStack$ and $SubList$ arrays
    Update n_{SS} and n_{SL} by equations (3.3) and (3.4)
    Update the matrix $S[n_{SL}, 1]$, $S[n_{SL}, 2]$, and $S[n_{SL}, 3]$ by (3.6)
    Set the row label of the matrix $S[n_{SL}]$ equal to the name of the current vertex stored in $pNodej$
    Add the current vertices stored in $pNodej0$ and $pNodej$ to $aS0$ and aS arrays
    Update $pNodej0$ to store the current vertex within $pNodej$
end if
while $n_s > 0$ and $i < MaxLoop$ **do**
    Set $Found = 0$ and $j = 1$
    while $j \leq n$ **do**
        Update $iM = A[LastStackBus_i, j]$, $nVisited = D[j, 1]$, and $D[j, 2]$ by equation (3.7)
        if $iM > 0$ and $nVisited = 0$ and $n_s \leq$ protection zones **then**
            Set $pNodejChk$ to store the vertex at $D[j]$
            Set $pNodei$ to store the current vertex within $pNodej$ and update $pNodej$ to store the current vertex within $pNodejChk$
            Add the current vertex stored in $pNodej$ to $Stack$
            Update n_S by equation (3.2)
            if $pNodej$ is the substation bus and its voltage level is the same as ϑ_{si0} **then**
                Update $LastStackBus_i = j$ and $Found = 1$
                Add the current vertex stored in $pNodej$ to $SStack$ and $SubList$ arrays
                Update n_{SS} and n_{SL} by equations (3.3) and (3.4)
                Add the current vertices stored in $pNodej0$ and $pNodej$ to $aS0$ and aS arrays
                Update $pNodej0$ to store the current vertex within $pNodej$
            end if
            Go to algorithm (4) (Push process)
            from algorithm (4)
            Update the matrix $S[n_{SL}, 3]$ by (3.6)
        end if
        $j = j + 1$
    end while
    Go to algorithm (5) (Pop process)
    From algorithm (5)
    Update the matrix $S[n_{SL}, 3]$ by (3.6)
    $i = i + 1$
end while

Algorithm 4 Pseudocode of Push or pop process.

Read $pNodei$, $pNodej$, $Branch$, $SStack$, $SubList$, LLe_{si0}, mk from the main MDFS
Set ii=1
while $ii \leq mk$ **do**
    if e_{ii} is the transmission line object class **then**
        Get ϑ_{ai} and ϑ_{aj}
        if ϑ_{ai} and ϑ_{aj} connected to e_{ii} **then**
            Set $pBranchNodei = \vartheta_{ai}$; $pBranchNodej = \vartheta_{aj}$
            if $pBranchNodei = pNodei$ **then**
                if $Push = 1$ **then**
                    $LL = LL + LLe_{ii}$; Break
                else($Pop = 0$)
                    $LL = LL$ - LLe_{ii}; Break
                end if
            end if
            if $pBranchNodej = pNodei$ **then**
                if $Push = 1$ **then**
                    $LL = LL + LLe_{ii}$; Break
                else($Pop = 0$)
                    $LL = LL$ - LLe_{ii}; Break
                end if
            end if
        end if
    end if
    $ii = ii + 1$
end while

Algorithm 5 Backtracking process.

1: $Found = 0$, update $pNodei$ to store the current vertex within $pNodej$
2: Remove the current vertex within $pNodej$ from $Stack$, also from $SStack$ if $pNodej$ is the vertex that represents the substation vertex
3: Update n_S and n_{SS} by equations (3.3) and (3.2), respectively
4: Check n_{aS}; the cardinality of aS and set $S0_i = 1$
5: **while** $S0_i \leq n_{aS}$ **do**
6: $pNodeChk = aS[S0_i, 1]$
7: **if** $pNodeChk = pNodej$ **then**
8: $pNodej0 = aS0[S0_i, 1]$; Break
9: **end if**
10: $S0_i = S0_i + 1$
11: **end while**
12: Update $pNodej$ to store the current vertex in $pNodej0$ (the latest in $Stack$)
13: Go to algorithm (4) (Pop process)
14: from algorithm (4)
15: Search for the row position of the $pNodej$ on the D matrix for all jj where $jj \in \{1, \ldots, n\}$, if it is discovered, set $LastStackBus_i = jj$

3.2 Automatized DR settings algorithm

In order to minimize effort and time while improving the efficiency of the DR setting process, the theoretical background and setting criteria outlined in Chapter 2, Section 2.2, are used to develop an automatized DR settings algorithm based on established paths and vertices, as detailed in Section 3.1, especially in (3.10) and (3.11) will be used as an exemplary of the DR settings for the entire process.

This algorithm gives the zone settings for both mho and quadrilateral characteristics for four zones, as well as parameters' settings of the additional functions, e.g., power swing, phase selection, etc., based on the recommendations from manufacturers and TSO's requirements [61, 64, 67, 86].

To illustrate the operation of the proposed algorithm according to the flow diagram presented in Figure 3.5, the operation of the algorithm can be detailed through the following steps.

1. Process P1: Read the number of DRs as input information from the network topology or the number of DRs to be configured and set, determined by users.

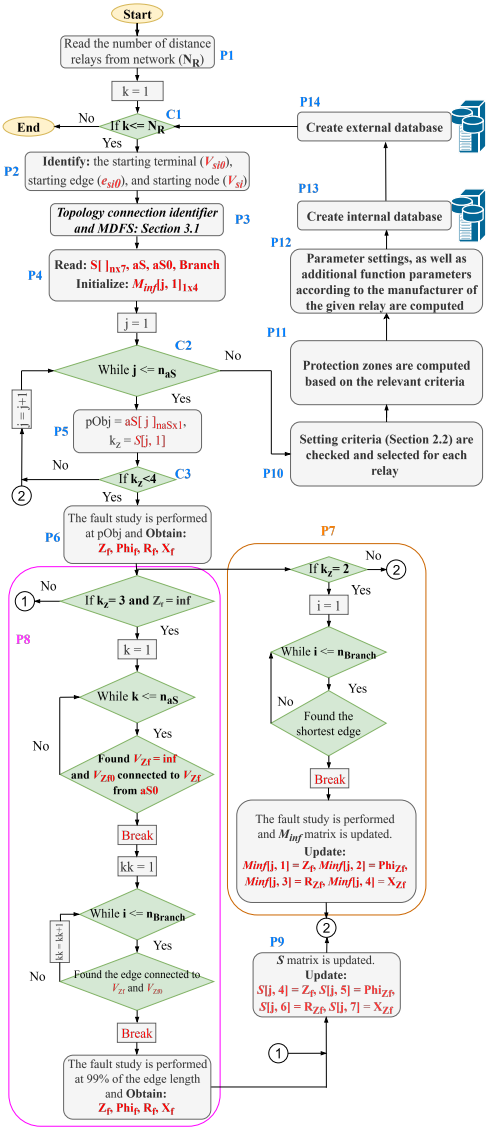

Figure 3.5: Flowchart of the proposed automatized DR settings.

2. Condition C1: Check the condition of the number of DRs to be configured and set. If the condition is verified as true, the process P2 will be executed. Conversely, if the condition is determined to be false, the DR settings process will stop.

3. Process P2: Determine the ϑ_{si0}, ϑ_{si}, and e_{si0} for each DR. After identifying these parameters, forward the values of ϑ_{si0}, ϑ_{si}, and e_{si0} to the "Network topology connection identifier" and MDFS subroutines, as elaborated in Section 3.1.

4. Process P3: Compute the S matrix and provide aS, $aS0$, and $Branch$ arrays based on the proposed methods described in Section 3.1.

5. Process P4: This process is then executed by retrieving the input information from the process P3. Moreover, the $Minf_{1x4}$ matrix is initialized, along with the initial conditions of the fault simulation study according to the IEC 60909 standard.

6. Condition C2: Check condition $C2$. If the condition is verified as false ($n_{as} > j$)—where n_{aS} represents the total number of vertices within aS array—the setting criteria corresponding the location of the current DR_k in the network is checked and executed further steps, as indicated in the process P10.

   This means the fault simulation study for all vertices within the aS array and some specific edges were performed, as well as the fault simulation study parameters, e.g, apparent fault impedance (Z_f) seen by the DR_k, fault angle (θ_f), resistance of Z_f (R_f), and reactance of Z_f (X_f), were recorded and stored in the matrix S for columns 4 to 7, respectively. More details on how to record and store the fault simulation study parameters in the matrix S will be explained later in the next steps.

   On the other hand, If the condition is verified as true, start traversing the aS array for all j and $j = 1....n_{aS}$.

7. Process P5: Obtain the vertex within the protection zones of the DR_k by traversing the S matrix and the aS array. For this purpose, the k_z variable is used to store the discovered vertex from the S matrix—indicating the vertex located within the protection zones of

the DR_k—and set equal to $S[j, 1]$, while $pObj$ is used to store the discovered vertex from the aS array and set equal to $aS[j]$.

8. Condition C3: Check condition C3 whether the discovered vertex is located within the protection zones of the DR_k. If the condition is true, the fault simulation study (bus fault simulation) will be executed. Conversely, if the condition is false, the next vertex will be examined by proceeding to step 6 by updating the index $j = j + 1$.

9. Process P6: The fault simulation study is executed on the vertex stored in $pObj$, i.e., by the order of the discovered vertex within aS array. Subsequently, Z_f, θ_f, R_f, and X_f are recorded.

   The possible infeed effect from the generation units in the system is taken into account if it occurs at any vertex for each fault simulation study; this effect is compensated by equations (2.2) and (2.3).

10. Process P7: To mitigate the infeed effect in mesh/multi-loop networks for $k_z = 2$, the fault simulation study is performed at the midpoint of the shortest edge (shortest line length in section 2). To do so, the shortest edge connected to vertices with degrees of 1 and 2 in the S matrix is identified by exploring the $Branch$ array, for all i and $i = 1....n_{Branch}$; where n_{Branch} represents the total number of edges within $Branch$. As a result, the fault impedance seen by the DR_k is determined. Subsequently, the variables Z_f, θ_f, R_f, and X_f are recorded and stored in the $Minf$ matrix. After this process, go to step 6 (Condition C2) by updating the index $j = j + 1$.

11. Process P8: Meanwhile, for $k_z = 3$, if Z_f seen by the DR is infinite for any vertex ($\vartheta_{Zf}^{k_z}$), the position index of ϑ_{Zf} in the aS array must be identified. To do so, the aS array is explored, for all k and $k = 1....n_{aS}$. When position index of ϑ_{Zf} is discovered, subsequently, the position index of the adjacency vertex (ϑ_{Zf0}) of ϑ_{Zf} can be determined by exploring the $aS0$ array for all k. Specifically, the position index of ϑ_{Zf0} in the $aS0$ array can be identified with the same position index of ϑ_{Zf}.

    Next, search for the edge connected to ϑ_{Zf0} and ϑ_{Zf} by exploring the $Branch$ array, for all kk and $kk = 1....n_{Branch}$. When the edge connected to ϑ_{Zf0} and ϑ_{Zf} is found, the fault simulation study is

performed at 99% of the edge length. Then, Z_f, θ_f, R_f, and X_f are recorded and forwarded to the process P9.

On the other hand, if $k_z = 3$ and Z_f seen by the DR is not an infinite value, the process P8 is skipped and process P9 will start.

12. Process P9: The fault simulation information at j^{th} is updated in the S matrix: $S[j,4] = Z_f$, $S[j,5] = \theta_f$, $S[j,6] = R_f$, and $S[j,7] = X_f$, respectively. Then, the next vertex will be examined by proceeding to step 6 (Condition C2) and updating the index $j = j + 1$.

13. Repeat steps 6 to 12 for the remaining vertices within the aS array and some specific edges within the protection zones of the DR_k.

14. Once the fault simulation study for all vertices within the array aS and some specific edges at $k_z = 2$ and $k_z = 3$ were performed, the complete matrices S and $Minf$ are forwarded to the process P10 to proceed with the next steps. As mentioned above, determined paths and vertices, as detailed in (3.10) and (3.11), are still used as examples for the sake of simplification. Hence, the complete matrices S and $Minf$ of the DR_k at the vertex ϑ_2, according to the test system, can be expressed by (3.12) and (3.13).

$$S = \begin{array}{c} \\ 3 \\ 1 \\ 6 \\ 5 \\ 4 \\ 7 \end{array} \begin{array}{c} \begin{array}{ccccccc} De & T & LL & Z_f & \theta_f & R_f & X_f \end{array} \\ \begin{pmatrix} 1 & 1 & 3.6 & 0.97 & 80.88 & 0.15 & 0.96 \\ 2 & 1 & 10.4 & 3.34 & 81.23 & 0.51 & 3.30 \\ 3 & 1 & 45.4 & 13.85 & 81.18 & 2.12 & 13.68 \\ 2 & 1 & 20.5 & 7.10 & 81.83 & 1.00 & 7.03 \\ 3 & 1 & 25.5 & 17.26 & 85.00 & 1.50 & 17.19 \\ 3 & 1 & 35.5 & 13.53 & 81.18 & 2.07 & 13.37 \end{pmatrix} \end{array} \tag{3.12}$$

$$Minf = \begin{array}{c} \\ 3-1 \end{array} \begin{array}{c} \begin{array}{cccc} Z_f & \theta_f & R_f & X_f \end{array} \\ \begin{bmatrix} 2.16 & 81.15 & 0.33 & 2.13 \end{bmatrix} \end{array} \tag{3.13}$$

Where De is the vertex's degree from the ϑ_{si0}, and T is the type of the vertex that represents the substation within the protection zones of the DR.

15. Process P10: Following the complete fault simulation study in step 14, this process obtains the complete S and $Minf$ matrices, aS, $aS0$, and $Branch$ arrays as an input information. Hence, the conditions will be checked and selected based on:

    Condition I

    - No DG connects to the remote substation.
    - The magnitude of the current passing through the DR_k and the adjacency line to the fault point is the same.

    Condition II

    - DG(s) connect to the remote substation.
    - The magnitude of the fault current passing through the DR_k differs from the current that passes through the adjacency line to the fault point.

    Condition III

    - No DG connects to the remote substation.
    - Only the transformer bay connects to the remote substation (no adjacency lines connect to the remote substation).

16. Process P11: Once the criteria are checked and selected, the zone settings of the DR_k are computed by algorithm (6) using information expressed in (3.12) and (3.13).

Algorithm 6 Criteria I, II, and III

if Criteria I and II **then**
Initialization for I and II
Zone 1:
1) Discover vertex, which has $De = 1$ and $T = 1$, by exploring the S matrix for all i, $i \in \{1, \ldots, n\}$
2) Z_1 is computed
Zone 2:
3) Discover the shortest vertex in zone 2 ($De = 2$)
4) Remove the Z_f between ϑ_{si0} and vertex, which has $De = 1$ to obtain only Z_f between vertices, which have $De = 1$ and 2 (shortest)
5) Z_2 is computed and $Z_{M_{inf}}$ is obtained from the M_{inf} matrix
6) $Z_{M_{inf}}$ is selected for the Z_2 setting
Zone 3:
7) Discover the longest vertex in zone 2 ($De = 2$)
8) Remove the Z_f between ϑ_{si0} and the longest vertex in zone 2 to obtain only Z_f between vertices, which have $De = 1$ and 2 (longest)
9) Z_{3a} is computed
10) Discover the longest vertex in zone 3 ($De = 3$)
11) Remove the Z_f between ϑ_{si0} and the longest vertex in zone 3 to obtain only Z_f between vertices, which have $De = 2$ and 3 (longest)
12) Z_{3b} is computed
13) $Max(Z_{3a}, Z_{3b})$ is selected; however, in the case of weak infeed, the forward direction is selected (positive value)
14) Z_4 is computed
else Criteria III
Zone 1:
1) Discover vertex, which has $De = 1$ and $T = 2$, by exploring the S matrix for all i, $i \in \{1, \ldots, n\}$
2) Z_1 is computed
Zone 2 and 3:
3) Remove the Z_f between ϑ_{si0} and vertex, which has $De = 1$ to obtain only Z_f between vertices, which have $De = 1$ and 2
4) Z_2 and Z_3 are computed
end if

However, the different locations of DRs in the system mean that the matrices S and $Minf$ differ depending on the paths and vertices established in Section 3.1. Furthermore, to express the S matrix of the DR based on criteria III, the DR at the vertex ϑ_{10} shown in the test system is taken as an example, and the complete S matrix based on the proposed method is shown in (3.14).

$$S = \begin{array}{c} \\ 11 \\ 12 \end{array} \begin{array}{c} \begin{array}{ccccccc} De & T & LL & Z_f & \theta_f & R_f & X_f \end{array} \\ \begin{pmatrix} 1 & 1 & 65 & 17.63 & 80.88 & 2.79 & 17.40 \\ 2 & 2 & 65 & 43.56 & 86.32 & 2.79 & 43.47 \end{pmatrix} \end{array} \tag{3.14}$$

17. Process P12: After zone characteristic settings are computed, the parameter mapping subroutine is initialized by reading information from process P11, such as zone characteristic settings, the DR manufacturer, DR model, as well as the CT and VT ratios.

    Next, the relay manufacturer and model of the DR_k are checked. If both information are detected, the computing and mapping process will start. Parameter settings are calculated and mapped according to the specifications recommended by manufacturers and TSOs, including additional functions [61, 64, 67, 86].

18. Process 13 and 14: After the parameter setting and mapping of the DR_k are computed, a protection database in PowerFactory and an external database are created. This information will be utilized for further analysis if any unexpected operations occur, i.e., it will aim to validate the coordination among DRs in the system periodically—a regular practice of TSO, or when the network topology is changed.

19. Then, the next DR ($k = k + 1$) is examined by repeating steps 2 to 18 (Go to condition $C1$).

The main setting routine will stop when all DRs within the N_R are discovered and configured. The pseudocode of an automatized DR settings is shown in algorithm (7).

Algorithm 7 Pseudocode of an automatized DR settings.

Read number of DR(s), N_R, determined by users or from the network model
Set k=1
while $k \leq N_R$ **do**
    Identify ϑ_{si0}, ϑ_{si}, e_{si0}
    Determine paths wtihin the protection zones of the DR(s):
    Go to algorithms (2) and (3)
    from algorithms (2) and (3) // Read $S[]nx7, aS, aS0, Branch$
    Initialize $Minf[j,1]_{1x4}$
    Set j=1 and check numbers of substation buses within aS (n_{aS})
    while $j \leq n_{aS}$ **do**
        Get the bus object from aS ($pObj = aS[j]$)
        Get the zone index from the S matrix ($k_z = S[j,1]$)
        Simulate the fault at $pObj$; then, Z_f, Phi_f, R_f, and X_f seen by the DR are obtained
        if $k_z = 2$ **then**
            Find the shortest line in zone 2
            Simulate the fault at 50% of the line length
            Update $Minf[j,1] = Z_f$, $Minf[j,2] = Phi_f$, $Minf[j,3] = R_f$, $Minf[j,4] = X_f$
        end if
        if $k_z = 3$ and $Z_f = inf$ **then**
            Simulate the fault at 99% of the line length, instead of simulating at the bus; then, Z_f, Phi_f, R_f, and X_f seen by the DR are obtained
        end if
        Update $S[j,4] = Z_f$, $S[j,5] = Phi_f$, $S[j,6] = R_f$, $S[j,7] = X_f$
        $j = j + 1$
    end while
    Setting criteria are checked and selected with respect to DR's location
    Go to algorithm (6)
    from algorithm (6) //Protection zones were computed
    Parameter settings, as well as additional function parameters according to the manufacturer are computed and mapped
    Write all parameter settings to the DR model
    Create summary report
    $k = k + 1$
end while

3.3 Automatized DRs coordination validation algorithm

In this section, details of the algorithm for DRs coordination validation will be discussed. Due to the various criteria and the individual standards set by each TSO for the DR settings, miscoordination may occur between

primary and backup relays. The miscoordination among DRs in the system can be caused by different lengths of transmission lines and the infeed effect at the remote substation. Hence, as outlined in Chapter 2, Section 2.3, coordination validation is required after updating the DR settings or after being changed in the network topology to guarantee the selectivity and reliability of the operation of DRs in the system. For this purpose, an automatized validation algorithm for DRs coordination is introduced to automatize DRs settings validation and identify the miscoordination issues between primary and backup relays in the system, creating lists of DRs with miscoordination problems. This ultimately reduces the computational resources and time, as the proposed method does not require the protection coordination study by performing fault simulation. Unlike, the approaches discussed in [16, 18, 22]. The overall operation of the proposed method is shown in Figure 3.6 and can be elaborated by the following steps.

1. Process P1: Read the number of DRs (N_R) and number of vertices (n) as input information from the network topology.

2. Condition C1: The flow control loop is checked. If any DRs in the network remain unexplored, proceed to the next step. Otherwise, the coordination validation process will stop.

3. Process P2: Identify the ϑ_{si}, e_{si0}, and the reference DR_{ref} at the j^{th} iteration.

4. Process P3: After initializing the coordination validation routine, the paths within the protection zones of DR_{ref} are determined using the proposed method described in Section 3.1.

5. Process P4: Following the process P3, this process acquires arrays $Branch$, aS, $aS0$, and the S matrix from the MDFS subroutine.

6. Condition C2: The flow loop control is established and verified in this step. The proposed method requires traversing the S matrix for all i, where i ranges from 1 to n to obtain the vertex object in zone-1. At this point, if the condition is true, proceed to process P5. Otherwise, proceed to process P11.

7. Process P5: Traverse the S matrix to obtain the vertex's zone and its status.

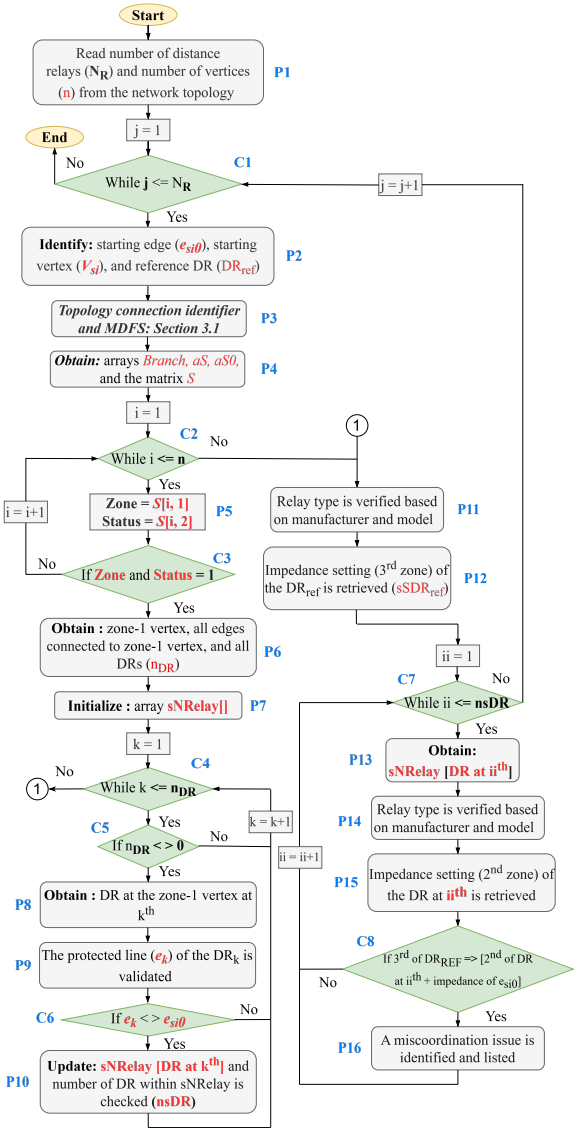

Figure 3.6: Flowchart of the proposed DRs coordination validation.

8. Condition C3: Once the vertex object and its status are found, the discovered vertex will be examined to determine whether the current vertex is located in zone 1 and its status represents the substation vertex. If this condition is false, step back to step 6 to discover the new vertex in the S matrix. Conversely, if the condition is true, the vertices and edges connected to the discovered zone-1 vertex will be searched.

9. Process P6: Once the the vertex object in zone-1 and its status represents the substation vertex ($Degree$ and $Status = 1$) are found, the vertices and edges connect to the discovered zone-1 vertex are obtained, as well as all DRs at the zone-1 vertex. Moreover, the total number of DRs at the zone-1 vertex is checked and stored it in the n_{DR} variable.

10. Process P7: Initialize $sNRelay$ object array and this array will be used to store all DRs at the zone-1 vertex, except the DR, which has a direction looking toward ϑ_{si0}.

11. Condition C4 and C5: The flow control loop is checked. If any DRs in the zone-1 vertex remain unexplored, proceed to the next step for all k and $k \in \{1, \ldots, n_{DR}\}$. Otherwise, proceed to process P11.

12. Process P8: Obtain DR_k at the zone-1 vertex.

13. Process P9: Obtain the protected line (e_k) of DR_k.

14. Condition C6: This condition is checked whether e_k is e_{si0}. If it is, step back to step 11 by updating variable k ($k = k + 1$). On the other hand, if it is not, proceed to the next step to add DR_k to $sNRelay$ array.

15. Process P10: Update $sNRelay$ array by adding DR_k to the array. Furthermore, The size of the array is updated by checking the number of DRs stored in the array, where ns_{DR} represents the total number of the DRs within $sNRelay$.

16. Repeat Steps 11 and 15 until all DRs at the zone-1 vertex are discovered.

17. Process P11: After all DRs at the zone-1 vertex are discovered and added to the $sNRelay$ array, the relay manufacturer and model of the DR_{ref} are checked and identified.

18. Process P12: After identifying the relay manufacturer and model of the DR_{ref} in process P11, the DR_{ref} zone-3 setting is retrieved and stored in the $sSDR_{ref}$ variable.

19. Condition C7: The flow control loop is checked. If any DRs in the zone-1 vertex remain unexplored, proceed to the next step for all ii and $ii \in \{1, \ldots, ns_{DR}\}$. Otherwise, proceed to condition C1 to discover new DR_{ref} in the system by updating j variable ($j = j + 1$).

20. Process P13: Obtain DR_{ii} at the zone-1 vertex from the $sNRelay$.

21. Process P14: Identify the relay manufacturer and model of the DR_{ii}.

22. Process P15: After identifying the relay manufacturer and model of the DR_{ii}, the DR_{ii} zone-2 setting is retrieved and stored in the $sSDR_{ii}$.

23. Condition C8: The settings of DR_{ref} and DR_{ii} are validated based on the conditions expressed in (3.15).

$$\begin{cases} Miscoordination \quad issue, \text{If } sSDR_{ref} \quad \geq \quad \mathrm{sSDR}_{ii} + Z_{e_{si0}} \\ No \quad issue, \text{If } sSDR_{ref} \quad < \quad sSDR_{ii} + Z_{e_{si0}} \end{cases} \tag{3.15}$$

24. If the condition is verified as "Yes," the miscoordination path is created and listed. Otherwise, the next DR in the array $sNRelay$ is examined by updating $ii = ii + 1$.

25. Repeat steps 19 to 24 until all DRs in the array $sNRelay$ is examined.

26. Then, the next DR_{ref} will be examined with the other relevant DRs in the system by updating $j = j + 1$.

The coordination validation algorithm routine will stop the process once all DRs in the system are discovered and performed as the DR_{ref}. The pseudocode of an automatized DR setting validation is shown in algorithm (8).

Algorithm 8 Pseudocode of an automatized DRs coordination validation.

Read DR(s) model, N_R, and the number of vertices, n, from the network model
Set j=1
while $j \leq N_R$ **do**
    Identify ϑ_{si}, $e_s i0$, and the reference DR at ϑ_{si0} (DR_{ref})
    Determine paths within the protection zones of the DR(s):
    Go to 2 and 3
    from 2 and 3 // Read $S[]nx3, aS, aS0, Branch$
    Set i=1
    while $i \leq n$ **do**
        Get the zone status $Zone = S[i, 1]$
        Get the type of the vertex $Status = S[i, 2]$
        if $Zone$ and $Status = 1$ **then**
            Get zone-1 vertex, edges connected to zone-1 vertex, and DRs (n_{DR})
            Initialize $sNRelay[]$ array
            Set k=1
            while $k \leq n_{DR}$ **do**
                if $n_{DR} \neq 0$ **then**
                    Get the DR at the zone-1 vertex at k^{th} (DR_k)
                    The protected line (e_k) of DR_k is validated whether it is e_{si0}
                    if $e_k \neq e_{si0}$ **then**
                        Update the $sNRelay[DR_k]^{ns_{DR}}x1$ and ns_{DR} variable
                    end if
                end if
                $k = k + 1$
            end while
        end if
        $i = i + 1$
    end while
    The DR model is checked based on the manufacturer and the model type
    Retrieve the impedance setting, 3^{th} zone, of DR_{ref} ($sSDR_{ref}$)
    Set ii=1
    while $ii \leq ns_{DR}$ **do**
        Get the DR model at ii^{th} (DR_{ii}) from $sNRelay$ array
        The DR model is checked based on the manufacturer and the model type
        Retrieve the impedance setting, 2^{th} zone, of DR_{ii} ($sSDR_{ii}$)
        Set $Z_{cum} = sSDR_{ii} + Z_{e_{si0}}$; $Z_{e_{si0}}$ is the line impedance of the e_{si0}
        if $sSDR_{ref} \geq Z_{cum}$ **then**
            A miscoordination issue is identified and listed
        end if
    end while
    Create summary report
    $j = j + 1$
end while

3.4 Validation and results

The proposed algorithms are applied to the modified 115 kV transmission network of the Provincial Electricity Authority (PEA), as illustrated in Figure 3.3, to evaluate and verify their effectiveness by comparing the results with the approaches presented in the literature. The multi-loop system consists of 11 substations, 13 transmission lines, and 1 transformer, all modeled in PowerFactory. The algorithms are developed using the digsilent programming language (DPL) [85]. The performance assessment of the proposed algorithms can be categorized into the following types of assessment.

3.4.1 Search algorithm assessment

To demonstrate the effectiveness of the proposed search algorithm for path determination, the proposed method and the traditional DFS from the literature are applied to a test system. This is done to determine paths within the protection zones of the DR. For this purpose, the DR at the vertex ϑ_2 (indicated by a red circle in the test system) is deployed as an example, and the results of the two approaches are compared.

Table 3.1: Path determination determined by DFS and proposed method

DFS in [21, 25, 73, 74]				Proposed MDFS			
Vertex	*De*	Status	km	Vertex	*De*	Status	km
3	1	1	3.6	3	1	1	3.6
1	2	1	10.4	1	2	1	10.4
6	3	1	45.4	6	3	1	45.4
7	4	1	85.4	5	2	1	20.5
8	5	1	100.4	4	3	1	25.5
9	6	1	105.9	7	3	1	35.5
10	7	1	123.9	-	-	-	-
11	8	1	188.9	-	-	-	-
12	9	2	188.9	-	-	-	-
4	8	1	154.9	-	-	-	-
5	9	1	159.9	-	-	-	-

The results presented in Table 3.1 show that after implementing the proposed method to determine the paths of the DR, it traverses the graph (the A matrix) and examines only the vertices and edges located within the protection zones; subsequently, it starts the backtracking process to search for alternative paths for any unvisited vertices. The path determination process based on the results expressed in Table 3.1 can be illustrated as follows: $2 \rightarrow 3_{n_s=1} \rightarrow 1_{n_s=2} \rightarrow 6_{n_s=3} \rightarrow 1_{n_s=2} \rightarrow 3_{n_s=1} \rightarrow 5_{n_s=2} \rightarrow 4_{n_s=3} \rightarrow 5_{n_s=2} \rightarrow 7_{n_s=3} \rightarrow 5_{n_s=2} \rightarrow 3_{n_s=1} \rightarrow 2_{n_s=0}$.

Unlike the MDFS, the DFS continues to traverse the graph and examine vertices and edges beyond the protection zones until it visits the deepest vertex and edge before beginning its backtrack, which path determination determined by DFS can be illustrated as follows: $2 \rightarrow 3_{n_s=1} \rightarrow 1_{n_s=2} \rightarrow 6_{n_s=3} \rightarrow 7_{n_s=4} \rightarrow 8_{n_s=5} \rightarrow 9_{n_s=6} \rightarrow 10_{n_s=7} \rightarrow 11_{n_s=8} \rightarrow 12_{n_s=9} \rightarrow 11_{n_s=8} \rightarrow 10_{n_s=7} \rightarrow 4_{n_s=8} \rightarrow 5_{n_s=9} \rightarrow 4_{n_s=8} \rightarrow 10_{n_s=7} \rightarrow 9_{n_s=6} \rightarrow 8_{n_s=5} \rightarrow 7_{n_s=4} \rightarrow 6_{n_s=3} \rightarrow 1_{n_s=2} \rightarrow 3_{n_s=1} \rightarrow 2_{n_s=0}$. As a result, the DFS introduces errors in path determination due to its search characteristic. For example, vertices 4 and 5 are supposed to be found within the protection zones, yet the results indicated that these vertices' degrees are located outside the protection zones. This ultimately results in errors when applying this method to the DR settings and coordination validation processes in the complex network topology. Nonetheless, this method remains effective when used in a radial system.

3.4.2 Setting and coordination algorithms assessment

In this assessment, a total of 25 DRs are tested and validated. The proposed algorithm for automatization of the DR settings is examined based on the computational time in the DR settings, including parameter settings of additional functions based on the manufacturers' recommendations and TSOs' requirements, as well as parameter mapping of the DRs from different manufacturers. Since only a few studies are focused on improving the efficiency of DR settings and their validation processes, the results from 2 different systems (11-bus and 3-bus systems) are compared, but the setting process from both systems is the same. Furthermore, the proposed method in this work is applied to the larger systems with higher numbers of DRs.

Two test cases are defined and deployed to assess the performance of the DR settings algorithm with the same number of DRs in the test system.

While both test cases involve the same number of DRs in the system, they differ in the number of manufacturers represented for the DRs.

In the first test case of the 11-bus system, only one specific manufacturer is involved in the testing and validation processes, and the computational time is achieved in 5.472 seconds. This computational result includes the whole process illustrated in Figure 3.5 for all DRs within the test system.

Seven different manufacturers are involved in the second test case, and the result is achieved in 8.168 seconds. The results indicate that using DRs from different manufacturers in the test system slightly increases the computational time. This increase in computational time is caused by different parameter settings of each manufacturer, i.e., each manufacturer has their own techniques for the fault detection algorithm for the distance protection function and additional functions.

Unlike the proposed method, although the test system is smaller and only one DR is tested and validated, the previous studies and conventional methods require more time— 24 times for method present in [16] and 120 times for conventional method compared to the proposed method—to complete the DR settings, excluding the computation of the additional functions. Moreover, only zone characteristics are provided. In practice, this ultimately results in time-consuming to complete the DR settings task when many DRs and DRs from different vendors are involved in the setting process, particularly in the complex network topology.

The results in terms of the computational time from 2 different systems using the conventional, previous, and the proposed methods are summarized in Table 3.2.

Table 3.2: Computational time of the setting algorithm

Proposed setting algorithm				
Case	No. DR	No. of vendor	Criteria	Computational time (s)
11-bus	25	1	1,2,3	5.472
11-bus	25	7	1,2,3	8.168
Proposed method presented in [16]				
3-bus	1	1	1	121.8
Conventional method (human manual work) presented in [16]				
3-bus	1	1	1	720

Table 3.3: Zone 2 settings (primary value) by vertex and DR location.

Vertex	DRs' location	Zone 2 setting (primary value)		
		in [22, 23]	Proposed method	|% Error|
1	1YB-01	79.541	26.508	200.06
	2YB-01	2.827	2.965	4.65
2	2YB-01	4.257	4.239	0.42
	6YB-01	2.159	2.164	0.23
3	1YB-01	6.588	6.588	0.00
	2YB-01	6.65	6.419	3.60
	3YB-01	7.657	19.657	61.05
4	1YB-01	5.030	4.862	3.46
	3YB-01	10.844	10.844	0.00
	5YB-01	7.658	6.473	18.31
5	1YB-01	16.491	13.571	21.52
	2YB-01	4.469	3.694	20.98
	4YB-01	5.549	5.445	1.91
6	1YB-01	10.411	10.411	0.00
	2YB-01	26.226	26.702	1.78
7	1YB-01	28.489	24.45	16.52
	2YB-01	5.074	5.140	1.28
	3YB-01	4.812	4.812	0.00
8	1YB-01	18.037	14.286	26.26
	2YB-01	9.085	8.489	7.02
9	1YB-01	9.082	9.082	0.00
	2YB-01	3.524	3.524	0.00
10	1YB-01	10.767	10.886	1.09
	2YB-01	8.958	8.730	2.61

Besides the computational time assessment, the methods to compute the setting of zone 2 are compared between the approach presented in [22, 23] and the proposed method within this work, and the results are reported in Table 3.3. According to the results reported in Table 3.3, in most cases, the zone 2 setting computed based on the previous methods results in under- and over-reach problems. This leads to DRs operating incorrectly if the fault occurs close to the boundary of zone 2.

Unlike previous approaches, the proposed method enhances the accuracy of zone 2 settings by directly determining the apparent fault impedance seen by the DRs at the boundary of zone 2, rather than relying on bus fault data during the computational process. This approach effectively minimizes the influence of infeed effects caused by generation units, which can lead to significant errors when using conventional bus fault current data and a fault at the line end. However, in the case of the adjacency line in zone 2 connected to the strong generation unit or strong grid, particularly in the meshed/loop topologies, the impedance seen by the DR may see the impedance in the reverse direction, like in the case of the DR at the vertex 3, 3YB-01.

To be more specific, the benchmark system—namely, the IEEE 39-bus test system, as illustrated in Figure 3.7—is employed to demonstrate the advantage of the proposed method over existing approaches reported in the literature when the under-reach problem is considered. Zone 2 is configured to cover 50% of the shortest adjacent line from the remote bus. Consequently, for example, when a three-phase fault occurs at 49% of the transmission line connecting Bus 25 and Bus 2, and the primary DR at Bus 25 protecting this line fails to operate, and assuming the primary DR at Bus 2 operates with zone 1. Hence, the backup DR located at Bus 26 is required to operate with the zone 2 delay time (300 ms) to mitigate equipment damage and to reduce the severity of voltage dips or sags caused by the fault.

As illustrated in Figure 3.8, for a three-phase fault occurring at 49% of the transmission line connecting Bus 25 and Bus 2 in the IEEE 39-bus test system, the zone 2 setting of the DR at Bus 26 based on the proposed method demonstrates correct operation. In contrast, the zone 2 setting derived using the methods reported in [22, 23] results in incorrect relay operation, as shown in Figure 3.9.

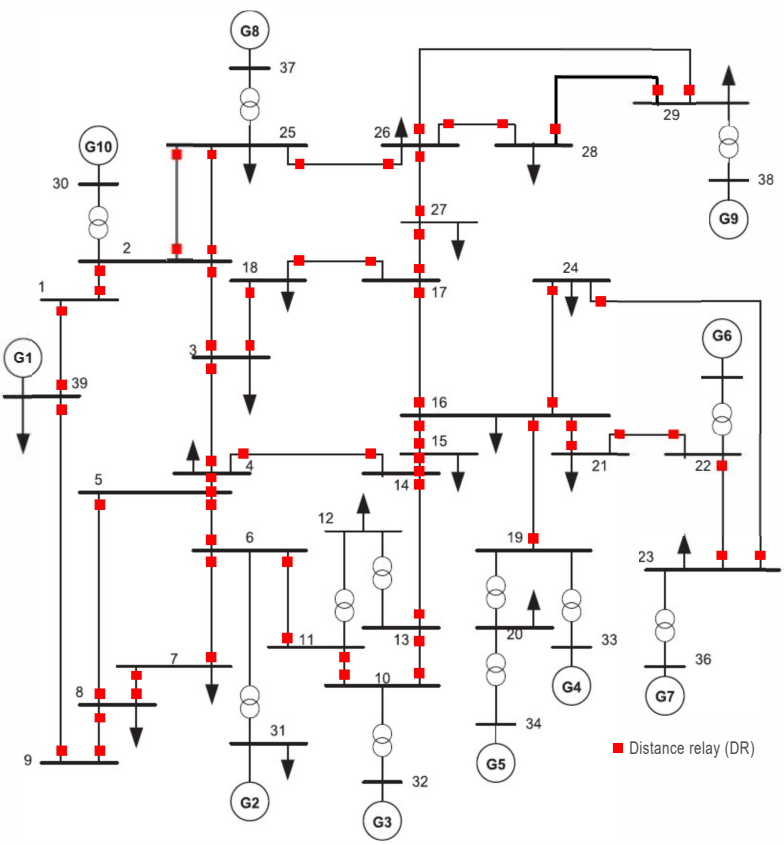

Figure 3.7: Modified IEEE 39-bus.

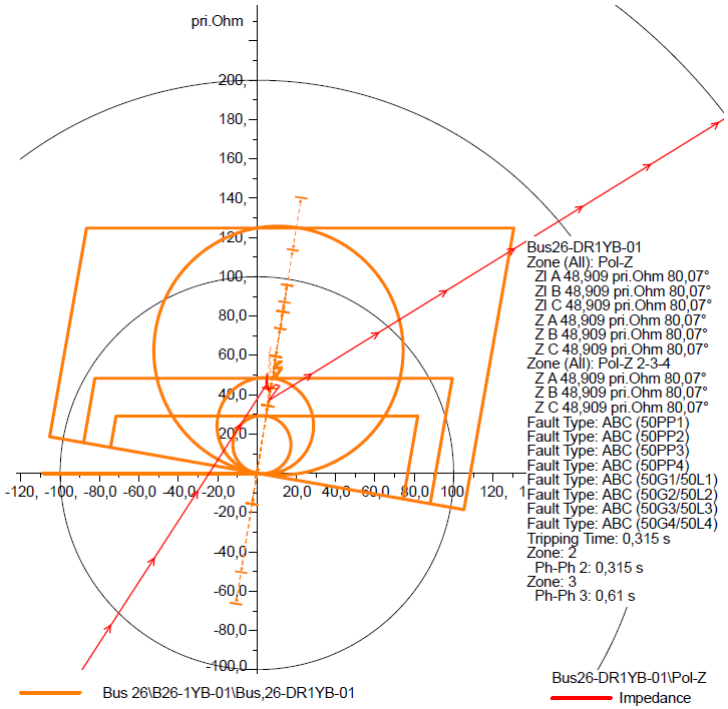

Figure 3.8: Zone 2 setting based on the proposed method.

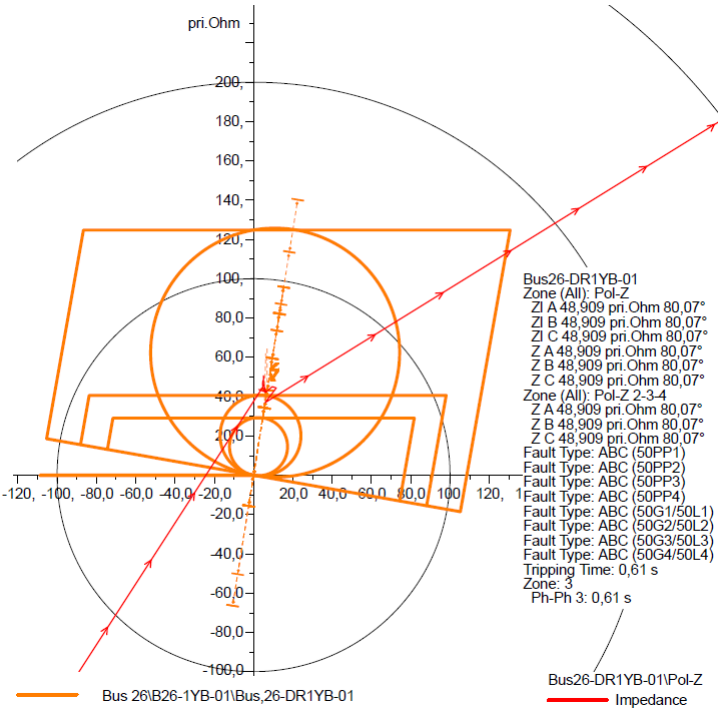

Figure 3.9: Zone 2 setting based on methods in [22, 23].

The DR settings obtained using the proposed method and those presented in [22, 23] of the DR at Bus 26 are summarized in Table 3.4.

Table 3.4: Comparison of zone 2 settings

DRs location Bus 26	**Protected line**	**Zone 2 setting (primary)**		**|% Error|**
		in [22, 23]	**Proposed method**	
DR26	25–26, 25–2	47.40	49.06	3.38

Hence, in general, the proposed method provides more accurate and reliable zone 2 settings, especially in complex network topologies with mul-

tiple infeeds. However, the proposed method requires high accuracy of the system model, particularly generator model parameters and transmission line parameters, etc.

In this study, besides the zone characteristic settings of the DRs, all parameter settings of the additional functions provided within a single package of the DR are computed and mapped. For this purpose, some parameters of the power swing and load encroachment functions of DRs at various points of interest in the test system, specifically at the vertices ϑ_2 (6YB), ϑ_8 (1YB), and ϑ_{10} (3YB), are deployed as an example. These parameters have been selected to demonstrate the process of parameter mapping in accordance with the requirements set by manufacturers and TSOs. Some results of this procedure are compiled and presented in Table 3.5.

Table 3.5: Excerpt of parameter mapping of a power swing, load encroachment, and zone setting

Function	ABB (ϑ_8) REL670 (Pri.)	SEL (ϑ_2) 311C (Sec.)	Schneider (ϑ_{10}) P443 (Sec.)
Power swing and Load Encroachment	X1InFw = 71.85	X1T6 = 21.49	PZ7 = 68.36
	R1LIn = 0.1	X1T5 = 19.49	PZ8 = 88.87
	R1FInFw = 36.89	R1R6 = 13.13	PZ7 = -68.36
	X1InRv = 71.85	R1R5 = 11.13	PZ8 = -88.87
	R1FInRv = 36.89	X1B6 = -21.49	PR7 = 39.40
	RLdOutFw = 46.11	X1B5 = -19.49	PR8 = 51.23
	ArgLd = 30	R1L6 = -13.13	PR7 = -39.40
	RLdOutRv = 46.11	R1L5 = -11.49	PR8 = -51.23
Zone reach	X1= 2.41	Z1 = 1.49	Z1 = 26.96
	R1 = 0.55	XG1 = 1.47	Z1G = 26.96
	RFPP = 7.24	Z2 = 3.89	Z2 = 47.35
	X2 = 14.08	XG2 = 3.84	Z2G = 47.35
	R2 = 2.44	Z3 = 14.99	Z3 = 52.59
	RFPP = 23.05	XG3 = 14.84	Z3G = 52.59
	X3 = 59.87	Z4 = 0.22	Z4 = 4.04
	R3 = 10.98	XG4 = 0.22	Z4G = 4.04
	RFPP = 57.13	k0M = 1.32	kZN = 1.32
	RFPE = 40	RG = 72	RG = 72

Table 3.6: Computational time of DRs coordination validation algorithm

Proposed coordination validation algorithm			
Case	No. DR	No. of vendor	Computational time (s)
11-bus	25	1	0.742
Proposed method presented in [16]			
3-bus	2	1	34.2
Conventional method (human manual work) presented in [16]			
3-bus	2	1	1440

For the DRs coordination validation algorithm, for the sake of simplification, the outcomes of the DR settings algorithm of test case 1 outlined above are used to test and validate its performance and effectiveness. The results provided by the proposed method are compared with those presented in [16]. The performance of the DRs coordination validation algorithm is evaluated based on the computational time, which is similar to the DR settings algorithm assessment.

The conventional and method presented in [16] requires high computational resources and time in completing the DRs coordination validation task, even if only two DRs are tested and validated. These are even more so when these methods are applied to a large system. Compared to the proposed method, even if the number of DRs is higher and the test system is more complicated, the computational resources and time are less expensive, approximately 50 times, as reported in Table 3.6. This effectively minimizes the time and effort needed to handle the validation of multiple DR settings.

The lists of DR miscoordinations achieved from the proposed method are summarized and reported in Table 3.7. Table 3.7 shows the lists of co-pairs and determined paths that experience a miscoordination issue in the third zone. It is important to note that in multi-loop systems with varying line lengths, when Z_2 for each DR is configured and set the zone characteristic setting at the boundary instead of relying on bus fault data for Z_2 calculations, there is no issue of miscoordination in zone 2 between the primary and backup DRs, as demonstrated in Figure 3.10. The results reveal that a coordination problem between the primary (Main) and backup (BU) of DRs arises due to variations in line lengths, weak infeed, infeed effect, and complex topologies.

Table 3.7: Lists of DR miscoordination among primary and backup relays

No. Pairs	Main	Vertex	BU	Vertex	Direction
1	1YB	6	1YB	7	$7 \rightarrow 6 \rightarrow 1$
2	2YB	5	2YB	7	$7 \rightarrow 5 \rightarrow 4$
	4YB	5	2YB	7	$7 \rightarrow 5 \rightarrow 3$
3	2YB	6	1YB	1	$1 \rightarrow 6 \rightarrow 7$
4	2YB	3	2YB	1	$1 \rightarrow 3 \rightarrow 5$
	3YB	3	2YB	1	$1 \rightarrow 3 \rightarrow 2$
5	1YB	4	2YB	2	$2 \rightarrow 4 \rightarrow 5$
	3YB	4	2YB	2	$2 \rightarrow 4 \rightarrow 10$
6	1YB	3	6YB	2	$2 \rightarrow 3 \rightarrow 1$
	2YB	3	6YB	2	$2 \rightarrow 3 \rightarrow 5$
7	2YB	5	6YB	3	$3 \rightarrow 5 \rightarrow 4$
	2YB	2	2YB	3	$3 \rightarrow 2 \rightarrow 4$
8	1YB	7	1YB	8	$8 \rightarrow 7 \rightarrow 6$
	2YB	7	1YB	8	$8 \rightarrow 7 \rightarrow 5$
9	1YB	9	2YB	8	$8 \rightarrow 9 \rightarrow 10$
10	1YB	4	1YB	10	$10 \rightarrow 4 \rightarrow 5$
	5YB	4	1YB	10	$10 \rightarrow 4 \rightarrow 2$
11	2YB	9	2YB	10	$10 \rightarrow 9 \rightarrow 8$
12	3YB	7	2YB	6	$6 \rightarrow 7 \rightarrow 8$
	2YB	7	2YB	6	$6 \rightarrow 7 \rightarrow 5$
13	1YB	5	1YB	4	$4 \rightarrow 5 \rightarrow 7$
	4YB	5	1YB	4	$4 \rightarrow 5 \rightarrow 3$
14	2YB	10	3YB	4	$4 \rightarrow 10 \rightarrow 9$
	3YB	10	3YB	4	$4 \rightarrow 10 \rightarrow 11$
15	6YB	2	5YB	4	$4 \rightarrow 2 \rightarrow 3$
16	1YB	7	1YB	5	$5 \rightarrow 7 \rightarrow 6$
	3YB	7	1YB	5	$5 \rightarrow 7 \rightarrow 8$
17	3YB	4	2YB	5	$5 \rightarrow 4 \rightarrow 10$
	5YB	4	2YB	5	$5 \rightarrow 4 \rightarrow 2$
18	1YB	3	4YB	5	$5 \rightarrow 3 \rightarrow 1$

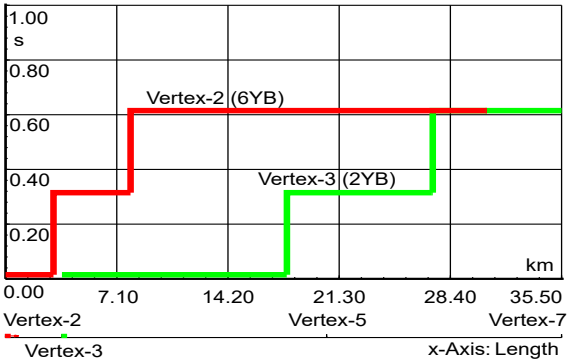

Figure 3.10: Miscoordination problem identified by the proposed method based on time distance diagram.

The coordination problem reported in Table 3.7 can assist TSOs in planning and decision-making regarding the appropriate network configurations and protection systems before implementation. As a result, the undesirable operations of DRs stemming from the miscoordination issue can ultimately be prevented. Based on the DR miscoordination lists, the problem can be resolved by the solution suggested by the authors in [87], but this will lead to a reduction in the protection zone. However, if TSOs must ensure coverage of all sections of the adjacent lines at the remote substation, the delay time for zone-3 of the backup DR can be adjusted.

3.5 Conclusions

The topology connection identifier and MDFS approaches are proposed to demonstrate the topological connections within the electrical grids and identify the vertices and edges, so-called "paths", within the protection zones of DR. The MDFS method is specifically proposed to enhance the performance of DFS during graph traversal, assisting in preventing path determination errors that can occur in the context of the DR settings and coordination validation regardless of the network topology. In addition, the proposed MDFS reduces search complexity and time compared to the traditional DFS, as indicated in Table 3.1. This ultimately results in the

path determination for the setting calculation and coordination validation of DRs being effectively determined.

The proposed algorithm for automatization of the DR settings is also proposed for covering settings, both zone characteristics and additional functions for modern DRs, by considering the possible infeed effects in the system, including mapping of parameter settings of the DRs from different manufacturers. In contrast to the approaches discussed in Chapters 1 and 2, which focus only on zone characteristics themselves and some specific criteria. Furthermore, the computation of the zone 2 setting at the boundary is proposed by considering all possible infeed effects in the system to avoid under- and over-reach problems. This approach is more efficient in the zone 2 setting than the previous approaches.

To reduce computational resources and time, graph theory-based algorithms and MDFS are presented to identify miscoordination problems and paths and to create the lists of DR miscoordination among primary and backup relays in the system. Moreover, the proposed method is able to retrieve the settings of DRs from different vendors to be validated. Hence, compared to the approaches discussed in Chapters 1 and 2, the proposed method is more efficient, considering computational resources and time, since it does not require performing the fault simulation to identify the miscoordination problems.

The results ultimately indicate that the proposed methods can effectively enhance DR settings and DRs coordination validation while also providing practical tools that improve efficiency and reliability in setting and coordination.

4

Distance Relay Testing

To address the challenges and drawbacks in the context of DR testing and validation formulated in Chapter 2, Section 2.5, this chapter presents:

(i) the developed test environment, transmission system model based on a real-time digital simulator, and methodologies for DR testing and validation to: assess the performance of the commercial DRs to overcome the limitations of the available testing methodologies by covering a broader of spectrum of functions, including additional functions, e.g., power swing, fault locator, etc. This approach offers advantages to both TSOs and manufacturers since the proposed methodologies enable a comprehensive evaluation of commercial distance relays, extending beyond zone characteristics and basic accuracy tests that are typically addressed by existing testing methodologies. The proposed method also allows the validation of the distance protection algorithm and the identification of operational errors in DR under different operating conditions. This, in turn, provides valuable insights for manufacturers to refine their approaches, thereby minimizing the risk of unintended relay operations,

(ii) the stat-DOE is introduced for the DR testing activity to: minimize the experiment effort by defining the most influential factors for performance testing and handling the constraints between factors in the design space based on the defined factors (avoiding unnecessary experiments, e.g., phase-to-phase fault with high fault resistance). Hence, the optimal choices of the testing activity focusing on the most impactful factors can be systematically selected (resource-saving context to properly collect data) while maintaining efficacy, objectivity, and generalization of the testing activity.

To effectively fulfill the research objectives of the proposed methods within the context of DR testing and validation, the requirements for performance evaluation are established as follows:

- the operating time should deviate less than 50 ms from the setting value for all scenarios;
- values of fault resistance from 0 to 9 ohms are applied for each fault type and fault location;
- fault inception angles can vary from 0 to 360 deg;
- DR must operate correctly, corresponding to its protection zones, in case of low fault resistance;
- during evolving fault, the fault detection element of DR must remain functional under changing conditions without any reset condition when a fault type evolves to another type;
- during simultaneous faults, DR must respond to the closest fault;
- for the tele-protection scheme, only the fault impedance detected by the distance protection element is sent to the remote DR;
- Switch-on-to-Fault (SOTF) must operate instantaneously after the CB is closed onto faulted line;
- if the fault occurs during a power swing, the DR should distinguish between fault and power swing events and should isolate the fault from the system without any delay;
- deadtime for the auto-reclose function is 1 s, reclaim time is 5 s;
- fuse failure condition blocks the operation of the DR to avoid unintended operation;
- the fault location reported by the fault locator should less than $\pm 2km$.

Therefore, this chapter focuses on the proposed methodologies for DR performance testing and validation based on established requirements to demonstrate a comprehensive evaluation of commercial DRs, as well

as show how the stat-DOE can provide advantages in DR performance testing activity compared to the available testing approaches. A major part of this chapter builds upon the methodology and HiL techniques of DR performance testing presented in [4, 6]. The proposed methods are specifically dedicated to complete DR testing schemes in order to bridge the gaps between manufacturers and other stakeholders in the protection community. Furthermore, the proposed techniques address the second research question and the third contribution motivated in Chapter 1. Similarly, the stat-DOE is introduced to determine an optimal set of scenarios and the number of tests [2], as well as to address also the second research question and the fourth contribution.

The rest of the chapter is organized as follows. Section 4.1 describes the developed test environment, proposed testing methodologies, transmission systems, as well as test and validation the performance of two commercial DRs based on the proposed testing methodologies. Section 4.2 demonstrates the guideline to conduct the DR performance testing via the stat-DOE, and identifies and synthesizes key lines of refinement and targeted recommendations for stakeholders within the protection community. The chapter conclusion is summarized in Section 4.3.

4.1 Testing methodology for performance evaluation

4.1.1 Proposed testing methodology

As outlined in chapter 2, the available DR testing approaches are limited to zone characteristics and basic accuracy tests, and the test methodologies are inadequate in practical testing for modern DRs. Moreover, the perspectives presented in [31] are limited to specific scenarios and do not encompass methodologies that could be interesting to TSOs, considering their operational needs [38]. In light of this, this subchapter presents a methodology for DR testing to assess the performance, including additional functions of multi-vendor DRs to encompass the viewpoints of manufacturers and other stakeholders in the protection community. To this scope, the test environment, transmission system model based on a real-time digital simulator, and methodologies for DR testing and validation are developed in order to encompass a broader spectrum of critical scenarios than those reported in [31, 34, 35, 36, 79]. In this work, the proposed testing methodology is deployed to investigate the DR performance of commercial DRs

according to established requirements. The proposed methodologies to evaluate the DR performance are summarized in Table 4.1.

The architecture of the developed testing methodology is proposed for the test, as shown in Figure 4.1. According to the proposed testing architecture, the power system model is modeled and simulated in an Real Time Digital Simulator (RTDS). The adoption of a real-time simulator enables comprehensive integration and testing of all components involved—namely, the power system model, developed algorithms, and physical devices—in a HiL environment prior to deploying the device under test in the field.

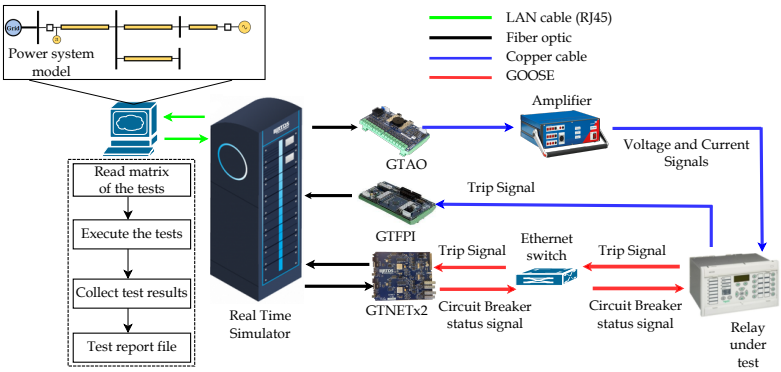

Figure 4.1: Testing platform for performance testing [© 2024 IEEE].

In the testing architecture, voltage and current measurement values in RSCAD are transmitted to the DR using a GTAO card. Once the DR detects that the fault occurs and the fault impedance falls into its protection zones, the DR releases the trip and auto-reclose signals (only for zone 1) to the RTDS via the GTFPI card with copper-wire connection and GOOSE signal via GTNETx2. In addition to zone characteristics and basic accuracy tests, additional functions that are provided to enhance DR operational performance can be studied with the proposed testing methodology, such as tele-protection, fuse failure, etc. Furthermore, a program routine has been developed to handle the test, e.g., system parameters changing, network reconfigurations, etc., based on the proposed methodology using the programming environment in RSCAD.

Table 4.1: Proposed test cases for evaluating the DR performance.

Case	Description	Characteristic	Fault type
1	Reach test–Internal fault with resistance	Mho, Quad (Zone 1)	AG, BG, CG, AB, BC, CA, ABG, BCG, CAG, ABC
2	Reach test–Internal fault with different fault inception angles	Mho, Quad (Zone 1)	AG, BG, CG, AB, BC, CA, ABG, BCG, CAG, ABC
3	Reach test–Forward and reverse fault	Mho, Quad (Zone 2, 3, 4)	AG, BG, CG, AB, BC, CA, ABG, BCG, CAG, ABC
4	Reach test–Evolving fault	Mho, Quad (Zone 1 and 2)	Evolving time: 30ms Zone 1 fault (50%), 200 ms Zone 2 fault (100%), AG to ABG, BCG to ABC, CA to ABC
5	Reach test–Simultaneous faults	Mho, Quad (Zone 1 and 2)	Simultaneous faults AG at 50% and BG at 0%, AG at 50% and BG at 100%
6	Reach test–Internal fault with different SIR	Mho, Quad (Zone 1 and 2)	AG, BG, CG, AB, BC, CA, ABG, BCG, CAG, ABC
7	Communication aided tripping (POTT, PUTT, etc.)	Mho, Quad (Zone 1 and 2)	AG, BC, CA, CAG, ABC
8	SOTF	Mho, Quad (Zone 1 and 2 and current supervision element)	Breaker closes onto faults: AG, BG, CG, AB, BC, CA, ABG, BCG, CAG, ABC
9	power swing detection	Swing detection; fault and power swing discrimination	Phase and ground fault
10	Auto-Reclose	Mho, Quad (Zones 1 and 2)	Temporary and permanent faults
11	Fuse failure, 1Ph, 2Ph, and 3Ph	Mho, Quad	No fault, AG, BG, CG, AB, BC, CA, ABG, BCG, CAG, ABC
12	Fault locator (Disturbance record)	Mho, Quad	AG, BG, CG, AB, BC, CA, ABG, BCG, CAG, ABC

Hence, the entire testing methodology is automated with the developed program routine, and the test results of the proposed methodology are automatically recorded and stored in .csv and Comtrade file formats. In such a test methodology, the operation of the DR can be monitored and investigated under all possible operating conditions of interest.

4.1.2 Validation and results

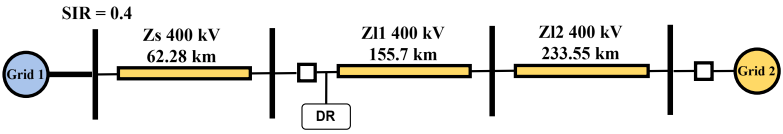

Figure 4.2: Transmission system model under study [© 2023 IEEE]

Table 4.2: Service settings of the DRs under test.

Zone	Characteristic	Impedance (ohm)	Resistive reach for Quad (ohm)	Operating time (ms)
1	Mho, Quad	4.34 (80%)	10	0
2	Mho, Quad	6.51 (120%)	15	300
3	Mho, Quad	9.22 (170%)	20	600
4	Mho, Quad	2.17 (40%)	20	600

The proposed testing methodology and architecture reported in Table 4.1 and Figure 4.1 are employed to test and investigate the performance of two commercial DRs, aiming to pinpoint possible unexpected operations under the same set of methodologies for the test. This includes comprehensive DR testing, encompassing the viewpoints of manufacturers and other stakeholders. All test cases are conducted and investigated. However, some results are reported here in this subsection, except test cases 2 and 6,

which will be deployed and elaborated more in detail in Section 4.2. The results reported in this subsection contribute to the test methodologies that are either missing or only partially elaborated in the [31] as well as in [34, 35, 36, 79]. The names of the two commercial DRs under test are anonymized and hereafter referred to as "Vendor 1" and "Vendor 2" for privacy concerns. DR configuration and parameter settings are computed according to the power system model in RSCAD, as illustrated in Figure 4.2 and their service settings (calculated based on secondary values) are reported in Table 4.2. The protection zones of the DRs under test are zone 1, 2, and 3 with forward direction and zone 4 as reverse direction.

Case 1: Reach test – Internal fault with resistance

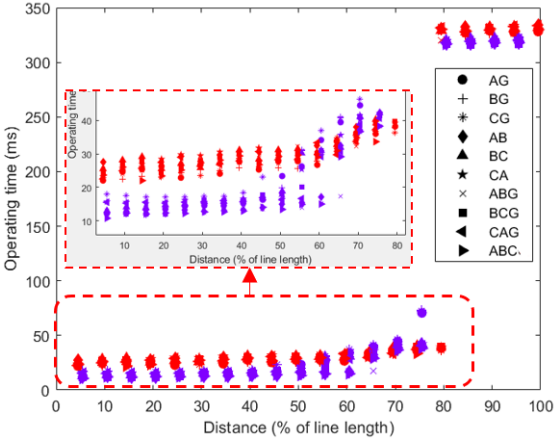

Figure 4.3: Case 1 – Operating times of Vendor 1 (red) and Vendor 2 (purple) with $R_f = 9$ ohms [© 2023 IEEE].

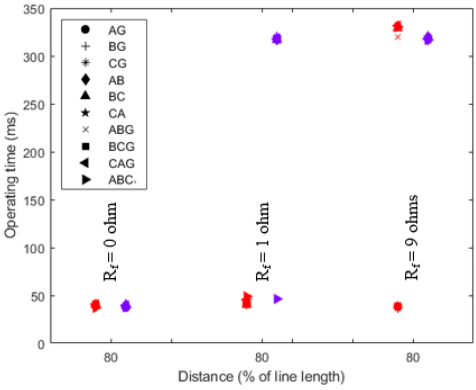

Figure 4.4: Case 1 – Operating times of Vendor 1 (red) and Vendor 2 (purple) with R_f equal to 0, 1 and 9 ohms at the boundary of zone 1 [© 2023 IEEE].

The main objective of this test methodology is to focus on the operating time and selectivity of the zone-1. In this experiment, ten fault types with varying resistances are simulated at different locations along transmission line $Zl1$. The fault locations are specified as percentages of the total line length, ranging from 5% to 100% in increments of 5%. Additionally, the R_f is set to 0, 1, and 9 ohms for each scenario. It is also important to assess the DR operation under different DC components and high-frequency components during fault conditions in the waveforms [88]. Hence, in this experiment, the fault inception angle is set and fixed to 0° since it is the extreme condition to generate the highest DC component [79]. Similarly, the SIR for the long transmission line configuration is implemented (SIR=0.4) [89]. More details of fault inception angles and SIR will be discussed in Section 4.2. Therefore, with the combination of the factors outlined above, 600 tests are performed for each DR.

Figure 4.3 presents the operating time results for $R_f = 9$ ohms across different fault locations. At 80% of the line length, corresponding to the boundary of zone 1, Vendor 1 consistently demonstrates better performance compared to Vendor 2 for the majority of fault types. Similar results were obtained for fault resistances of $R_f = 0$ and 1 ohm.

Figure 4.4 illustrates the performance of the two relays at the zone-1 boundary for R_f equal to 0, 1, and 9 ohms. Vendor 1 successfully detects all ten fault types when R_f is 0 or 1 ohm; however, with $R_f = 9$ ohms, only five fault types—AG, BG, CG, CA, and BCG—are correctly identified. In contrast, Vendor 2 fails to operate within zone-1 in the presence of fault resistance. Notably, the activation of zone-2 results in the DR driving to a lockout condition, potentially triggering a blackout in the transmission system in case of a temporary fault.

Case 3: Reach test – Forward and reverse faults

This test case aims to assess the fault parameter sensitivity study affecting zones 2 to 4. Ten fault types are investigated at different locations along transmission line $Zl1$ for the forward zones. The fault locations are specified as percentages of the total line length, ranging from 65% to 245% in increments of 20%. On the other hand, for the reverse zone, the locations range from -3% to -48% in decrements 5% along transmission line Zs. The fault inception angle and SIR are still the same values as reported in test case 1. Hence, in this experiment, 200 test cases are conducted for each vendor. Comparisons of the operating time and standard deviation between Vendor 1 and Vendor 2 for 10 fault types are reported in Figures 4.5 and 4.6. Based on the test results, it is noticed that the DR of Vendor 2 operates incorrectly (overreach than 170% for forward zones and 40% for reverse zone) in case of faults AN, BN, CN, BCN, and CAN. Therefore, TSOs can easily select the DR(s) that are most appropriate for their applications.

Case 4: Evolving fault

Table 4.3: Performance of Vendors 1 and 2 in addressing the evolving fault

Distance (%)	Fault Type 1	Fault Type 2	Vendor 1 (ms)	Vendor 2 (ms)
50	AG	ABG	35.05	26.90
50	BCG	ABC	29.80	24.90
50	CA	ABC	29.55	28.30
100	AG	ABG	336.50	318.70
100	BCG	ABC	331.10	320.30
100	CA	ABC	330.90	321.10

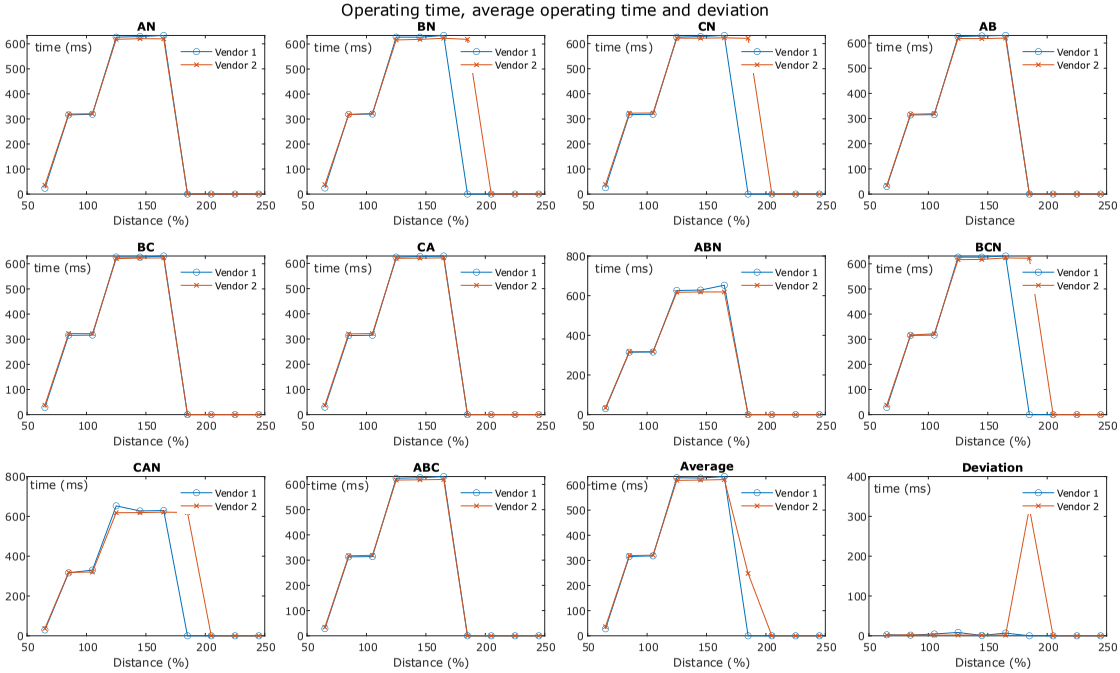

Figure 4.5: Results comparison between Vendor 1 and Vendor 2 (forward zones).

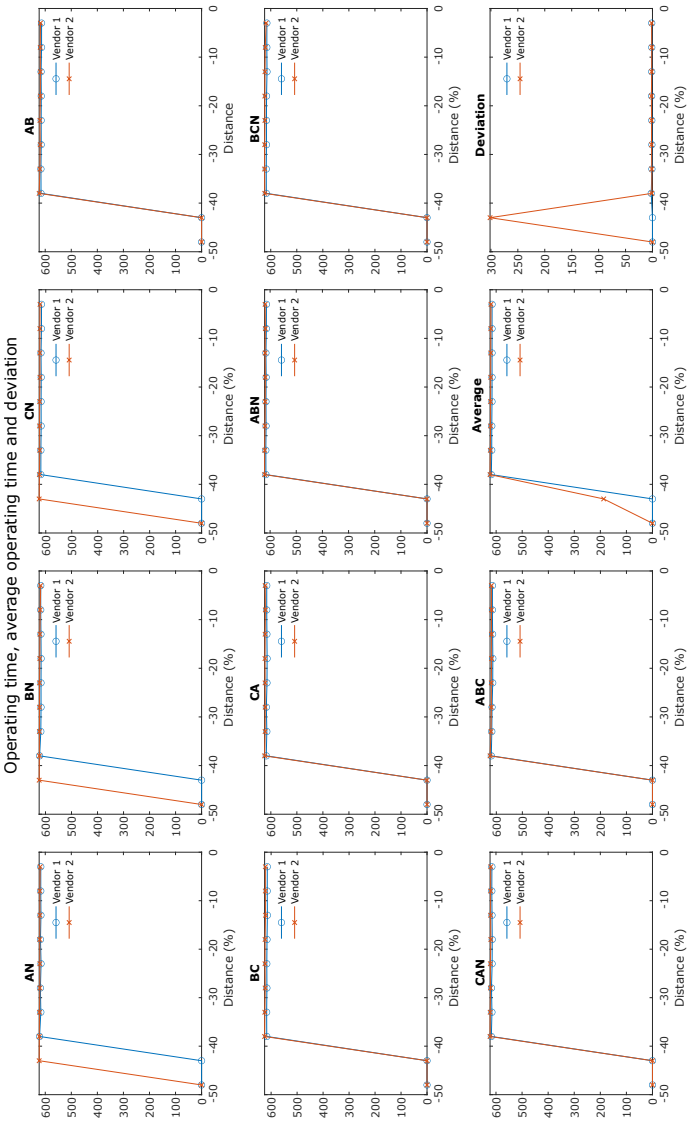

Figure 4.6: Results comparison between Vendor 1 and Vendor 2 (reverse zones).

In this test scenario, the DR performance is assessed as the initial fault evolves into another fault type. This fault scenario aims to assess the fault clearing time when a fault type changes over time, and the fault detection function must remain functional under changing conditions, without any reset condition when a fault type evolves to another type. The DR performance respond to evolving fault are reported in Table 4.3. In this experiment, DRs Vendor 1 and 2 correctly address the evolving faults without any drop-off conditions. Suppose one specific DR vendor experiences any drop-off conditions due to this fault type. In that case, the main and backup DRs may operate simultaneously, or the backup DR may operate faster than the main DR (DR coordination issue), which results in wide-area blackouts in the transmission systems.

Case 5: Simultaneous faults

This test scenario aims to ensure accurate detection and clearing of multiple faults occurring at the same time, as well as ensure that DR can correctly respond to faults in different zones. Two different fault types (type 1 and 2) are simultaneously applied at different locations. The different fault scenarios are automatically conducted by varying the fault type 1 from AG to ABC with another fault type 2 simultaneously for each test. Out of the 90 tests performed for each vendor, results are reported in Figures 4.7 and 4.8, respectively. The average and standard deviation operating times for both vendors across different fault types reveal distinct trends in their performance.

Vendor 1 consistently illustrates average value and standard deviation of operating times for all fault types, which could indicate better baseline efficiency and stability in detecting and clearing in case of simultaneous faults. In contrast, Vendor 2 demonstrates significantly lower average operating time. However, the average value and the variability of operating times of Vendor 2 in the case of AG fault indicate higher values than those of other fault types. Although most standard deviations for Vendor 2 are less than those for Vendor 1, the larger deviations in the case of AG fault imply that Vendor 2's performance may fluctuate depending on the fault type. Therefore, the performance in detecting and clearing in case of simultaneous faults for Vendor 1 demonstrates that its performance is more stable than that of Vendor 2.

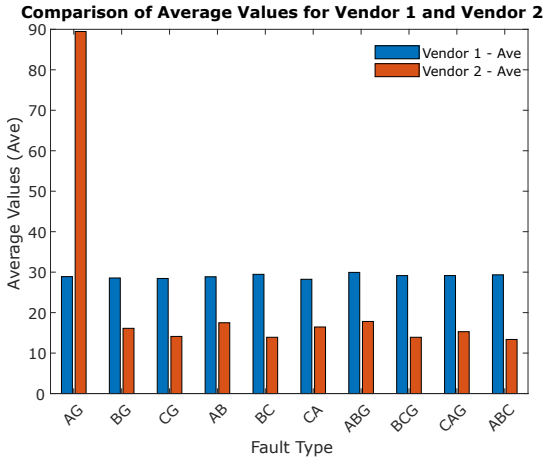

Figure 4.7: Average operating time for Vendor 1 and Vendor 2.

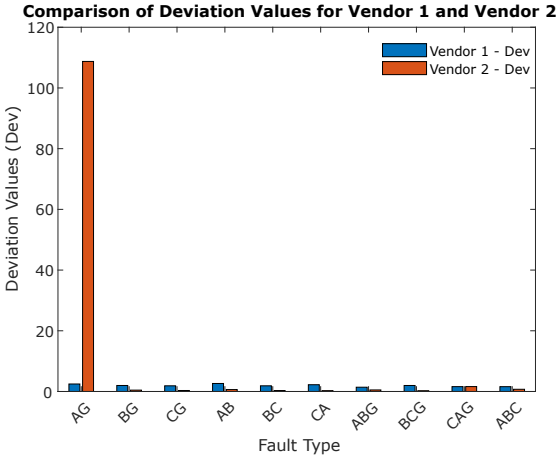

Figure 4.8: Standard deviation of operating times for Vendor 1 and Vendor 2.

Case 7: Communication aided tripping

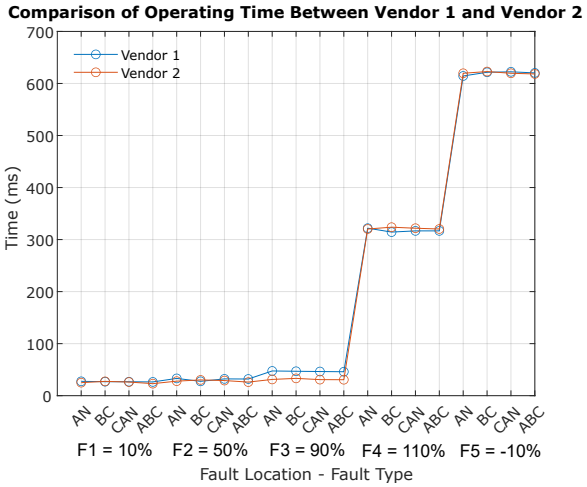

Figure 4.9: Comparison of response time between Vendor 1 and Vendor 2 in case of POTT scheme operation.

In this experiment, the tele-protection scheme (POTT) of the DR is evaluated. The main goal of this test is to confirm the correct operation of transfer trip signals. Principally, when DR detects the fault within the protected line, zone-2 with the POTT scheme of each DR must operate without delay time. Furthermore, the transfer trip signals should be originated from the fault detection element of the DR. To achieve the objectives of this experiment, four fault types are applied at 10%, 50%, 90%, 110%, and -10% of the line $Zl1$. The performance of Vendors 1 and 2 is similar in this case, as reported in Figure 4.9. However, the internal function of Vendor 2 has an issue since the transfer trip signal can be generated from other functions. This results in the transfer trip signal being sent from any starting function (e.g., overcurrent, voltage functions), as shown in Figure 4.10. Since the user cannot modify such a configuration, maloperation of the DRs may occur when implementing DRs with the POTT scheme.

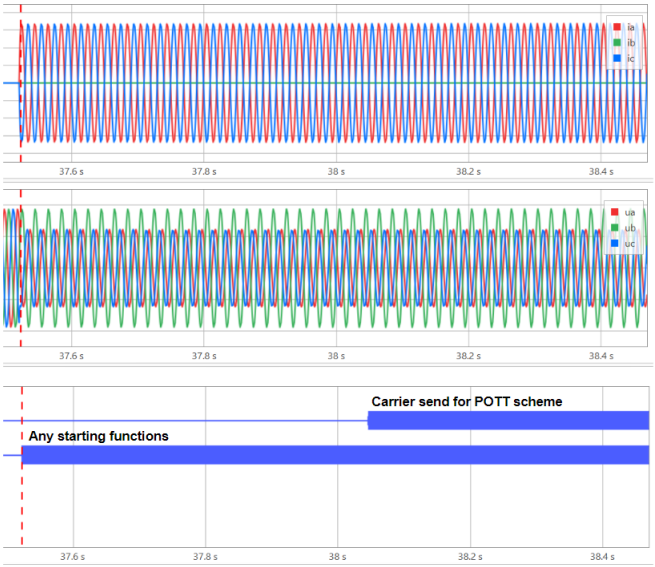

Figure 4.10: Transfer trip signal of Vendor 2 is generated when the fault is detected outside the protection zone [© 2024 IEEE].

Case 8: SOTF

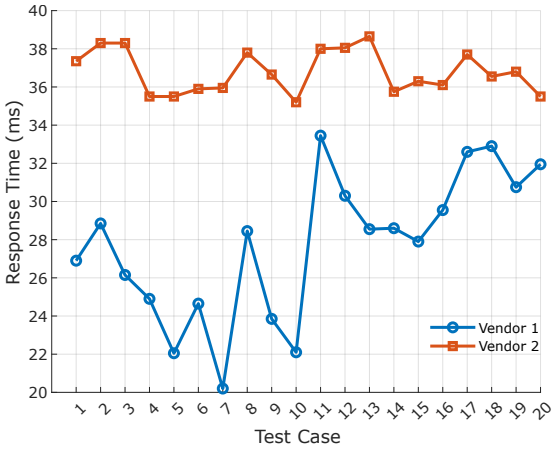

Figure 4.11: Response time of Vendor 1 and Vendor 2 in case of SOTF operation.

SOTF is the protection function intended to trip the associated CB when CB is closed onto the faulted line. Current or impedance-based fault detection must be set to cover the entire line or protection zones [90]. The main goal of this experiment is to verify the ability to detect different fault types when the CB is closed into a faulted line and the DR must release the trip signal to open the CB immediately to minimize equipment damage. The 10 fault types are applied to emulate the fault at 0% (test cases 1 to 10) and 100% (test cases 11 to 20) of the line $Zl1$, and the results are reported in Figure 4.11.

The findings indicate that the performance of Vendor 1 consistently indicates lower response times than that of Vendor 2 for all test cases, demonstrating a slightly faster operation than Vendor 2.

Case 9: Power swing

In this test case, the response time of power swing detection is examined for each vendor. Additionally, the capability to distinguish between power

swings and faults is investigated. During a power swing, the impedance changes more gradually, moving as a circular or spiral trajectory on the impedance plane, whereas, during a fault, the impedance becomes very low (impedance-based detection commonly used for DR). To achieve the objective of this test, phase and ground faults are applied to emulate faults in zone 2 after the power swing occurs in the system. The results are reported in Table 4.4.

Table 4.4: Performance of Vendor 1 and 2 for power swing detection and distinguish between power swings and faults

Test case	**Fault Type**	**Power swing**	**Vendor 1 (ms)**	**Vendor 2 (ms)**
1	No	Yes	69.30	-
2	ABC	Yes	371.1	551.6
3	AG	Yes	372.4	553.4

Since Vendor 2 does not have the power swing detection element, it cannot be reported as timing detection. Additionally, during power swing followed by phase or ground faults, the DR of Vendor 2 is able to detect and separate a fault from the system with a 500 ms delay (fixed parameter from manufacturer). In such a time delay, even if a fault occurs in zone 2, the DR of Vendor 2 operates after 500 ms, which is slower than the operating time of zone 2 itself. This may result in a coordination issue since a backup DR may operate (600 ms) simultaneously due to a small margin (less than 50 ms) between primary and backup DRs. On the contrary, Vendor 1 is able to detect the swing and distinguish between power swings and faults correctly.

Case 10: Auto-reclose

The auto-reclose function is examined by applying temporary and permanent faults within zone 1 and zone 2 of DR, respectively. This test aims to ensure the operation of the auto-reclose function under synchronized conditions to validate dead time and reclaim time when the fault occurs in the system. In this experiment, the auto-reclose function is initiated by the DR zone-1 trip signal, and it is dived into a lock-out state for zones 2 to 4. To avoid closing on to fault and minimize equipment damage in case the transformer protection or bus bar protection fails to operate, the

auto-reclose function for zones 2 to 4 is disabled since these zones are used as backup protections for power transformers and bus bars.

Table 4.5: Test results for Vendor 1

Test case	Fault type	Fault zone	Vendor 1 (s)		Reclose success	Lock out
			Dead time	Reclaim time		
1	AG(T)	zone 1	1.020	5.108	Yes	No
2	ABC(T)	zone 1	1.027	5.109	Yes	No
3	BCG(P)	zone 2	-	-	No	Yes
4	CA(P)	zone 2	-	-	No	Yes

Table 4.6: Test results for Vendor 2

Test case	Fault type	Fault zone	Vendor 2 (s)		Reclose success	Lock out
			Dead time	Reclaim time		
1	AG(T)	zone 1	1.023	4.999	Yes	No
2	ABC(T)	zone 1	1.030	5.103	Yes	No
3	BCG(P)	zone 2	-	-	No	Yes
4	CA(P)	zone 2	-	-	No	Yes

The results reported in Table 4.5 and Table 4.6 indicate that Vendors 1 and 2 are able to re-close successfully in the case that temporary faults (T) for phase and ground occur in Zone 1. Similarly, in the case of permanent faults (P) for phase and ground occurring in Zone 2, both DRs operates and dives to lock-out condition. In addition, since the faulted in zone 2 dives the auto-reclose function to the lock-out condition, the dead time and reclaim time cannot be measured.

Case 11: Fuse failure

The key purposes of this test case are i) to identify abnormal voltage conditions and ii) to avoid incorrect operation of DR due to fuse failure conditions. The fuse failure or loss of VT input causes the voltage input to the DR to be lost or unbalanced, which leads to false tripping since DR may be considered as a close-in fault. To investigate the operation of DR under a fuse failure condition, fuse failure is emulated for single-phase,

phase-to-phase, and three-phase scenarios. In such scenarios, 77 test cases need to be conducted for each DR. Under this condition, the operation of DR is blocked to prevent incorrect impedance calculations and false trips when voltage is lost.

Table 4.7: Fuse failure test results

Fuse failure	**Fault Type**	**Vendor 1 (ms)**	**Vendor 2 (ms)**
A B C AB BC CA ABC	No fault No fault No fault No fault No fault No fault No fault	blocked	blocked
A, B, and C	10 fault types for each phase	blocked	blocked
AB, BC, and CA	10 fault types for each phase-to-phase	blocked	blocked
ABC	10 fault types	blocked	blocked

Upon the fuse failure on a single phase, phase-to-phase, and three phases, DRs from both vendors successfully detect the abnormal conditions. Simultaneously, all DR protection zones are blocked, as illustrated in Table 4.7. Based on the results, Vendors 1 and 2 correctly identified the VT loss.

Case 12: Fault locators

The main objective of this test case is to verify whether the DR can accurately estimate the distance to the fault (typically in kilometers or as a percentage of the line length), which enables TSOs to pinpoint fault locations for faster repair and system restoration. To comply with the objective of this test case, 10 fault types are applied to the $Zl1$ at 10%, 50%, and 80% of its length, resulting in 30 test cases that need to be performed for each DR.

The test results of 2 vendors illustrated in Figure 4.12 indicate that at 10% of the line length, Vendor 1 shows a slight deviation from the actual

fault location, with errors typically within ±0.05 km. In contrast, Vendor 2 shows significantly higher errors, ranging from approximately -0.39 km to -0.78 km. Similarly, at 50% of the line length, Vendor 1 maintains high accuracy, with errors generally within ±0.2 km, whereas Vendor 2 shows a broader spread and increased magnitude of errors, with some fault types experiencing location errors exceeding -1.9 km. For the fault at 80% of the line length, even if the magnitude of errors of Vendor 1 increases gradually, the errors remain under -1 km. On the other hand, Vendor 2 reveals significant errors in identifying the fault localization, with errors as large as -3.3 km. The increasing deviation with distance indicates that the fault locator algorithm of Vendor 2 is less robust when the length of transmission lines increases.

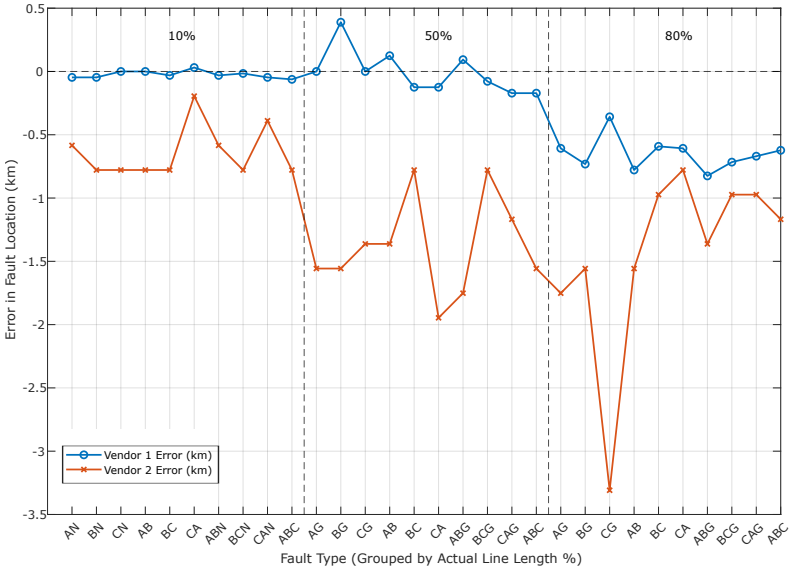

Figure 4.12: Fault location error comparison: Vendor 1 vs Vendor 2.

4.2 Performance testing based on statistical design of experiments

In the previous section, complete DR scheme testing is elaborated according to the proposed methodologies, which aim to go beyond the existing approaches outlined in the literature. Notice that to comply with the guidelines and requirements outlined in [31, 39], as well as the complete testing of the DR scheme, the size of the experiment becomes significantly large. This aspect presents considerable challenges, particularly concerning the experiment burden and duration of testing. Hence, the stat-DOE is introduced and integrated to determine an optimal set of scenarios and the number of tests, as well as handling the constraints between factors to avoid unnecessary experiments. The features and steps of the stat-DOE are reported in Table 4.8. Based on the steps illustrated in Table 4.8, the stat-DOE is applied to perform the performance testing of the commercial DRs, and each step is elaborated on in Section 4.2.2.

Table 4.8: Overview of the workflow for the stat-DOE [80].

STEP 1. Specify problem and objectives
STEP 2. Select the response variable
STEP 3. Choose factors, levels and ranges
STEP 4. Select the design
STEP 5. Conduct the experiment
STEP 6. Statistically analyse the data
STEP 7. Extract conclusions and recommendations

4.2.1 Test setup and experiment assumption

The test set-up shown in Figure 4.1 and the power system model depicted in Figure 4.13 are used for the experiment with the stat-DOE approach. The instrument transformers modeled in this study are ideal voltage and current transformers (with 115kV/115V and 1800A/1A ratios, respectively); no saturation is considered.

The device under test is the Schneider P543 relay, with four protection zones implemented therein (different from those 2 vendors mentioned in Section 4.1). The phase and ground characteristics of the P543 DR are

mho and quadrilateral, respectively. The resistive reach for all the zones of the quadrilateral element is set to 40 ohms by taking into account the utility requirements. The service settings of the P543 DR, calculated based on the power system model illustrated in Figure 4.13, are reported in Table 4.9.

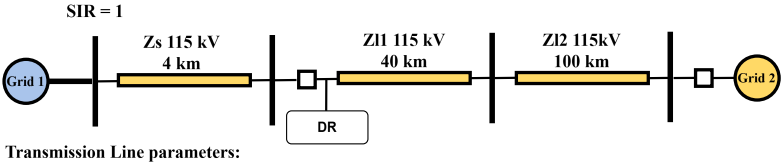

Figure 4.13: Transmission system model for stat-DOE study

Table 4.9: Service settings of the DR under test.

Zone	Setting (% of line impedance)	Operate time [ms]
1	85% of A-B	0
2	100% of A-B plus 50% of B-C	300
3	100% of A-B plus 120% of B-C	600
4	15% of the Zone 1 setting	600

Assumptions of this experiment

The assumptions used in this experiment are described hereafter.

- The measured response of the system is the operating time t, defined as the duration of the time interval between the fault inception and the receiving of the trip signal via GOOSE (excluding the CB operation).
- The typical operate time of the CB (including mechanical process and arc extinguishing) is 100 ms.
- For the sake of simplicity, only the performance of the DR at Zone 1 is evaluated.

- Unless otherwise specified, in this assumption when discussing pass/-fail criteria and operability regions for the DR, Although the main protection zone (Zone 1) shall operate "instantaneously", it can be acceptable to have the main protection operate just *faster* than the backup protection (Zone 2 and 3), to prevent wide-area blackout caused by the latter. As shown in Table 4.9, the operating time of Zone 2 is set at 300 ms. This is done to account for the CB operation and to introduce some safety margin, which is quantified in 200 ms to include the relay error, the overshoot time of the relay, and the error of the instrument transformers. Hence, the Zone 1 operation of the DR is assumed to be "correct" as long as $t < 200$ ms, with 200 ms being considered as the maximum acceptable operating time.

- The simulation is run for 12 seconds for each scenario to ensure that the power system returns to normal conditions before proceeding to the next test.

4.2.2 Application guideline of statistical design of experiments for performance testing

Step 1 – Specify problem and objectives

Prior to deployment, the electricity utility has to perform an acceptance test of the P543 DR. Without loss of generality, the focus is emphasized on the DR's Zone 1 operation. According to the technical manual provided by the manufacturer [65], the average operating times in Zone 1 range between 30 and 35 ms. Furthermore, considering the assumption for this experiment mentioned in Section 4.2.1, the operating time of DR can be accepted as long as $t < 200$ ms, i.e., *correct* operation, and when considering the constraints of both time and financial resources, it is assumed that a maximum of 100 tests can be conducted.

Step 2 – Choose the response variable

The response variable measured to test the DR performance is the operating time t of DR, defined as the duration of the time interval between the fault inception and the receiving of the trip signal by RTDS, excluding the operation time of the CB.

Step 3 – Choose factors, levels and ranges

According to the IEC 60255-121:2014 standard, four factors influence DR performance, which consists of fault location, fault inception angle, SIR, and fault type. These factors should be tested and evaluated, considering the levels reported in [31]. Furthermore, to reflect more realistic operating conditions, the effect of fault resistance (similar to other literature works, e.g., [6, 79, 91]) needs to be considered. Accordingly, the five design factors are subject of the experiment, which—along with their respective levels and the factors held constant—are presented in Table 4.10. The rationale for selecting these design factors and their corresponding levels is discussed in the following section.

Table 4.10: Design factors, their levels, and held-constant factors used for the experiment designed for the performance testing.

Design factors	Factor levels	Constant factors
Fault resistance [Ω]	0.001, 3, 6, 9	Service settings
Fault location [%]	5, 25, 50, 75, 85	based on
Fault inception angle [°]	0, 15, 30	Table 4.9
SIR [-]	0.2, 2, 5	
Fault type [-]	BN, AC, ABC, ACN	

- Faults of type BN, AC, ABC, and ACN are studied, as outlined in the IEC 60255-121:2014 standard [31].
- Given that the IEC 60255-121:2014 standard recommends only the positive half-cycle of the fault inception angle, with the most severe condition occurring at 0°—where the fault current reaches its peak magnitude—faults are simulated with inception angles of 0°, 15° and 30°.
- Since the focus is on evaluating the DR performance within Zone 1—configured to cover 85% of the protected line—faults are applied at locations representing 5%, 25%, 50%, 75% and 85% of the line length, with particular emphasis on locations near the boundary between Zones 1 and 2.
- Long, medium, and short transmission lines are investigated in accordance with the classifications outlined in the IEC 60255-121:2014

standard [31]. Since the SIR is the recommended criterion for classifying the types of transmission line configuration for the purpose of applying protective relays, representative SIR values of 0.2, 2 and 5 are selected for short, medium, and long lines, respectively [13].

- The IEC 60255-121:2014 standard [31] does not consider the fault resistance as a design parameter, recommending it be set to 0Ω—or to the minimum feasible value in cases of numerical limitations. However, non-zero fault resistances frequently occur in practical scenarios. Therefore, fault resistance values of 0.001Ω, 3Ω, 6Ω, 9Ω are considered in this study, with the selected range based on the recommendations in [92].

Step 4 – Select the design

Following Step 3, a mixed-level hybrid design space is established, characterized by five factors with varying numbers of levels. These factors include both quantitative variables—namely fault resistance, fault location, fault inception angle, and SIR—and a qualitative variable, fault type. It is important to highlight that the IEC 60255-121:2014 standard [31] recommends employing a full factorial design, which, given the current design space, would entail $4 \times 5 \times 3 \times 3 \times 4 = 720$ test runs. When each test is replicated four times to account for fault inception variability, a total of 2880 tests would be required. Given that only 5 tests can be performed per minute (as discussed in the assumption), the total experiment time would exceed 9 hours. Furthermore, if performance evaluations were to be extended to protection zones beyond Zone 1, or expanded to include more complex scenarios—such as evolving or simultaneous faults—or additional functionalities like tele-protection [6], several days of continuous testing would be inevitable. This size of experimentation may not align with the utility's available time and financial resources (which are presumed to restrict the number of feasible tests to 100), and this leads to considering a custom design.

Furthermore, Step 3 indicates that the set of design factors encompasses both fault type and fault resistance; therefore, the full factorial design would consist of scenarios that lack practical significance in reality, such as phase-to-phase faults (AC, ABC) occurring with non-zero resistance. From a mathematical perspective, this results in a limited design space that full factorial designs and other conventional designs cannot effectively handle.

Conversely, custom designs can effortlessly accommodate such features. Therefore, for all these reasons, a custom optimal design is chosen.

In detail, the custom design is generated with JMP [93] by:

(i) the *D*-optimality criterion is chosen to define the optimal design matrix based on the five design factors. The D-optimality of the design matrix (U) can be computed by [94]:

$$det(U^T U) = \frac{1}{det(U^T U)^{-1})} \tag{4.1}$$

(ii) the fault resistance of AC and ABC fault types shall be 0.001Ω;

(iii) the total number of tests = 100, as defined in Step 1.

The first ten runs of the 100-test custom design are shown in Table 4.11. It can be observed that phase-to-phase fault types are particularly linked to zero fault resistance values (0.001 Ω). To demonstrate and compare

Table 4.11: Excerpt of the design matrix generated with the custom design.

Run	**Fault Resistance** [Ω]	**Fault Location** [%]	**Fault Inception Angle** [°]	**Fault Type** [-]	**SIR** [-]
1	6	5	0	BN	2
2	6	25	0	ACN	2
3	0.001	25	30	ABC	0.2
4	9	25	0	BN	2
5	9	85	30	BN	2
6	6	25	0	BN	0.2
7	0.001	85	0	ABC	5
8	3	25	15	ACN	0.2
9	0.001	25	30	ABC	0.2
10	3	0	30	BG	5

the optimal design matrix between the 100-test custom design and the full factorial design based on the approach outlined in IEC 60255-121:2014 standard [31], the D-optimality index and the required numbers of tests are computed, and results reveal that the custom design has higher values of the optimality criteria compared to the full factorial design, as illustrated in Table 4.12. Based on the results shown in Table 4.12, the custom design is generated *without* the constraint (ii) since the full factorial design cannot

deal with constraints on the design space (here, the presence of disallowed combinations of factors) to be fair in evaluation with the same constraints between these two approaches. Moreover, when a minimum number of required tests is considered as a constraint, the custom design is way more "economical". The custom design matrix with constraint (ii) will be used for Steps 5 to 7.

Table 4.12: Comparison of the custom design (neglecting the constraint (ii)) and the full factorial design outlined in IEC 60255-121:2014 standard [31].

	Custom design without constraint (ii)	**Full factorial design**
D-optimality	57.09%	50.53%
N_{MIN}	26	1920

Step 5 – Conduct the experiment

The custom design has produced a 100-test design matrix, which includes constraint (ii), and this matrix is used to perform the experiment according to the test setup shown in Figure 4.1. The results from the experiment, reflecting the operating time, are recorded and further discussed in the following sections.

Step 6 – Statistically analyse the data

The experimental results are summarized in Figure 4.14 and indicate that the distribution of the operating time values is classified into two groups, with a clear distinction between test results where the relay operates "correctly" and "incorrectly" (indicated by green and red bars, respectively), based on the operability threshold of 200 ms, as defined in the experimental assumption. The cumulative distribution plot illustrates that $t < 200$ ms in almost 80% of the tests.

The histogram indicated in Figure 4.14 implies that the most significant effects on the operating time of DR are fault location, fault resistance and SIR. The interaction between fault location and fault resistance plays a significant role in the selectivity and impacts directly on the DR performance. Furthermore, the faults simulated for short lines result in

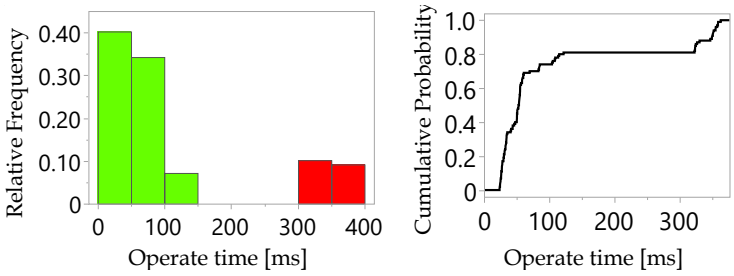

Figure 4.14: Histogram (left) and cumulative distribution plot (right) of the values of operating time [© 2024 IEEE].

longer operating times compared to medium and long lines, primarily due to the larger measurement error from instrument transformers stemming from the higher ratio of impedance in front of and behind the relay.

It is important to highlight that these findings correspond with those achieved through the full factorial design involving 2880 tests recommended by the IEC 60255-121:2014 standard [31]; in other words, the experiment based on the custom design with the stat-DOE can be achieved with an efficiency that is nearly 30 times greater while producing the same results—more details will be described in step 7.

Step 7 – Conclusions and recommendations

Ultimately, the experimental findings enable to draw conclusions that are beneficial not only for the utility but also for other stakeholders. As mentioned in Step 6, the most significant factors are fault location, fault resistance and SIR. Thus, plots involving the three significant factors can be produced. For instance, Figure 4.15 shows a modified version of the "SIR diagrams" recommended by the IEC 60255-121:2014 standard [31]. Fundamentally, in the standard, the SIR diagrams display the average, minimum, and maximum operating times (y-axis) for the different fault locations (x-axis) at different SIRs. Contrary to these, the SIR diagrams illustrated in Figure 4.15 display all the recorded operating times at each fault location, and the classification is determined using the operability threshold of $t = 200$ ms. Specifically, the average operating times' SIR diagrams are omitted since this data would hold little importance for

scenarios where, at a specific fault location, some operating times exceed the threshold while others fall below it, as illustrated in Figure 4.15a-b-c for a fault location equal to 85%.

It is also useful to create similar diagrams for various fault resistance values. These diagrams are displayed in Figure 4.16, which indicates that, for zero fault resistance values, the DR consistently operates within the threshold even at locations near the boundary (i.e., 85%); conversely, as fault resistance increases, the DR performance degrades and operates above the threshold even for faults point located far from the boundary.

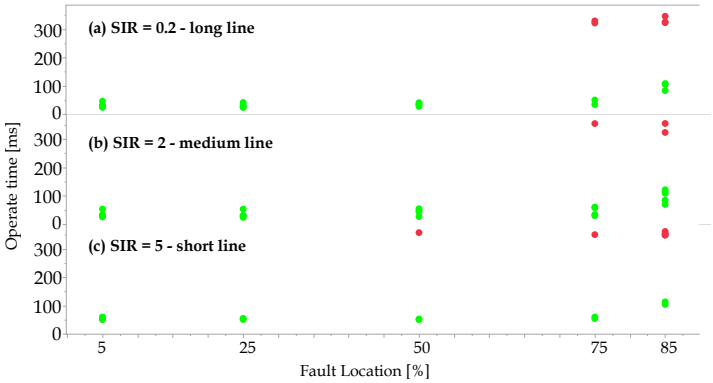

Figure 4.15: Operating times for long (a), medium (b) and short lines (c) [© 2024 IEEE].

Overall, some lines of refinement and recommendations for all stakeholders can be extracted, as discussed hereafter.

- The reporting of the test results as per the IEC 60255-121:2014 standard [31] could be enhanced. Specifically, regarding the SIR diagrams, it would be beneficial to consolidate all the operating times collected from every test into a single diagram, as illustrated in Figure 4.15, to prevent the use of meaningless average values when there is a significant variation in the operating times. Additionally, when incorporating other factors like fault resistance, similar diagrams (for instance, Figure 4.16) would help in thoroughly characterizing the relay's performance.

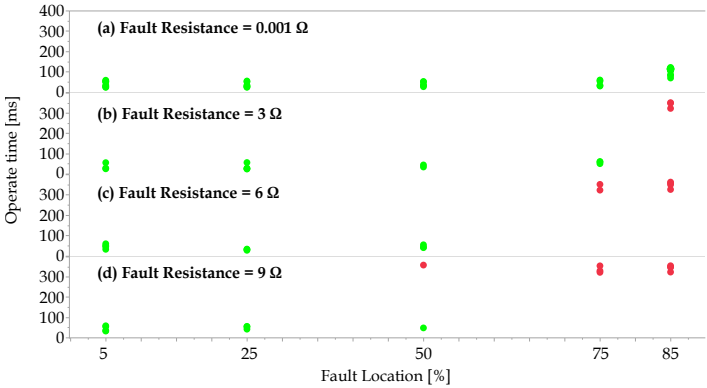

Figure 4.16: Operating time for Zone 1 for different fault resistance values [© 2024 IEEE].

- The IEC 60255-121:2014 standard [31] recommends conducting performance tests by maintaining a fault resistance of 0 Ω, which is presumably to align with the relay manufacturer's perspective. However, in realistic operating conditions, the relay performance is significantly impacted by fault resistance, both independently and in conjunction with fault location; thus, it cannot be neglected in a comprehensive evaluation of the relay performance test. Using stat-DOE, it is demonstrated that utilities can effectively analyze the influence of the most important factor, e.g., fault resistance, alongside other factors. Specifically, there are two advantages in examining the impact of fault resistance on relay performance covering a broader spectrum, for instance, from 0 to 9 Ω, as illustrated in Figure 4.16. In fact, firstly, the tests applying faults with zero resistance (e.g., Figure 4.16a) allow the utility to verify the compliance of the manufacturer's claims with the IEC 60255-121:2014 standard [31] (as reported in the relay technical manual). Secondly, the tests that involve faults with resistance values exceeding 0 Ω (e.g., Figure 4.16b-c-d) help the utility in determining the fault resistance levels at which relay misoperation occurs under realistic conditions. This information helps pinpoint further areas for improvement, such as the types

of additional protection functions that should be integrated into the protection system to handle high-resistance faults.

4.3 Conclusions

The developed test environment, transmission system model based on a real-time digital simulator, and methodologies for DR testing and validation are presented in this chapter to pinpoint possible unexpected operations under different operating conditions in power systems prior to deployment and to bridge the gaps between manufacturers and other stakeholders in the power system protection community—beyond the existing approaches outlined in the literature (only zone characteristics evaluation).

The performance of the two commercial DRs has been assessed in an ad-hoc developed use case by resorting to the proposed methodology and established requirements. This approach has proven to be a useful method for the TSOs to verify the compliance of DRs to specific requirements and identify any potential unexpected operations prior to their integration in the field. Moreover, the results in this chapter indicate that the proposed methodology based on established requirements reveals the following characteristics of some of the DRs tested:

- The DR of Vendor 2 lacks the selectivity for faults located at the boundary of zone 1 when the fault resistance is presented.
- The tele-protection scheme (POTT) of Vendor 2 may lead to maloperation since the carrier signal for POTT can be generated from any other function, even alarm functions, e.g., fuse failure.
- Regarding the power swing function, although the DR of Vendor 2 is able to differentiate the characteristics between power swing and fault, it operates with a time delay (500 ms). This ultimately may cause a coordination problem between primary and backup DRs., i.e., the primary and backup may operate simultaneously under this system condition.
- When the DR of Vendor 2 is applied to protect the long transmission line, it may cause errors in the fault localization.

By testing a broader spectrum of critical scenarios with respect to state-of-the-art testing approaches, the proposed methodology can effectively

help TSO assess the performance of commercial DRs in the acceptance and commissioning tests in a comprehensive manner. Ultimately, TSOs can easily select the DR(s) that are most appropriate for their applications.

Furthermore, a guideline for the application of the stat-DOE in DR performance testing is presented to minimize the number of scenarios and experiments, aligning with experiment burden and time constraints. The stat-DOE can (i) deal with constraints concerning resources and the input space more efficiently, (ii) minimize experimental burden by providing the optimal set of tests to perform, and (iii) facilitate a robust and objective interpretation of the experimental results through statistical analysis. Applying stat-DOE to determine the set of tests enables the consideration of operator-specific requirements (such as the maximum number of affordable tests) or physical constraints among inputs more effectively; ultimately, it allows a more comprehensive assessment of the DR performance under realistic operating conditions instead of just randomly deciding which and how many tests to perform.

When compared to advanced experimental approaches like OAT and full factorial, stat-DOE is significantly more efficient in producing the same amount of information at a much lower cost in terms of the number of tests conducted. For example, in the performance testing outlined in this chapter, the design matrix (number of tests) based on stat-DOE indicates an efficiency nearly 30 times higher than the full factorial design recommended by the IEC 60255-121:2014 standard. This ultimately illustrates that the stat-DOE can be beneficial for the testing activity, especially in resource-saving contexts.

5

Protection Scheme Development and IOP Testing

To address the challenges and drawbacks in the context of the overcurrent protection scheme and methodologies for IOP testing and validation formulated in Chapter 2, Section 2.6, this chapter presents:

(i) a GOOSE-based protection scheme to address MFFs to: enhance the performance of the overcurrent protection scheme within the digital substation in dealing with MFFs to avoid a wide area blackout of the distribution systems. The proposed method consists of two different approaches for fault detection: (i) impedance-based fault detection, and (ii) the voltage and current polarized method.

(ii) the developed test environment, distribution system model with the integration of distributed generation based on a real-time digital simulator, and methodologies for IOP testing and validation to: assess the comprehensive performance of the protection schemes of multi-vendor relays at the bay level by considering the impact of the distributed generation on the protection scheme under different operating conditions of the system, flexibly facilitate and replicate in testing other protection schemes, e.g., breaker failure, arc protection scheme, etc.

To effectively fulfill the research objectives of the proposed methods within the context of the overcurrent protection scheme and methodologies for IOP testing and validation, the requirements for performance evaluation are established as follows:

- the average operating time of the proposed protection scheme should be less than 100 ms for all scenarios where fault resistance is $\leq 2\Omega$;

- the average in percentage for fault detection accuracy should be higher than 95% for all scenarios without DG connection;
- the average percentage for the data exchange success rate should be higher than 95% for all scenarios without DG connection;
- the IOP verdict is determined as either "pass" or "fail" based on the following criteria: (i) **"pass" if the operating time of the proposed protection scheme** > 0, and (ii) **"fail" if the operating time of the proposed protection scheme** $= 0$

Therefore, this chapter focuses on how the proposed protection scheme can enhance the existing overcurrent protection scheme, as well as demonstrate how proposed methodologies for IOP testing can comprehensively validate the performance of the protection schemes with multi-vendor relays at the bay level. The proposed techniques and methodologies for addressing MFFs and IOP testing issues build upon the key findings presented in [3, 5, 7, 9] to tackle the third research question, as well as contribute to the fifth and sixth points mentioned in Chapter 1.

The rest of the chapter is organized as follows. Section 5.1 introduces the MFFs characteristic in the distribution system. The protection scheme based on IEC 61850 is elaborated in Section 5.2. Additionally, the proposed methodology for testing IOP at the bay level is presented in Section 5.3. The validations and results are expressed in Section 5.4, and the chapter conclusion is summarized in Section 5.5.

5.1 Multiple feeder faults (MFFs) in distribution systems

Figure 5.1: Multi-feeders structure on the same corridor [© 2023 IEEE].

As outlined in chapter 2, the economic reasons and the right-of-way limitations result in the construction of overhead distribution lines that contain multiple feeders on the same support structure, as indicated in Figure 5.1. This configuration can lead to the appearance of MFFs, which occurs due to fallen trees during thunderstorms or from trucks and cars colliding with the structure.

To describe the MFFs characteristic and its effect on the coordination of existing ORs within digital substations, the setting and coordination of ORs shown in Figure 5.2 are analyzed. This analysis is based on the substation topology depicted in Figure 5.3. It aims to highlight the vulnerability of the operation of the existing ORs to MMFs, even if all ORs can be coordinated.

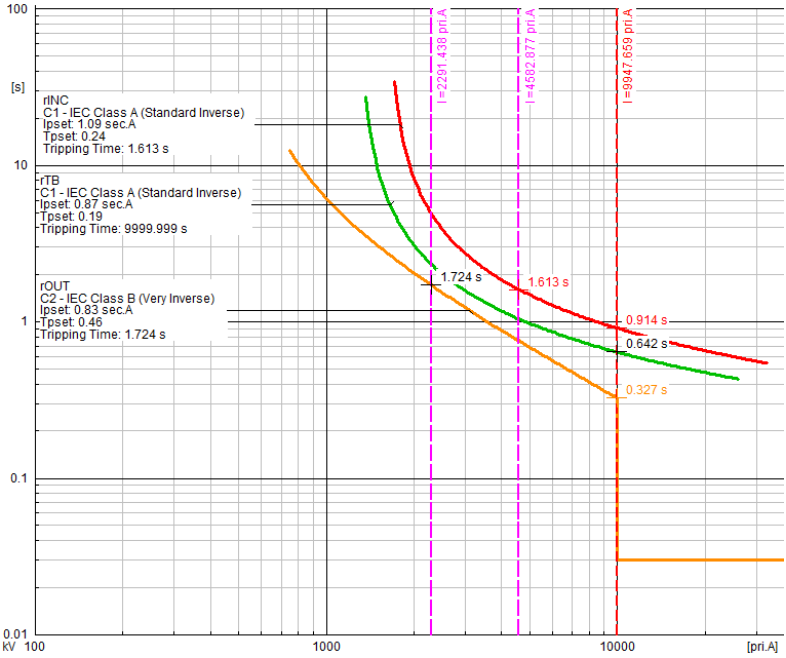

Figure 5.2: Overcurrent relays setting and coordination [© 2023 IEEE].

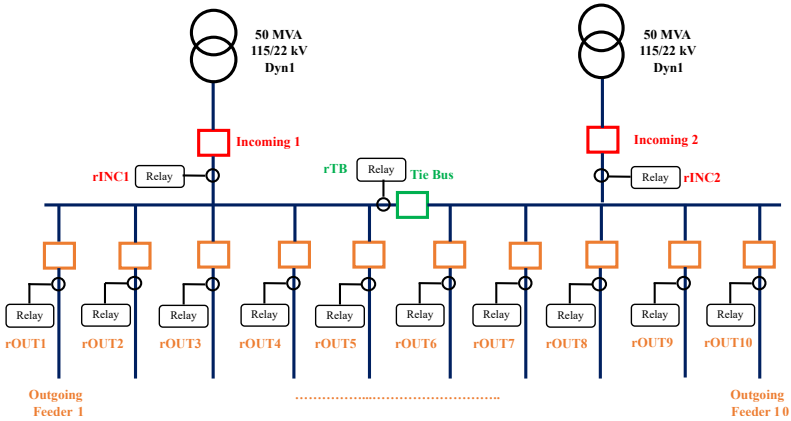

Figure 5.3: Substation topology [© 2023 IEEE].

In practice, the setting and coordination are derived from the short circuit study involving single feeders based on inverse time characteristics, as expressed in equation (5.1).

$$t = \frac{TMS \times A}{\left(\frac{I}{I_s}\right)^{\alpha} - 1} \tag{5.1}$$

where TMS is the time multiplier setting, I and I_s are the short circuit current and setting current, respectively. A and α are represented by 0.14 and 0.02 for standard inverse time characteristic, whereas for very inverse time characteristic, A and α are represented by 13.5 and 1. Principally, the maximum short circuit current magnitude of both phase and ground at the medium-voltage (MV) bus and the safety margin range of 0.3 and 0.4 seconds between main and backup relays are deployed for setting and coordination [40, 61].

In reference to Figure 5.3, the substation topology consists of 2 medium-voltage buses, two power transformers, and 10 feeders. During normal operating conditions, the CB at the tie bus is open, while the "Incoming 1" and "Incoming 2" CBs, along with all outgoing CBs, are closed. Consequently, after the short circuit study, the setting and coordination of ORs in such a substation can be derived and illustrated in Figure 5.2, where

the dashed-red line represents the maximum 3-phase short circuit current at the low-voltage side of the power transformer or MV bus. In such a coordination study, it is noticed that ORs can discriminate a feeder fault for all ranges of current values based on the defined safety margin.

On the other hand, once the MFFs occur in the system, the short circuit current magnitude seen by the incoming relay (rINC) is higher than that seen by the outgoing relays (rOUTs); here, two simultaneous feeder faults are used as an example to describe the characteristics of MFFs. In such a case, rINC measures the short circuit current approximately two times greater than that measured by the rOUTs. This leads to the rINC tripping faster than rOUTs, as indicated by the purple-dashed line in Figure 5.2 (1.613 s vs 1.724 s). Consequently, all feeders, including healthy ones, are de-energized from the system, leading to electrical blackouts in wide areas.

To delve into the details of the operation of rINC and rOUTs responding to MFFs in terms of operating times, the disturbance record of MFFs depicted in Figure 5.4 is used to elaborate on the OR operations based on inverse time characteristics and short circuit current. Hence, the operating times of the rINC and rOUTs to respond with the MFFs of two feeders can be expressed as follows:

$$t_{rINC} = \frac{0.24 \times 0.14s}{\left(\frac{6,687}{1,635 \times \sqrt{2}}\right)^{0.02} - 1} = 1.565s \tag{5.2}$$

$$t_{rOUT1} = \frac{0.46 \times 13.50s}{\frac{3,291}{498 \times \sqrt{2}} - 1} = 1.691s \tag{5.3}$$

$$t_{rOUT2} = \frac{0.24 \times 13.50s}{\frac{3,250}{498 \times \sqrt{2}} - 1} = 1.718s \tag{5.4}$$

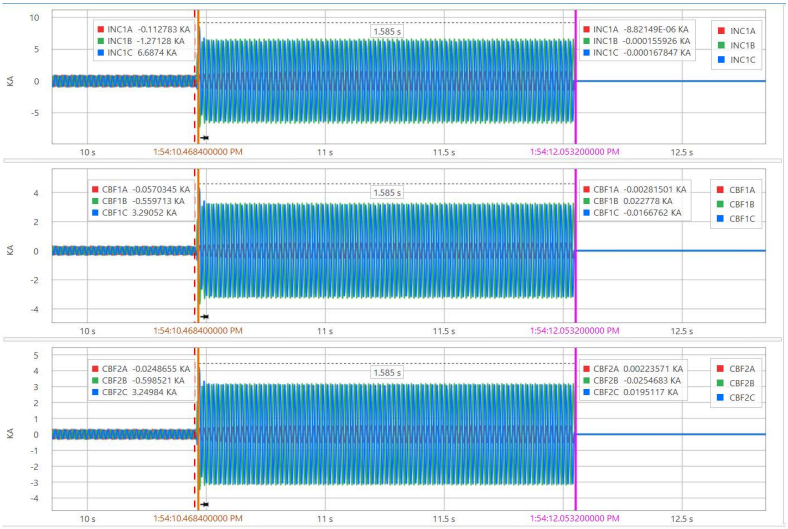

Figure 5.4: MFFs characteristic [© 2023 IEEE].

5.2 Proposed protection scheme based on IEC 61850

In addressing the MFFs within distribution systems and mitigating the risk of widespread blackouts resulting from rINC operating faster than rOUTs, a proposed protection scheme is developed based on the GOOSE communication protocol as specified in the IEC 61850 standard. The development of a protection scheme based on the IEC 61850 standard facilitates interoperability, enabling effective information exchange between relays from different vendors or between relays and systems, such as monitoring and control systems [95], as no proprietary protocol is required and no vendor-specific device is needed. Thus, the proposed protection scheme can be deployed in the digital substations using the internal logic and programming environment provided by OR manufacturers without the need for any additional equipment installation. The architecture of the proposed scheme is illustrated in Figure 5.5, and its operation, along with the information flow between rINCs, OR at the tie bus (rTB), and rOUTs, is detailed hereafter.

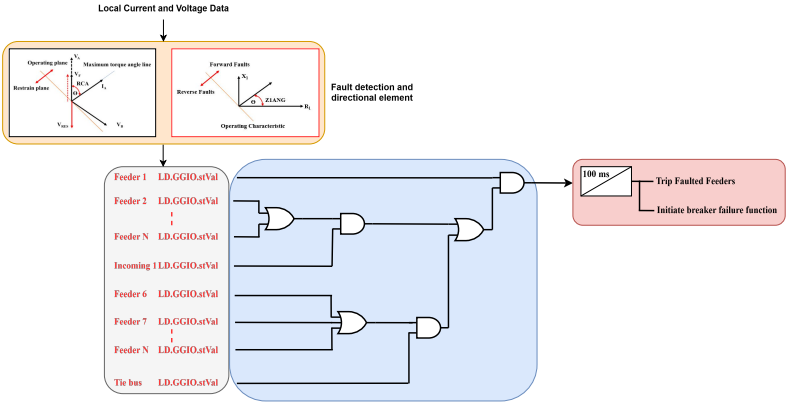

Figure 5.5: IEC 61850-based protection scheme for MFFs [3].

Operation of the overcurrent protection function

Since different types of DGs are connected to the distribution systems, the proposed scheme may experience unintended operation due to the DG in-feed effect. For example, if a fault occurs on an adjacent feeder, the rOUT may detect the fault in the reverse direction. For this purpose, a directional current detection is implemented to avoid the proposed scheme's maloperation and improve the selectivity in the presence of DGs. In the proposed protection scheme, two different approaches are deployed for MFFs detection: the so-called impedance-based fault detection and Relay characteristic angle (RCA) operation modes.

1) Impedance-based fault detection mode

The operation of this mode can be represented by:

$$(-90^\circ + \Theta_{Z_1}) < \widehat{\Theta}_{Z_1} < (90^\circ + \Theta_{Z_1}) \tag{5.5}$$

$$Z_2 = \frac{1}{I_2^2} Re[\overline{V_2}(\overline{I_2} \times 1\angle\Theta_{Z_1})^\star] \tag{5.6}$$

$$threshold = \begin{cases} Z_{2F} > 0, & 1.25 \times Z_{2F} - 0.25 \times |\frac{V_2}{I_2}| \\ Z_{2F} \leq 0, & 0.75 \times Z_{2F} - 0.25 \times |\frac{V_2}{I_2}| \end{cases} \tag{5.7}$$

where:

- $\overline{V_2}$ and V_2 are the complex value of the negative sequence voltage and its magnitude, respectively;
- $\overline{I_2}$ and I_2 are the complex value of the negative sequence current and its magnitude;
- Θ_{Z_1} is the positive sequence impedance angle;
- $\widehat{\Theta}_{Z_1}$ is the operating plane;
- Z_{2F} is the forward/reverse fault threshold.

It is important to note that Equation (5.5) is used to detect three-phase faults and activate the directional element (32PF), which corresponds to the relay word bit of the SEL relay for detecting three-phase faults [96]. This element measures the positive sequence voltage and current to derive the operating region on the R-X plane.

Equations (5.6) and (5.7) facilitate the detection of phase-to-phase, phase-to-phase-to-ground, and single-phase-to-ground faults, as these fault types are characterized by the presence of negative-sequence current and voltage components. Such fault types, the directional element (32QF), can also be activated by Equations (5.6) and (5.7) to identify forward and reverse faults. In the context of the 32QF element, the negative-sequence impedance (Z_2) is evaluated against a predefined forward fault threshold (Z_{2F}). If Z_2 is found to be less than Z_{2F}, the element identifies the fault as occurring in the forward direction. Conversely, if Z_2 exceeds Z_{2F}, a reverse fault condition is declared [57, 96]. The 32PF and 32QF directional elements determine the fault direction by analyzing the impedance characteristics on the R-X plane.

2) Relay characteristic angle operation mode

In the RCA operation mode for fault detection, a phase-to-phase voltage and the opposite phase current are measured to identify phase faults, as summarized in Table 5.1. This measurement approach typically follows a 90° connection principle, corresponding to an operating plane oriented ± 90° from the maximum torque line, as illustrated in Figure 5.6.

Table 5.1: Measured voltage and current for phase fault detection

Phase	Current	Voltage
A	I_A	V_{BC}
B	I_B	V_{CA}
C	I_C	V_{AB}

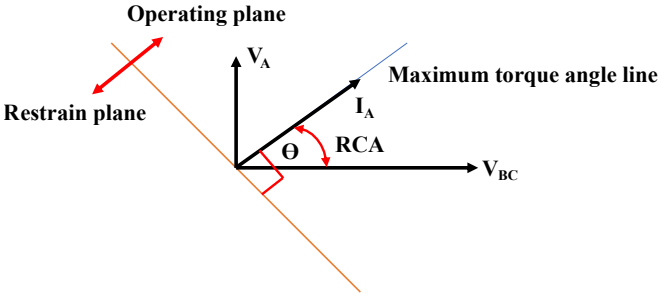

Figure 5.6: Phase fault detection based on 90° connections [© 2023 IEEE].

The selection of the RCA angle for phase fault detection is influenced by the specific characteristics of the power system. For example, (i) an angle of 30° is recommended for systems with a low R/X ratio and plain feeders where the zero-sequence source is located behind the relay, (ii) 45° is advised for transformer feeders with the zero-sequence source positioned in front of the relay, and (iii) 60° is recommended for systems connecting with a short section of cable [40, 65, 97]. In this work, an RCA angle of 30° is adopted.

To detect single-phase-to-ground faults, the residual voltage ($-3V_0$) is employed, as depicted in Figure 5.7. In this approach, the relay characteristics are influenced by the system's grounding. Recommended characteristic angles include (i) 0° for resistance-earthed systems, (ii) –45° for the distribution system with solidly-earthed, and (iii) –60° for the transmission system with solidly-earthed [40, 65, 97].

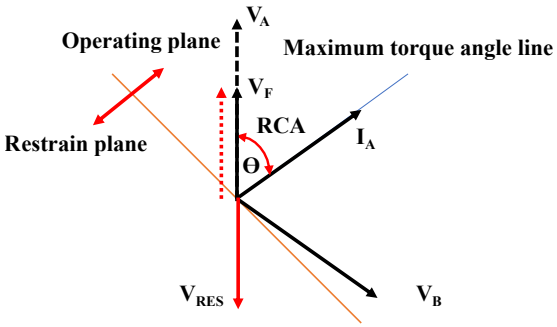

Figure 5.7: Ground fault detection based on 90° connections [© 2023 IEEE].

Incoming feeder relays

In the proposed scheme, rINCs are employed to transmit the GOOSE signal, which is responsible for activating and deactivating the proposed scheme during maintenance periods. As part of its design, the rINC receives "ON" and "OFF" status signals from the cut-off switch located at the switchgear panel.

Tie breaker relays

The rTB provides both phase and ground current detections, and the non-directional current detection is used, as the current can flow in both directions when the tie CB is closed. The GOOSE signal of the current detection is transmitted from the rTB to rOUTs, and the rTB does not need to subscribe to the GOOSE signal from other relays. Basically, the tie CB is closed when one of the power transformers at the substation is unable to be energized or requires maintenance.

Outgoing feeder relays

When MFFs occur in the system, the rOUTs independently detect them and must wait for confirmation signals from other rOUTs to verify that the MFFs have occurred in the system. Subsequently, the rOUTs transmit trip signals to open the associated CBs of the faulted feeders. In practice,

A delay time of 100 ms is implemented to prevent unnecessary operations triggered by transient events in the system, such as on-load switching or motor starting. In this work, to assess the performance and sensitivity of the proposed protection scheme responding to the MFFs, a delay time (100 ms) is not considered in the experiment. Each rOUT must be configured to publish both phase and ground current detection with directional elements to other relays to proceed according to the proposed scheme. In terms of the subscription, the rOUT receives signals from other rOUTs, the rTB (e.g., when the tie CB is closed for specific purposes such as maintenance), and the rINC.

IEC 61850 data model of the proposed protection scheme

An IEC 61850-based proposed protection scheme is developed and implemented with the data model illustrated in Figure 5.8, which consists of:

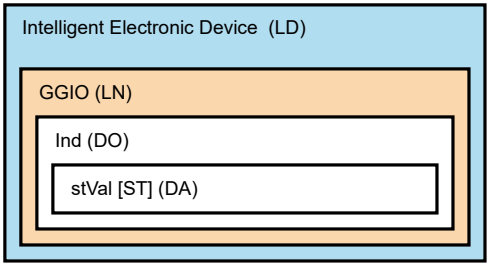

Figure 5.8: Proposed protection scheme data model [© 2023 IEEE].

- the Logical Device (LD), which represents the name of the physical relay;
- the "Generic process Input/Output (GGIO)" Logical Node (LN), which is used to represent the proposed protection scheme;
- the "Ind" Data Object (DO), which represents the information exchanged (in the form of binary output), belonging to the single point status (SPS) common data class [98];

- the "stVal" Data Attribute (DA), which contains a boolean signal for the proposed scheme [99].

Using this hierarchical data model, information can be exchanged between relays from different manufacturers through the Substation Configuration Language (SCL) [100, 101]. Specifically, the data model presented in Figure 5.8 is employed to represent the data model of the proposed protection scheme, as no LN is typically associated with the MFFs protection function within ORs. Furthermore, this data model is utilized to combine different types of boolean signals into one single GOOSE signal, e.g., phase and ground fault detection. Given that certain manufacturers impose restrictions on the number of GOOSE input signals. Hence, to avoid this problem, these signals are combined into one boolean signal. This approach reduces the number of GOOSE inputs to the subscriber, thereby facilitating protection engineers to test the proposed protection scheme and other schemes, e.g, breaker failure and arc detection, efficiently and conveniently with the same data model. The complete path of the hierarchical data model, which represents the "ON" and "OFF" status of the proposed protection scheme, is presented in Table 5.2. In this context, [ST] denotes the functional constraint "status information" of the "stVal" data attribute.

Table 5.2: Status of the proposed protection scheme signal

Logical expression	Binary value
LD.GGIO.IndX.stVal [ST] = “ON”	1
LD.GGIO.IndX.stVal [ST] = “OFF”	0

5.3 Proposed testing methodology for multi-vendor bay-level relays

5.3.1 Testing platform architecture

To validate the IOP of the protection and control schemes with multi-vendor relays at the bay level, the testing architecture shown in Figure 5.9 is developed and proposed. In this work, the proposed protection scheme discussed in Section 5.2 with multi-vendor relays is deployed to test as

an example. Hence, the IOP testing can be automated using a custom-developed script written in a C-type programming language to validate protection schemes of multi-vendor bay-level relays, as well as handle experiments, such as fault emulation, changing network topology, and recording results. The proposed testing architecture consists of the HiL connection of RTDS, amplifiers, and the relays under test. The details of each component involved in the proposed testing architecture are described hereafter.

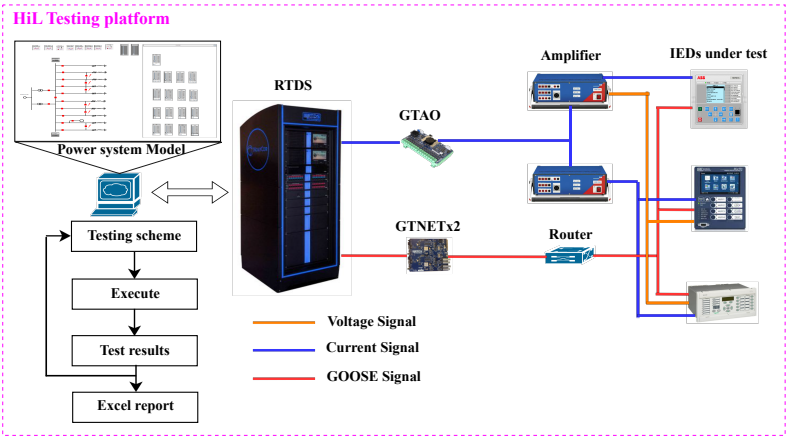

Figure 5.9: Proposed HiL testing platform for multi-vendors bay-level relays [© 2023 IEEE].

All binary signals—including starting signals for MFFs detection, trip commands, CB status indicators, and enable/disable MFFs control signals—are transmitted via GOOSE messages and are illustrated by red lines in Figure 5.9. Similarly, voltage and current signals are depicted using orange and blue lines, respectively.

Real Time Digital Simulator

The power system is modeled using RSCAD, whereas the simulation of faults and the communication of binary signals—such as circuit breaker

status, protection, and control signals—as well as the transmission of analog voltage and current signals to the physical devices connected to the testing platform, are performed by the NovaCore processing unit of the RTDS. The analog signals are transmitted to the power amplifiers integrated with the testing platform through the GTAO module, which directly interfaces with the physical GTAO card of the RTDS system. These signals, originating from the power system model, are delivered to the power amplifiers within a voltage range of ±10 V.

In this setup, the analog signals are delivered to the amplifiers through a wired connection from the GTAO card, while the NovaCore processor communicates with the GTAO module via a fiber optic connection through the GT port. Each analog channel of the GTAO module requires a defined scaling factor, determined by the amplifier's gain and the desired analog signal levels for the relays. For the exchange of boolean signals between the RTDS and the physical devices under test, the GTNETx2 card is utilized. The GTNETx2 card is connected to the NovaCore processor via a fiber optic cable through the GT port and interfaces with the testing platform using an RJ45 cable. The GOOSE protocol is activated through the GTNETx2 configuration. Hence, GOOSE signals can be published from the RTDS to the physical equipment through the GTNETx2 card by configuring the GSE module to determine a set of data to be exchanged.

Besides publishing the signals to the communication network, the GSE module is also used to subscribe to GOOSE signals from the relays. For this purpose, a word-to-bit converter element is required to map GOOSE input signals by transforming multi-word integers into multiple logical signals.

Relays under test

Three commercial ORs from different manufacturers, ABB, SEL, and Schneider, are used as devices under test and are integrated into the testing platform. These relays receive voltage and current signals from the secondary sides of voltage and current transformers. In this study, ideal current and voltage transformers (CTs and VTs) are employed, and the effects of transformer saturation are not considered. The CT ratio is set to 1500 A:1 A for the rINC and rTB, and 600 A:1 A for rOUTs. Additionally, the rOUTs require a three-phase voltage input to polarize the directional element, enabling them to determine the forward or reverse direction of

faults within the system. Hence, the VT ratio is configured as 22 kV:110 V.

Apart from analog values, starting and tripping signals for detecting and identifying MFFs generated by the relays are transmitted back to the RTDS and used for performance evaluation of the proposed scheme.

Amplifiers

In the developed testing platform, two power amplifiers—configurable via a web-based interface—are utilized to amplify the voltage and current signals supplied by the GTAO module, thereby enabling accurate generation of analog voltage and current signals at the secondary side for the relays. An analog input range of ± 7.071 V peak (corresponding to 5 Vrms) is adopted. One amplifier is configured to deliver both voltage and current outputs (3×300 V and 3×32 A), while the other is dedicated exclusively to current output (6×32 A) for the relays. At an input range of 5 Vrms, the amplification ratios of the two amplifiers are 60 V per 1 V for voltage signals and 6.4 A per 1 V for current signals [102]. These amplifiers are connected to both the GTAO card and the relays through wired connections.

5.3.2 Use case under study

A specific use case was developed to validate the IOP of the proposed protection scheme with the relays from different vendors. Such use cases involved modeling a part of the Provincial Electricity Authority of Thailand's (PEA) real distribution system, illustrated in Figure 5.10, using RTDS. The power system model includes two buses and five feeders, with detailed parameters provided in Table 5.3. The distribution line's length of 25 km represents the typical distance found in areas serving large commercial and industrial customers.

Real-time signal exchange among physical devices in the testing platform architecture is facilitated through RTDS, while Digsilent Power Factory software is utilized to derive equivalent parameters (source parameters illustrated in Table 5.3) from the power plant to the selected substation of interest for this investigation.

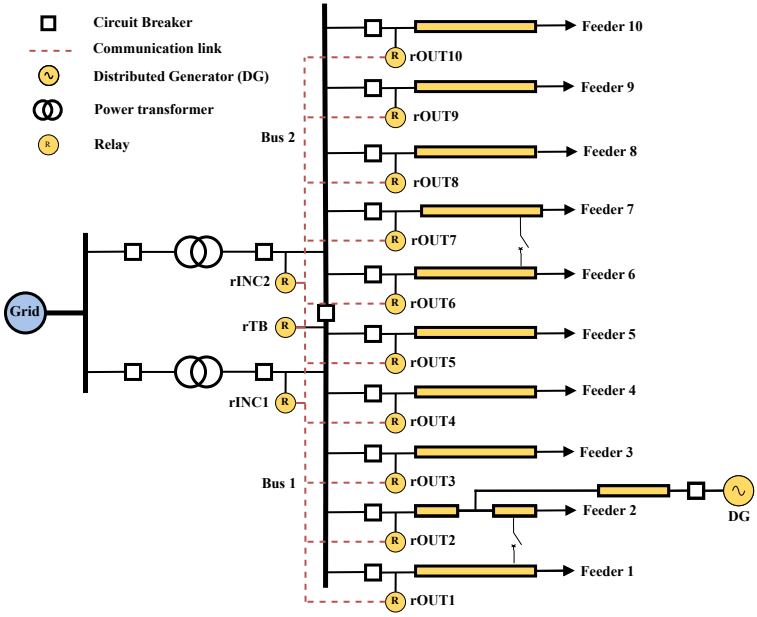

Figure 5.10: Power system model adopted for IOP testing [© 2023 IEEE].

The devices under test include three commercial relays: the ABB REF615, SEL 751, and Schneider P543. Specifically, the ABB REF615 is employed to represent the relay on the low-voltage (LV) side of the power transformer and at the tie CB (rINC1 and rTB). Meanwhile, the Schneider P543 is used as the feeder relay for protecting feeder 1 (rOUT1), and the SEL 751 is utilized for protecting feeder 2 (rOUT2).

The overcurrent settings for each relay, as expressed in Table 5.4, are calculated and coordinated according to the criteria set by the PEA [61]. A developed script will be executed to perform the tests, with the results of each test case being automatically recorded and stored in the form of CSV and Comtrade files.

Three test cases are developed to specifically represent scenarios of interest, encompassing the impact of all potential switching operations and the possible integration of DG. In each test case, ten signals from three

relays are transmitted back to the RSCAD when the relays can detect and identify the MFFs emulated within the RSCAD. Additionally, each relay receives the CB status from the simulated power system through the GOOSE protocol for the breaker failure function. To enable the proposed method, the Cut-off switch needs to be switched "ON" for all test cases.

Table 5.3: Parameters of the power system model.

Source parameters		
Positive sequence impedance	Z = 2.76 Ω	85.08°
Zero sequence impedance	Z = 3.47 Ω	86.26°
Power transformer at the substation		
Rated MVA		50 MVA
Rated Voltage (HV)		115 kV
Rated Voltage (LV)		23.10 kV
Short circuit impedance		13.80%
Vector group		Dyn1
Line parameters		
Positive sequence impedance	Z = 0.21 + j0.41 Ω/km	
Zero sequence impedance	Z = 0.35 + j1.63 Ω/km	
Power transformer at the point of common coupling		
Rated MVA		12.50 MVA
Rated Voltage (HV)		23.10 kV
Rated Voltage (LV)		6.60 kV
Short circuit impedance		10.00%
Vector group		YNyn0
Generator parameters		
Rated MVA		12.37 MVA
Rated Voltage		6.60 kV
Power factor		0.80
Direct Axis Synchronous Reactance, Xd		233.10%
Direct Axis Transient Reactance, X'd		21.60%
Direct Axis Sub-transient Reactance, X"d		15.60%
Negative Sequence Reactance, X2		17.10%
Zero Sequence Reactance, X0		7.30%

Table 5.4: Setting parameters of the three relays under test.

Information on the relay setting			
	rINC	rTB	rOUT
Manufacturer	ABB	ABB	SEL, Schneider
Model	REF615	REF615	751, P543
CT ratio HV	1500	1500	600
CT ratio LV	1	1	1
Phase overcurrent setting (50/51)			
Curve	SI	SI	VI
I>	1.09	0.87	0.83
TMS	0.24	0.19	0.46
I> >	-	-	16.60
Time (s)	-	-	Instantaneous
Ground overcurrent settings (50N/51N)			
Curve	SI	SI	VI
IN>	0.26	0.22	0.25
TMS	0.53	0.40	0.84
IN> >	-	-	16.60
Time (s)	-	-	Instantaneous

The IOP of the relays under test with the proposed method is assessed by evaluating the performance of the scheme's operation. The interoperability verdict is determined as either "pass" or "fail" based on the following criteria:

$$\text{verdict} = \begin{cases} \text{“pass” if operating time} > 0 \\ \text{“fail” if operating time} = 0 \end{cases} \tag{5.8}$$

From a practical standpoint, IOP testing is conducted by measuring the operating time, defined as the interval between the fault inception and the reception of binary signals from the relays by the RTDS. If the measured operating time is zero, the IOP test is considered to have failed, indicating that the proposed protection scheme fails to detect the MFFs. Nevertheless, under such conditions, alternative protection functions—such as high impedance fault (HiF) detection or existing overcurrent protection functions—are expected to respond to and isolate the fault with a delay time depending on the magnitude of the fault current. Such IOP testing

is critically important, as it enables the identification and verification of potential IOP issues that may arise when relays are integrated into a system. Furthermore, performing the IOP testing prior to field implementation facilitates the identification of the IOP boundary—the set of conditions (such as fault resistance values, MFFs types, and fault locations, etc.) that determine the IOP region, where a “pass” verdict is achieved, from the non-IOP region, where a “fail” verdict is observed. Ultimately, this may lead to the development of recommendations for relevant stakeholders, such as electric utilities, and bring guidance for future findings focused on complying with defined technical and operational requirements.

5.4 Validation and results

In this section, the power system model and parameters outlined in Figure 5.10 and Table 5.3, along with the relay settings specified in Table 5.4, are used to test three test cases using the HiL testing platform illustrated in Figure 5.9. The IOP testing is conducted in three different test cases, each specifically designed to evaluate the impact of all possible switching operations and the integration of the DG on the proposed scheme. Each test case involves ten types of the MFFs, encompassing single-phase-to-ground faults (AG, BG, CG), phase-to-phase faults (AB, BC, CA), and multi-phase-to-ground faults (ABG, BCG, CAG, and ABCG). To assess the IOP, ten binary signals are transmitted from the relays to the RTDS using the following designated names:

- "SELStr" represents the starting signal, both phase and ground fault detection of the rOUT2.
- "SELTr" represents the trip signal, both phase and ground fault of the rOUT2.
- "P543Str" represents the starting signal, both phase and ground fault detection of the rOUT1.
- "P543Tr" represents the trip signal, both phase and ground fault of the rOUT1.
- "SELMF" represents the trip signal operated by the proposed scheme of the rOUT2.

- "P543MF" represents the trip signal operated by the proposed scheme of the rOUT1.
- "ABBEFStr" represents the starting signal of a ground fault detection of the rINC and rTB.
- "ABBEFTr" represents the tripping signal of a ground fault detection of the rINC and rTB.
- "ABBPHStr" represents the starting signal of a phase fault detection of the rINC and rTB.
- "ABBPHSTr" represents the tripping signal of a phase fault detection of the rINC and rTB.

For each test case, a total of 300 scenarios are executed by emulating the MFFs occurrence between feeder 1 and feeder 2, using the parameter values specified in Table 5.5. Specifically, ten different MFFs types are simulated at each fault location. The fault resistance R_f is varied from 0.001 Ω to 10 Ω, encompassing both common and uncommon values of fault resistances in distribution networks, with increments of 2 Ω. Additionally, the fault location along the line varies from 5 km to 25 km in 5 km intervals.

Table 5.5: Parameter values for the IOP testing.

Fault Resistance (Ω)
0.001, 2, 4, 6, 8, 10
Fault distance (km)
5, 10, 15, 20, 25
Fault type
AG, BG, CG, AB, BC, CA, ABG, BCG, CAG, ABCG

5.4.1 Test case 1: No DG connected

In this test case, the network topology corresponds to the power system model depicted in Figure 5.10, where no DG is connected. Both incoming CBs are closed, while the tie CB remains open. This configuration represents normal operating conditions, allowing the power transformers at the substation to supply power to both buses. As illustrated in Figure 5.11,

the simulation results obtained using the parameter values specified in Table 5.5 indicate that a lack of IOP, as defined by equation (5.8), occurs exclusively for the single-phase-to-ground fault types AG, BG, and CG, which are represented by red dots. In contrast, all other fault types consistently result in a "pass" IOP outcome, depicted by green dots, regardless of fault location or the value of the resistance.

Further insights are provided in Figure 5.12, which illustrates the operating times of the proposed scheme for the two relays under an AG-type MFFs. As depicted, the region of non-IOP (indicated by red cells) is confined to scenarios where the fault resistance $R_f \geq 8\ \Omega$ and the fault occurs at a distance of 25 km. In such cases, the rINC trips more rapidly than the rOUTs, potentially leading to a wide-area blackout. A similar pattern is observed for BG and CG fault types. However, it is important to note that due to the nature of MFFs, which typically involves at least two conductors across two feeders, single-phase-to-ground MFFs are less probable compared to multi-phase-to-ground or phase-to-phase faults.

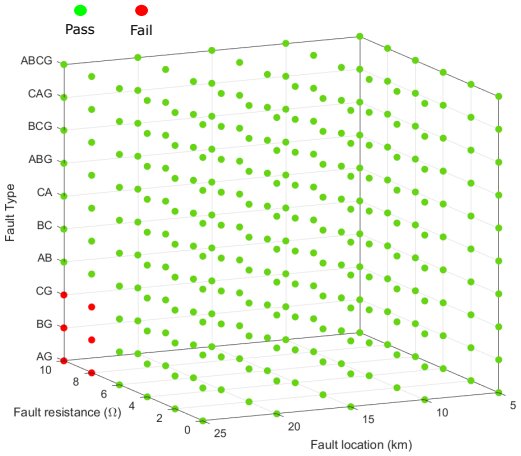

Figure 5.11: Test case 1. IOP verdict for rOUT1 of all fault types for different fault resistance values and fault locations. Same results are observed for rOUT2 [© 2023 IEEE].

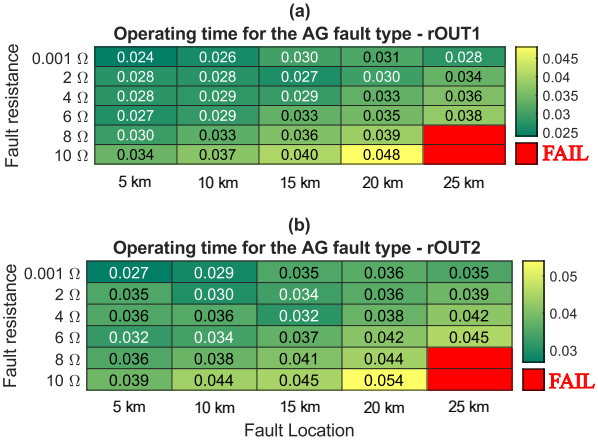

Figure 5.12: Test case 1. Operating times of rOUT1 and rOUT2 in the case of an AG MFFs type for different fault resistance values and fault locations [© 2023 IEEE].

Furthermore, Figure 5.13 shows the starting and tripping signals issued by the three relays under test in response to an AG-type MFFs occurring at a distance of 25 km in the system, for two fault resistance values: $R_f = 0.001\ \Omega$ (a) and $R_f = 8\ \Omega$ (b). As illustrated in Figure 5.13a, the proposed scheme demonstrates correct operation with both rOUTs, as indicated by the activation of the "SELMF" and "P543MF" binary signals.

In this scenario, only the relays associated with the faulted feeders operate to isolate the MFFs, allowing the healthy outgoing feeders to remain continuously energized without interruption. Such an operation is applied for all parameter combinations that result in a "pass" IOP outcome, as depicted in Figure 5.11. Conversely, when $R_f = 8\ \Omega$, the proposed scheme fails to detect the AG-type MFFs when the fault occurs 25 km from the substation. Under these conditions, the IOP test results in a failure verdict, as the proposed scheme is unable to detect and identify the high-resistance MFFs. In this case, only the rINC detects the MFFs, as indicated by the activation of the "ABBEFStr" binary signal in Figure 5.13b. A similar response is observed for the BG and CG MFFs fault types.

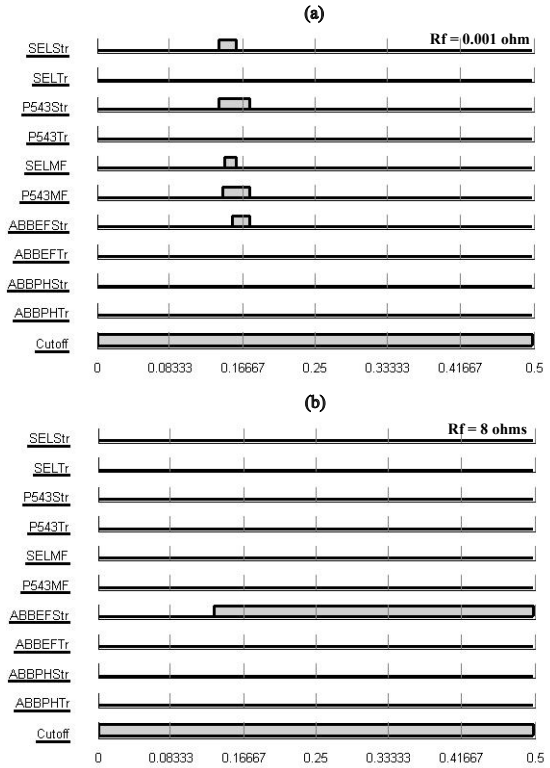

Figure 5.13: Test case 1. Detection of the AG MFFs type at 25 km with fault resistance 0.001 ohm (a) and 8 ohms (b) [© 2023 IEEE].

5.4.2 Test case 2: only one transformer energized on bus 2 without DG connected

The network topology for this test case corresponds to the power system configuration shown in Figure 5.10, where no DG units are connected. In this test case, incoming 2 and the tie CBs are closed, while incoming 1 CB is open. This topology represents a scenario in which the power transformer

connected to bus 1 is either de-energized or undergoing maintenance. As illustrated in Figure 5.14, simulation results based on the parameter values listed in Table 5.5 indicate that, consistent with the findings from Test Case 1, IOP failures—defined by equation (5.8)—occur exclusively for fault types AG, BG, and CG. All other fault types consistently result in a "pass" verdict for IOP, regardless of the fault location or the value of the resistance.

Further insights are provided in Figure 5.15, which presents the operating times of the proposed scheme for the two relays under BG-type MFFs. The results indicate that the proposed scheme maintains IOP for all fault locations when the fault resistance $R_f \leq 6\ \Omega$. However, for $R_f \geq 8\ \Omega$, the proposed scheme fails to detect BG-type MFFs occurring 25 km from the substation. Similar behavior is observed for AB and CG MFFs types. The same considerations were discussed in Test Case 1 concerning the low probability of occurrence of single-phase-to-ground MFFs.

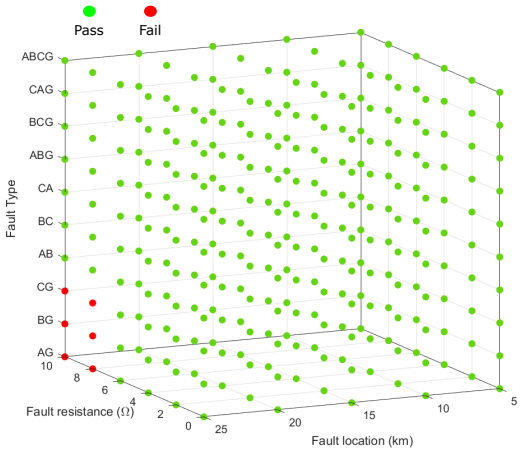

Figure 5.14: Test case 2. IOP verdict for rOUT1 of all fault types for different fault resistance values and fault locations. Same results are observed for rOUT2 [© 2023 IEEE].

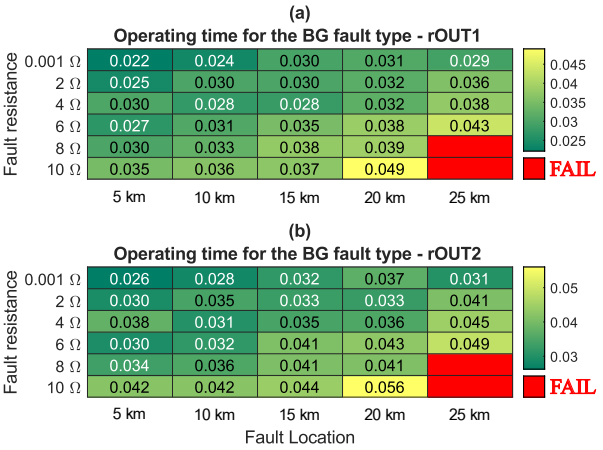

Figure 5.15: Test case 2. Operating times of rOUT1 and rOUT2 in the case of an BG MFFs type for different fault resistance values and fault locations [© 2023 IEEE].

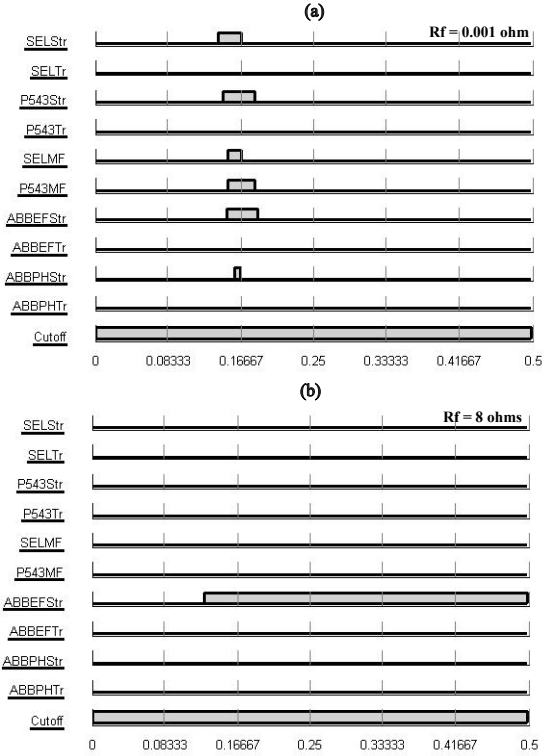

Figure 5.16: Test case 2. Detection of the BG MFFs type at 25 km with fault resistance 0.001 ohm (a) and 8 ohms (b) [© 2023 IEEE].

When the fault resistance is equal to $R_f = 0.001\ \Omega$, the proposed scheme successfully detects the MFFs, as indicated by the activation of the "SELMF" and "P543MF" signals shown in Figure 5.16a. In contrast, for $R_f = 8\ \Omega$, only the rTB is capable of detecting the MFFs, as indicated by the "ABBEFStr" binary signal in Figure5.16b. This behavior is recorded for AG and CG MFFs types as well. In such cases, the rTB operates more

rapidly than the outgoing feeders, resulting in the disconnection of all feeders connected to bus 1, including healthy feeders.

5.4.3 Test case 3: two transformers energized with DG connected

The network topology for this test case is based on the power system model depicted in Figure 5.10, with a DG unit connected to feeder 2, located 3 km from the substation. Both incoming CBs are closed, while the tie CB remains open. The operation of the OR at the DG connection point is not taken into account, as the analysis focuses solely on assessing the IOP of the proposed scheme in the presence of the DG's in-feed effect.

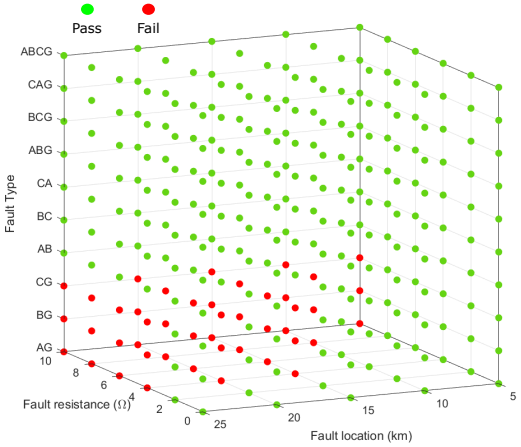

Figure 5.17: Test case 3. IOP verdict for rOUT1 of all fault types for different fault resistance values and fault locations. Same results are observed for rOUT2 [© 2023 IEEE].

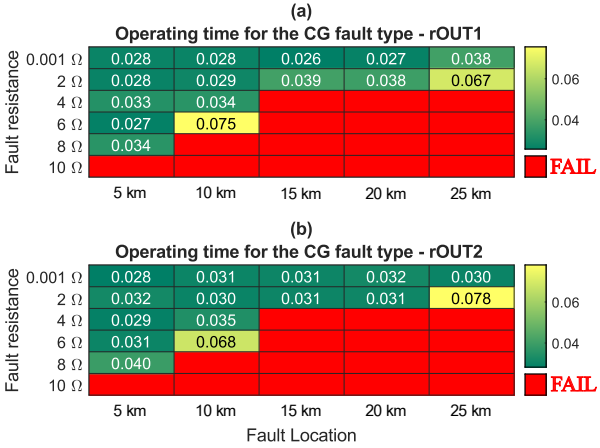

Figure 5.18: Test case 3. Operating times of rOUT1 and rOUT2 in the case of an CG MFFs type for different fault resistance values and fault locations [© 2023 IEEE].

As illustrated in Figure 5.17, simulation results obtained using the parameter values specified in Table 5.5 indicate that non-IOP—defined by equation (5.8)—occurs exclusively for fault types AG, BG, and CG. For all other fault types, the IOP criterion is consistently satisfied, regardless of fault location or resistance value.

Additional insights are provided in Figure 5.18, which displays the operating times of the prooposed scheme for the two relays under a CG-type MFFs. Compared to Test Cases 1 (Figure 5.12) and 2 (Figure 5.15), the non-IOP region is noticeably broader. Specifically, IOP failures are observed for fault resistances $R_f \geq 4\ \Omega$ and fault locations beyond 10 km. When $R_f \geq 10\ \Omega$, a failure verdict is recorded regardless of the fault location. A similar pattern is observed for AG and BG fault types. This reduction in the proposed scheme's IOP is primarily attributed to the in-feed effect of the DG, which adversely affects current detection by the outgoing feeders (rOUTs) in the case of single-line-to-ground faults. Overall, the integration of DG, along with increases in fault resistance and fault location, reduces the protection coverage of the rOUTs. Furthermore, Figure 5.19 presents the starting and tripping signals issued by the three

relays under test in response to a CG-type MFFs occurring 15 km from the substation, for fault resistance values of $R_f = 0.001\ \Omega$ (a) and $R_f = 4\ \Omega$ (b).

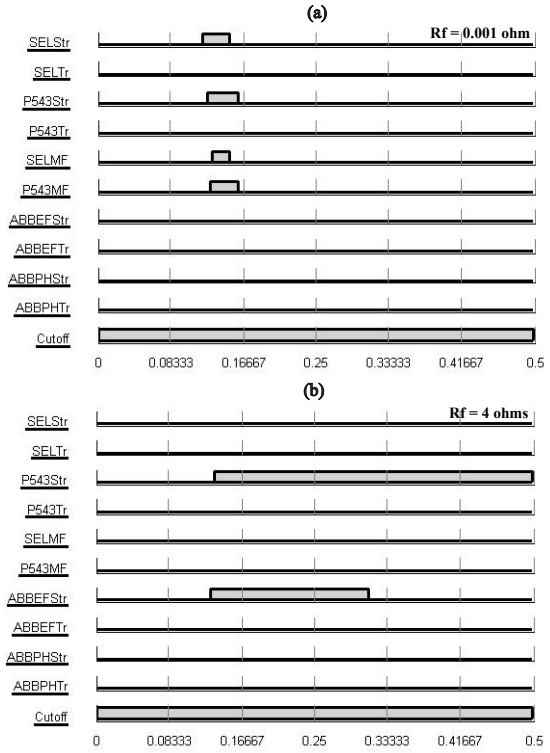

Figure 5.19: Test case 3. Detection of the CG MFFs type at 15 km with fault resistance 0.001 ohm (a) and 4 ohms (b) [© 2023 IEEE].

As illustrated in Figure 5.19a, the proposed scheme demonstrates correct operation for all fault types and locations for both rOUTs. However, when $R_f = 4\ \Omega$, the proposed scheme fails to detect a CG-type MFFs located

15 km from the substation. In this case, only rOUT1 and rINC respond to the fault, as indicated by the activation of the "P543Str" and "ABBEFStr" signals in Figure 5.19b. Although the fault occurs in front of both rOUT1 and rOUT2, detection is achieved only by rOUT1. Accordingly, rOUT1 operates to separate the fault based on its inverse time characteristic.

5.5 Conclusions

An IEC 61850-based protection scheme is introduced in this chapter to address MFFs in the distribution systems. The proposed scheme can improve the selectivity and reliability of the ORs within digital substations by isolating only the faulted feeders while the healthy ones remain energized in the case of MFFs.

In addition, testing methodologies and techniques are developed to test and validate the proposed protection scheme in the context of the IOP of multi-vendor bay-level relays at a system level. Furthermore, since a custom-developed script for handling experiments, such as fault emulation, changing network topology and system parameters, and recording results, is integrated into the proposed testing architecture, the IOP testing can be conducted automatically. The data model represented in the proposed scheme can be replicated to test other protection functions at the bay level, e.g, breaker failure and arc detection. Ultimately, the proposed testing methodologies are more efficient and convenient compared to the approaches provided in the literature discussed in Chapter 2. With the proposed testing methodologies, electricity utilities can test and validate the protection and control schemes according to their requirements more efficiently and flexibly before the field implementation.

All test cases are elaborated to investigate all possible switching operations and the impact of DG integration, excluding the operation of OR at the DG connection point. Except for the case of single-line-to-ground MFFs, with the proposed scheme, customers connected to the unfaulted feeders experience uninterrupted service during MFFs, ultimately improving service quality and availability, minimizing outage-related costs, and improving network reliability. Unlike conventional ORs applied for MFFs scenarios, the proposed approach ensures that healthy feeders remain fully connected and energized to the system.

Considering the average operating time of the proposed scheme for test cases 1 and 2, when the MFFs are detected, the average operating time

for all scenarios is less than 100 ms, as illustrated in Figure 5.20. However, the fault detection accuracy is slightly dropped to 94%, as depicted in Figure 5.21, when $R_f \geq 8\ \Omega$ and faults occur at the end of the feeder (e.g., 25 km).

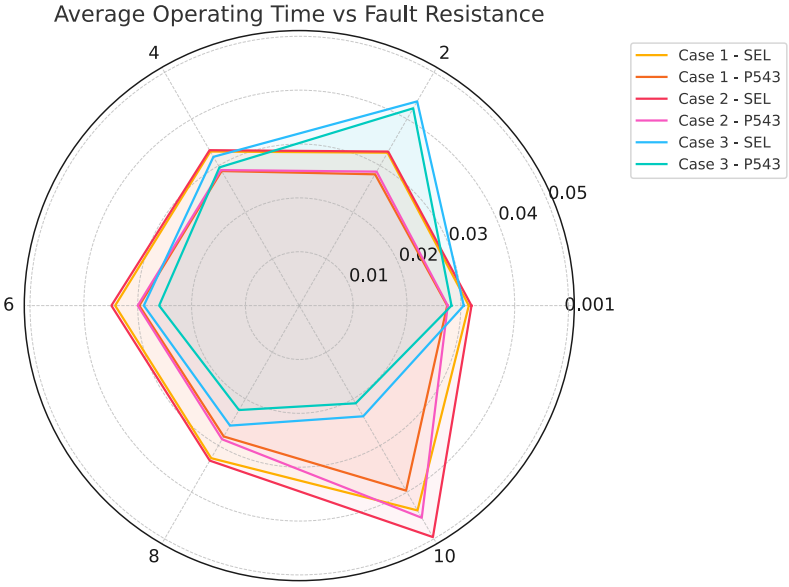

Figure 5.20: Average operating time of the proposed protection scheme for test cases 1 to 3.

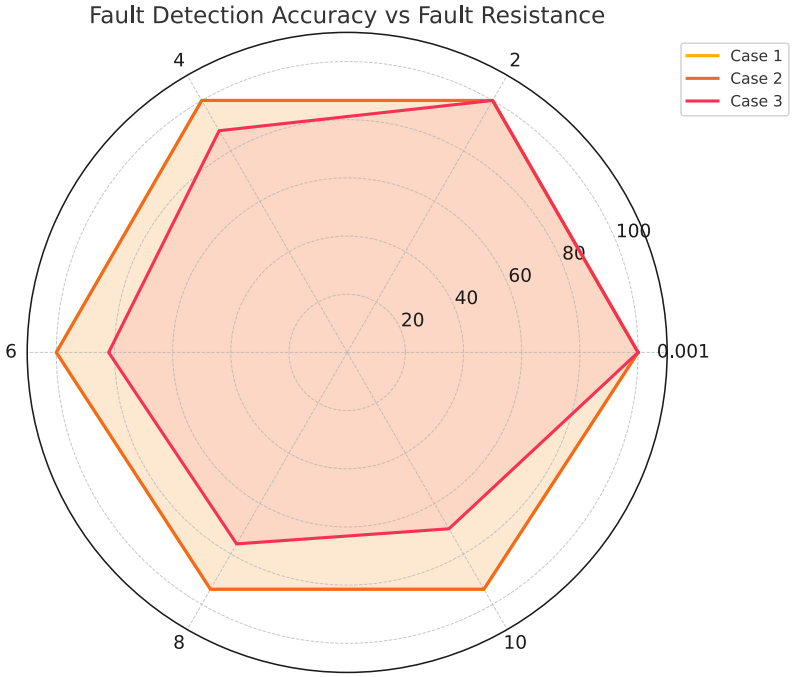

Figure 5.21: Fault detection accuracy with different R_f.

In the case of DG connection, test case 3, when the MFFs are detected, the average operating time of the proposed scheme is less than 100 ms, as illustrated in Figure 5.20. However, fault detection accuracy drops to approximately 85% when $R_f = 4$ and reaches its lowest accuracy of around 68% at $R_f = 10$, as depicted in Figure 5.21. In this test case, the region of non-IOP is expanded when a DG is connected to the distribution network, particularly for $R_f \geq 4$ and for fault locations situated relatively close to the substation. Such worsening of interoperability occurs when the DG is installed near the substation, as examined in this study, representing a potential worst-case scenario for current detection in both forward and reverse directions.

In addition, seamless communication between relays at the bay level is presented (scoring = 98%) for all scenarios of test cases 1 and 2, as depicted in Figure 5.22, when four different manufacturers exchange information via GOOSE to implement the proposed protection scheme. For test case 3, the success rate of data exchange decreases to 86% when fault resistance increases beyond 2 Ω, and this issue is caused by external factors (uncontrollable), specifically, power system fault-related issues that result in information not being exchanged between relays.

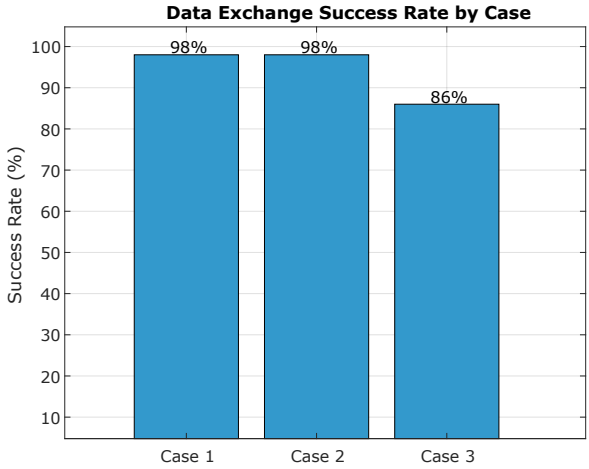

Figure 5.22: Data exchange success rate in percentage in case of the proposed scheme operated success

Last but not least, since the MFFs characteristic typically involves at least two conductors from different outgoing feeders, the magnitude of the fault current is sufficiently high to enable detection by the proposed scheme. Furthermore, it is important to highlight that high-resistance faults can potentially be addressed by using a HiF function, which is commonly available in commercial relays. However, the effectiveness of HiF technologies in mitigating the impact of such faults requires thorough validation and might be a topic for further investigation.

6

Conclusion

This work addresses the gaps in the DR setting and coordination, DR and IOP testing, as well as the performance of ORs within digital substations. Since this work is motivated and guided by three research questions, the key findings based on those questions are as follows:

- The proposed method based on graph theory and MDFS can be applied to determine paths within protection zones for DR setting and coordination, regardless of the network topologies without errors. Furthermore, the proposed methods can reduce the computational burden and time by limiting the search space with respect to the protection zones of the DRs—less complexity and time during graph traversal compared to the conventional approaches presented in the literature.

- An MDFS-based algorithm for DR setting is able to automatize the entire process of DR settings with multiple DRs, providing the parameter settings for both mho and quadrilateral characteristics, as well as additional functions for modern DRs, by taking into account potential infeed effects in the system. Furthermore, various setting criteria can be applied, and parameter settings from different manufacturers can be mapped, resulting in better accuracy and less computational time; unlike the approaches discussed in chapter 2, which focus only on zone characteristics themselves and some specific criteria.

- An MDFS-based algorithm for DRs coordination validation is able to validate multiple settings of DRs from different manufacturers, as well as identify miscoordination problems and paths to provide

lists of DR miscoordination among primary and backup relays in the system with less expensive the computational resources and time, approximately 50 times compared to the approaches discussed in the literature.

- Considering DR testing, findings in this work indicate that the proposed methodology for DR testing can cover critical scenarios beyond the existing testing approaches outlined in the literature in which TSOs can perform the tests to: (i) verify the DR performance based on their own specific requirements for acceptance and commissioning tests, and (ii) to check the compliance with IEC 60255-121:2014 standard according to the manufacturer's claimed.

- In case of experiment burden and time constraints in the DR testing activity, stat-DOE can be applied to the DR testing to reduce the experimental time by determining the optimal set of scenarios and the number of tests to conduct without harming or limiting the efficacy and generalization. The stat-DOE has proven that, producing the same results, the experiment based on the custom design with the stat-DOE can be achieved with an efficiency that is nearly 30 times that of the full factorial approach.

- A proposed protection scheme has proven that it is able to deal with MFFs in the distribution systems by identifying and separating only the faulted feeders without any impact on the healthy feeders, resulting in the reduction of outage areas.

- The proposed methodology and technique indicate that the performance of the protection scheme of multi-vendor bay-level relays can be comprehensively tested and validated at the system level to identify the potential IOP issues of the protection schemes under different operating system conditions before deployment, more efficiently and flexibly compared to the available approaches that require predefined analog values to generate initial signals for each test scenarios.

6.1 Research achievements

Throughout this work, the setting and coordination of DRs in transmission systems are developed, followed by a methodology and approach for DR

testing to validate DR's characteristics and the additional functions that enhance DR performance under different system conditions. Furthermore, IEC 61850-based protection scheme and a methodology for IOP testing within digital substation are presented.

As motivated in Chapter 1 for the first and second contributions, in Chapter 3, an algorithm based on graph theory and MDFS is developed and proposed to determine the paths within protection zones of DRs for setting and coordination. With the proposed method, the paths within protection zones of DRs can be correctly identified without errors stemming from the network topologies. Unlike, the approaches presented in the literature that is limited to the simple network topology. This ultimately leads to a decrease in search complexity and an increase in efficiency compared to the conventional approach, as discussed in Chapter 3. In addition, algorithms for DR setting and coordination are presented: (i) to automatize the entire DR settings process and handle DR setting under different TSOs' criteria, considering the possible infeed effects, (ii) parameter settings mapping based on commercial DRs since different manufacturers have different techniques (different parameter settings) in fault detection, (iii) to mitigate under- and over-reach problems at zone 2 setting. In contrast, previous works focus on specific criteria and defining reference DRs to be used as references for DR setting and coordination, but they still lack a complete DR setting. This leads to still requiring effort and time for DR setting.

Furthermore, to reduce computational resources and time, graph theory and MDFS-based algorithms are developed to identify miscoordination problems and paths to provide lists of DR miscoordination among primary and backup relays, without requiring the protection coordination study by performing fault simulation. With such an approach, the miscoordination problems between pairs of DRs in the system can be validated more efficiently, as discussed and expressed in Chapter 3. Unlike the approaches presented in the literature discussed in Chapter 2. As discussed aforementioned, it is noted that these two contributions enhance DR setting and coordination, providing practical tools that improve efficiency and reliability in setting and coordination.

To align with contributions 3 and 4, the proposed methodology and stat-DOE are presented for DR testing, as discussed in Chapter 4. Compared to the previous approaches discussed in Chapter 2, the proposed methodology for DR testing, in addition to focusing on zone characteristics and basic

accuracy of the DR, enables TSOs to verify the full scheme of DR under various system conditions beyond the existing approaches. Based on the proposed methodology leads the TSOs to observe and capture some specific properties of the DRs before implementation. Ultimately, it enables TSOs to make decisions in selecting DRs from different manufacturers that meet their specific application requirements. Furthermore, suppose the experiment burden and time constraints are considered in the testing activity. In that case, the stat-DOE can be applied to the DR testing to minimize the set of the input design matrix (the number of tests) to be conducted without loss of generality. As discussed in Chapter 4, the stat-DOE has demonstrated that, given the same results, it is more effective when compared to OAT and full factorial approaches. Furthermore, compared to advanced experimental approaches like OAT and full factorial, with the stat-DOE, it is not only physical constraints among inputs, e.g., the constraint of fault resistance in the case of phase-to-phase fault, can be handled, but also the interaction between design factors, e.g., SIR and fault inception angle can be captured, unlike, OAT and full factorial approaches. This leads to stat-DOE being more efficient at a much lower cost in terms of the number of tests conducted compared to the other approaches, especially the approach outlined in the IEC 60255-121:2014 standard, which the findings in this work indicated that stat-DOE has an efficiency nearly 30 times higher than the full factorial design.

Regarding contributions 5 and 6 discussed in Chapter 5, to fill the gap in the operation of ORs in addressing MFFs in the distribution system, the IEC 61850-based protection scheme is proposed. Three commercial relays and two approaches in fault detection are implemented: (i) current and voltage polarization and (ii) impedance-based fault detection to perform the proposed scheme. The findings discussed in Chapter 5 indicate that the outage areas caused by the MFFs can be reduced by the proposed method. This leads to an improvement in the quality of services and the reliability of the system. Moreover, the IOP region and boundary of the operation of the protection scheme based on multi-vendor bay-level relays can be identified; this information reveals the limitations (caused by controllable and uncontrollable factors) of the protection scheme before the deployment. Hence, DSOs are able to identify solutions to handle such scenarios in advance to maintain the system more secure and reliable.

Furthermore, the methodology and technique for IOP testing to assess the performance of the protection schemes at the bay level of the digital

substation are proposed. Since the conformity of relays with the standard does not guarantee their IOP from different vendors, the proposed method aims to validate the IOP problems that may arise when integrating relays from different manufacturers. This validation process is essential for ensuring that the protection schemes function correctly at the system level before deployment. With the proposed method, DSOs can comprehensively investigate the IOP problem under various system conditions, which are overlooked by the works in the literature, to ensure that protection schemes operate properly, even in transient scenarios, without predefining the analog values for each test scenario, e.g., voltage and current signals, like the previous works discussed in Chapter 2. This results in the proposed method being more flexible and efficient compared to previous approaches when scaling up and replicating the test setup are needed.

6.2 Outlook

Looking ahead, some opportunities exist to build upon the findings of this work. Referring to the DRs coordination discussed in Chapter 3, further investigations are required to optimize the zone 3 reaches of the DR in case miscoordination problems are presented, as well as provide solutions by considering the stability aspects in the case of high penetration of inverter-based renewable energy resources.

The integration of inverter-based renewable energy resources introduces specific challenges for DR due to their limited and controlled fault current contributions. Hence, in such system conditions, further investigations are needed other than the findings discussed in Chapter 4, particularly in examining the differences between grid-forming and grid-following inverter control strategies. Such a study would offer deeper insights into how it impacts the performance of the DR, as well as the response of the DR to such system conditions.

According to the findings presented in Chapter 5, the IOP region and boundary are caused by different factors, which include both controllable and uncontrollable factors that directly impact the proposed protection scheme, particularly in the cases of high resistance fault and DG connected to the distribution systems. Although high-resistance faults may be addressed using a HiF function, the effectiveness of HiF technology in mitigating high-resistance faults needs to be verified appropriately and may require further investigation. Moreover, further investigations are

needed to thoroughly validate how different fault detection techniques of ORs respond to the in-feed effects of DG across various locations and capacities. This will include examining the MFFs resistance, the MFFs location, and the MFFs types.

A

Curriculum Vitae

Work experiences

September 2020 – December 2025: Research Assistant at the *Institute for Automation of Complex Power Systems* of the RWTH Aachen University, Aachen, Germany.

2010 – 2020: Electrical engineer with the *Provincial Electricity Authority of Thailand (PEA)*, Bangkok, Thailand.

2008 – 2009: Electrical engineer with the *PowerGrid international limited*, Bangkok, Thailand.

Education

September 2020 – December 2025: Doctoral degree (Dr.-Ing.) at the RWTH Aachen University, Aachen, Germany.

2009 – 2013: Master of Engineering in *Electrical Power* at the Kasetsart University, Bangkok, Thailand.

2005 – 2008: Bachelor of Engineering in *Electrical Power* at the King Mongkut's Institute of Technology Ladkrabang, Bangkok, Thailand.

List of Acronyms

CB Circuit Breaker 13

DFS Depth-First Search 2, 161

DG Distributed Generators xviii

DR Distance relay 1, 161

DSO Distribution System Operator 6

GOOSE Generic Object-Oriented Substation Events 4

HiF high impedance fault 132

HiL Hardware-in-the-Loop 3

IOP interoperability 4, 163

MDFS Modified Depth-First Search 8, 162

MFFs Multi-Feeders Faults 4, 163

OAT one-at-a-time 3

OR Overcurrent relay 4

RTDS Real Time Digital Simulator 86

SIR Source Impedance Ratio 32, 161

stat-DOE Statistical Design of Experiments 8, 162

TSO Transmission System Operator 3

List of Figures

List of Tables

Bibliography

[1] Thanakorn Penthong, Antonello Monti, and Ferdinanda Ponci. "Distance Relay Setting and Validating Based on Graph Theory and Modified Depth-First Search". In: *Under review IEEE Transactions on Industrial Informatics* (2025).

[2] Mirko Ginocchi et al. "Statistical Design of Experiments for Power System Protection Testing: A Case Study for Distance Relay Performance Testing". In: *IEEE Access* 12 (2024), pp. 27052–27072. DOI: 10.1109/ACCESS.2024.3367591.

[3] Thanakorn Penthong et al. "IEC 61850-Based Protection Scheme for Multiple Feeder Faults and Hardware-in-the-Loop Platform for Interoperability Testing". In: *IEEE Access* 11 (2023), pp. 65181–65196. DOI: 10.1109/ACCESS.2023.3280128.

[4] Mirko Ginocchi et al. "Global sensitivity analysis of distance protection performance for submarine transmission systems". In: *14th Mediterranean Conference on Power Generation Transmission, Distribution and Energy Conversion (MEDPOWER 2024)*. Vol. 2024. 2024, pp. 406–411. DOI: 10.1049/icp.2024.4694.

[5] Thanakorn Penthong et al. "Hardware-in-the-Loop Validation of AC/DC Service Restoration including industrial IED and Communication Protocols". In: *2024 Open Source Modelling and Simulation of Energy Systems (OSMSES)*. 2024, pp. 1–6. DOI: 10.1109/OSMSES62085.2024.10668962.

[6] Thanakorn Penthong et al. "Testing Methodology for Performance Evaluation of Distance Protection Relays for Transmission Systems". In: *2023 IEEE Belgrade PowerTech*. 2023, pp. 1–6. DOI: 10.1109/PowerTech55446.2023.10202837.

[7] Thanakorn Penthong, Erdem Gümrükcü, and Ferdinanda Ponci. "Laboratory of Power System Automation: an example of activity". In: *2022 IEEE German Education Conference (GeCon)*. 2022, pp. 1–6. DOI: 10.1109/GeCon55699.2022.9942765.

[8] Muhammad Zeeshan Khattak et al. “Evaluation of the Impact of the Cable Model on the Distance Protection Performance in a Submarine Transmission System”. In: *PESS 2024; Power and Energy Student Summit*. 2024, pp. 137–142.

[9] Thomas I. Strasser et al. “Towards interoperability testing of smart energy systems – an overview and discussion of possibilities”. In: *14th Mediterranean Conference on Power Generation Transmission, Distribution and Energy Conversion (MEDPOWER 2024)*. Vol. 2024. 2024, pp. 263–268. DOI: 10.1049/icp.2024.4670.

[10] Cesar Cazal et al. “Automation Framework for Blockchain-Based Coordination of Distributed Energy Resources”. In: *2024 IEEE 15th International Symposium on Power Electronics for Distributed Generation Systems (PEDG)*. 2024, pp. 1–6. DOI: 10.1109/PEDG61800.2024.10667360.

[11] Ramin Vakili et al. “An Algorithmic Approach for Identifying Critical Distance Relays for Transient Stability Studies”. In: *IEEE Open Access Journal of Power and Energy* 8 (2021), pp. 107–117. DOI: 10.1109/OAJPE.2021.3064514.

[12] N. Praneeth et al. “Finding Optimal Zone II Settings for Distance Relays in Coordination With Directional Overcurrent Relays Using QCQP Algorithm”. In: *IEEE Access* 12 (2024), pp. 143658–143674. DOI: 10.1109/ACCESS.2024.3466557.

[13] Institute of Electrical and Electronics Engineers. *IEEE Std C37.113-2015 (Revision of IEEE Std C37.113-1999). IEEE Guide for Protective Relay Applications to Transmission Lines*. 2016.

[14] Siemens. *SIPROTEC 5 Basic Structure of the Function 2 Distance Protection, Line Differential Protection, and Breaker Management for 1-Pole and 3-Pole Tripping System Functions 3 Applications 4 Function-Group Types and Bay Proxy 5 7SA87, 7SD87, 7SL87, 7VK87, Technical manual*. Tech. rep. accessed Apr. 18, 2025. Siemens, 2024. URL: chrome-extension://efaidnbmnnnibpcajpcglclefindmkaj/https://support.industry.siemens.com/cs/attachments/109742440/SIP5_7SA-SD-SL-VK-87_V09.90_Manual_C011-Q_en.pdf.

[15] General Electric. *MiCOM Agile P443 Distance Protection for Central European Applications, Brochure*. Tech. rep. accessed Apr. 18, 2025. General Electric, 2018. URL: chrome-extension://efaidnbmnnnibpcajpcglclefindmkaj/https://www.gevernova.com/grid-solutions/products/brochures/p443_fw85-brochure-en-2018-08-grid-ga-1059.pdf.

[16] Juan F. Piñeros. "Intelligent model to automatically determine and verify distance relays settings". In: *Electric Power Systems Research* 217 (2023), p. 109137. ISSN: 0378-7796. DOI: https://doi.org/10.1016/j.epsr.2023.109137.

[17] ETAP. *Transmission and Distribution Protection*. Tech. rep. accessed Sep. 14, 2025. 2025. URL: Availableonline:https://etap.com/product/starz-distance-relay-coordination.

[18] Asma Assouak and Rabah Benabid. "Setting and coordination of distance relays in interconnected power systems using DIgSILENT PowerFactory software". In: *2022 2nd International Conference on Advanced Electrical Engineering (ICAEE)*. 2022, pp. 1–5. DOI: 10.1109/ICAEE53772.2022.9962071.

[19] Jon Kleinberg and Eva Tardos. *Algorithm design*. Pages: 73. Boston, MA, US: Pearson Education, Inc., 2006.

[20] J.L. Gross and J. Yellen. *Graph Theory and Its Applications (2nd ed.)* Chapman and Hall/CRC, 2005. ISBN: 9780429190544. DOI: https://doi.org/10.1201/9781420057140.

[21] Ji-Soo Kim et al. "An Islanding Detection Method for Multi-RES Systems Using the Graph Search Method". In: *IEEE Transactions on Sustainable Energy* 11.4 (2020), pp. 2722–2731. DOI: 10.1109/TSTE.2020.2972948.

[22] M. Tasdighi and M. Kezunovic. "Automated Review of Distance Relay Settings Adequacy After the Network Topology Changes". In: *IEEE Transactions on Power Delivery* 31.4 (2016), pp. 1873–1881. DOI: 10.1109/TPWRD.2016.2524654.

[23] T.S. Sidhu et al. "A new approach for calculating zone-2 setting of distance relays and its use in an adaptive protection system". In: *IEEE Transactions on Power Delivery* 19.1 (2004), pp. 70–77. DOI: 10.1109/TPWRD.2003.820202.

[24] Kleber M. Silva et al. “An Algorithm to Mitigate the Infeed Effect on Overreaching Distance Zones Settings”. In: *IEEE Transactions on Power Delivery* 37.4 (2022), pp. 3345–3356. DOI: 10.1109/TPWRD.2021.3128131.

[25] R. Ramaswami et al. “Enhanced Algorithms for Transmission Protective Relay Coordination”. In: *IEEE Transactions on Power Delivery* 1.1 (1986), pp. 280–287. DOI: 10.1109/TPWRD.1986.4307920.

[26] Mohammad Dolatabadi and Yaser Damchi. “Graph Theory Based Heuristic Approach for Minimum Break Point Set Determination in Large Scale Power Systems”. In: *IEEE Transactions on Power Delivery* 34.3 (2019), pp. 963–970. DOI: 10.1109/TPWRD.2019.2901028.

[27] Lufeng Liu and Lijun Fu. “Minimum Breakpoint Set Determination for Directional Overcurrent Relay Coordination in Large-Scale Power Networks via Matrix Computations”. In: *IEEE Transactions on Power Delivery* 32.4 (2017), pp. 1784–1789. DOI: 10.1109/TPWRD.2016.2583222.

[28] *Technical requirements for the connection and operation of customer installations to the high voltage network (TAR high voltage)*. 2018.

[29] Provincial Electricity Authority. *Provincial Electricity Authority's Regulation on the Power Network System Interconnection Code*. Tech. rep. B.E.2559. accessed Jan. 4, 2023. Provincial Electricity Authority, 2016. URL: https://www.pea.co.th/Portals/0/Document/vspp/PEA%20Interconnection%20Code%202016.pdf.

[30] IEEE-PSRC-Working-Group. *Processes, Issues, Trends and Quality Control of Relay Settings*. Tech. rep. accessed Apr. 18, 2025. IEEE-PSRC-Working-Group, 2007. URL: chrome-extension://efaidnbmnnnibpcajpcglclefindmkaj/https://www.pes-psrc.org/kb/report/095.pdf.

[31] International Electrotechnical Commission. *Measuring relays and protection equipment – Part 121: Functional requirements for distance protection*. 2014.

[32] Alexander Novikov, Jose Jesus de Chavez, and Marjan Popov. “Performance Assessment of Distance Protection in Systems with High Penetration of PVs”. In: *2019 IEEE Milan PowerTech*. 2019, pp. 1–6. DOI: 10.1109/PTC.2019.8810491.

[33] Jonathan Loebel, Florian Mahr, and Johann Jaeger. “HiL Ground Fault Distance Protection Tests of Novel Zero Sequence Control VSC”. In: *2024 IEEE Power Energy Society General Meeting (PESGM)*. 2024, pp. 1–5. DOI: 10.1109/PESGM51994.2024.10689074.

[34] Li Yang et al. “Design and Performance Testing of a Multivendor IEC61850–9-2 Process Bus Based Protection Scheme”. In: *IEEE Transactions on Smart Grid* 5.3 (2014), pp. 1159–1164. DOI: 10.1109/TSG.2013.2277940.

[35] Juan R. Camarillo-Peñaranda, Mauricio Aredes, and Gustavo Ramos. “Hardware-in-The-Loop Testing of a Distance Protection Relay”. In: *IEEE Transactions on Industry Applications* 57.3 (2021), pp. 2326–2331. DOI: 10.1109/TIA.2021.3066328.

[36] Atieh Delavari et al. “Real-Time Modeling and Testing of Distance Protection Relay Based on IEC 61850 Protocol”. In: *2019 IEEE Canadian Conference of Electrical and Computer Engineering (CCECE)*. 2019, pp. 1–5. DOI: 10.1109/CCECE43985.2019.9052403.

[37] Bin Wang et al. “RTDS Environment Development of Ultra-High-Voltage Power System and Relay Protection Test”. In: *IEEE Transactions on Power Delivery* 23.2 (2008), pp. 618–623. DOI: 10.1109/TPWRD.2008.915818.

[38] Andrea Bonetti, Murty V.V.S. Yalla, and Stig Holst. “The IEC 60255-121:2014 standard and its impact on performance specification, testing and evaluation of distance protection relays”. In: *2016 IEEE/PES Transmission and Distribution Conference and Exposition (T&D)*. 2016, pp. 1–6. DOI: 10.1109/TDC.2016.7520031.

[39] Provincial Electricity Authority. *Acceptance Requirements*. Tech. rep. PEA-AC 1/2561. accessed Apr. 14, 2025. 2017. URL: Availableonline:https://www.pea.co.th/Webapplications/tor/Attachments/09e3a977-3321-4f4c-a71a-ecaff6e36e29/%E0%B8%A3%E0%B9%88%E0%B8%B2%E0%B8%87%E0%B9%80%E0%B8%AD%E0%B8%81%E0%B8%AA%E0%B8%B2%E0%B8%A3%E0%B8%9B%E0%B8%A3%E0%B8%B0%E0%B8%81%E0%B8%A7%E0%B8%94%E0%B8%A3%E0%B8%B2%E0%B8%84%E0%B8%B2.pdf.

[40] ALSTOMGRID. *Network Protection and Automation Guide*. Alstom Grid, 2011. ISBN: 978-0-9568678-0-3.

[41] Jorge Betanzos Manuel et al. “Protecting distribution feeders for simultaneous faults”. In: *2010 63rd Annual Conference for Protective Relay Engineers*. 2010, pp. 1–9. DOI: 10.1109/CPRE.2010.5469496.

[42] Xi Chen, Peter A Crossley, and Hao Guo. “Design, construction and validation of a next generation protection and control system based on IEC61850 standards”. In: *12th IET International Conference on Developments in Power System Protection (DPSP 2014)*. 2014, pp. 1–6. DOI: 10.1049/cp.2014.0037.

[43] International Electrotechnical Commission. *IEC 61850 - Communication networks and systems for power utility automation*. 2013.

[44] Provincial Electricity Authority. *SUBSTATION CONTROL AND PROTECTION SYSTEM (SCPS)*. Tech. rep. RSUB-010/2560 (Rev. 1.0). 2017.

[45] Metropolitan Electricity Authority. *SUBSTATION AUTOMATION SYSTEMS Based on the IEC 61850 Communications Standard*. Tech. rep. PM9-0028-WBX. 2016.

[46] S. Roostaee, R. Hooshmand, and Mohammad Ataei. “Substation automation system using IEC 61850”. In: *2011 5th International Power Engineering and Optimization Conference*. 2011, pp. 393–397. DOI: 10.1109/PEOCO.2011.5970443.

[47] Patrick Montignies, Philippe Angays, and Laurent Guise. “IEC 61850 in the Oil and Gas Industries”. In: *IEEE Industry Applications Magazine* 17.1 (2011), pp. 36–46. DOI: 10.1109/MIAS.2010.939430.

[48] Mohammad Aurangzeb, Bruno Andre, and Luc Hossenlopp. “IEC 61850 capabilities applied to Oil and Gas industry”. In: *2010 Record of Conference Papers Industry Applications Society 57th Annual Petroleum and Chemical Industry Conference (PCIC)*. 2010, pp. 1–7. DOI: 10.1109/PCIC.2010.5666843.

[49] Giovanni Manassero et al. “IEC61850–Based Systems—Functional Testing and Interoperability Issues”. In: *IEEE Transactions on Industrial Informatics* 9.3 (2013), pp. 1436–1444. DOI: 10.1109/TII.2012.2217977.

[50] Xi Chen. “Performance Analysis of IEC 61850 Process Bus and Interoperability Test among Multi-Vendor System”. In: *Published PhD thesis*. accessed Apr. 18, 2025. 2016. URL: chrome-extension://efaidnbmnnnibpcajpcglclefindmkaj/https://research.manchester.ac.uk/files/60826406/FULL_TEXT.PDF.

[51] Jian-Cheng Tan, Vince Green, and John Ciufo. “Testing IEC 61850 based multi-vendor substation automation systems for interoperability”. In: *2009 IEEE/PES Power Systems Conference and Exposition*. 2009, pp. 1–5. DOI: 10.1109/PSCE.2009.4840228.

[52] Power System Relaying and Control Committee Relaying Communication and COntrol Subcommittee Working Group H6. *Application Testing of IEC 61850 Based Systems*. 2020.

[53] Jian-Cheng Tan, Vince Green, and John Ciufo. “Testing IEC 61850 based multi-vendor substation automation systems for interoperability”. In: *2009 IEEE/PES Power Systems Conference and Exposition*. 2009, pp. 1–5. DOI: 10.1109/PSCE.2009.4840228.

[54] R. Aguilar and J. Ariza. “Testing and configuration of IEC 61850 multivendor protection schemes”. In: *IEEE PES TD 2010*. 2010, pp. 1–8. DOI: 10.1109/TDC.2010.5484210.

[55] Hany F. Habib, Nevin Fawzy, and Sukumar Brahma. “Performance Testing and Assessment of Protection Scheme Using Real-Time Hardware-in-the-Loop and IEC 61850 Standard”. In: *IEEE Transactions on Industry Applications* 57.5 (2021), pp. 4569–4578. DOI: 10.1109/TIA.2021.3091417.

[56] Aushiq Ali Memon and Kimmo Kauhaniemi. “Real-Time Hardware-in-the-Loop Testing of IEC 61850 GOOSE-Based Logically Selective Adaptive Protection of AC Microgrid”. In: *IEEE Access* 9 (2021), pp. 154612–154639. DOI: 10.1109/ACCESS.2021.3128370.

[57] H.J.A. Ferrer and E.O. Schweitzer. *Modern Solutions for Protection, Control, and Monitoring of Electric Power Systems*. Schweitzer Engineering Laboratories, 2010. ISBN: 9780972502634.

[58] DIgSILENT GmbH. *DIgSILENT PowerFactory Technical Reference Documentation: Distance protection coordination*. 2023.

[59] Mengxiao Chen et al. “Research on a Distance Relay-Based Wide-Area Backup Protection Algorithm for Transmission Lines”. In: *IEEE Transactions on Power Delivery* 32.1 (2017), pp. 97–105. DOI: 10.1109/TPWRD.2016.2599198.

[60] Seung Jae Lee et al. “An expert system for protective relay setting of transmission systems”. In: *IEEE Transactions on Power Delivery* 5.2 (1990), pp. 1202–1208. DOI: 10.1109/61.53142.

[61] *Criteria Setting of Protection Functions in Transmission and Distribution System, Provincial Electricity Authority of Thailand*. 2009.

[62] *Best Protection Practices for HV and EHV AC-Transmission Systems of ENTSO-E Electrical Grids*. 2018.

[63] Pratim Kundu and Ashok Kumar Pradhan. “Enhanced Protection Security Using the System Integrity Protection Scheme (SIPS)”. In: *IEEE Transactions on Power Delivery* 31.1 (2016), pp. 228–235. DOI: 10.1109/TPWRD.2015.2459231.

[64] SEL. *SEL-311C Transmission Protection System, Instruction Manual*. Tech. rep. SEL, 2015.

[65] Schneider Electric. *Technical Manual – Easergy MiCOM P54x (P543, P544, P545 & P546) – Current Differential Protection Relay*. Software Version K3. 2020.

[66] ABB. *Line distance protection REL650 1.1 IEC, Application Manual*. Tech. rep. ABB, 2011.

[67] ABB. *Line distance protection REL670 2.0 IEC, Application Manual*. Tech. rep. ABB, 2014.

[68] *Determination and Application of Practical Relaying Loadability Rating Version 1*. NERC, Princeton, NJ, USA, Tech. Rep., 2008.

[69] Panupong Maneerat, Suttichai Premrudeepreechacharn, and Autthaporn Supannon. “Development of Wide Area Protection Coordination for PEA’s 115 kV Closed Loop Transmission Lines in Chiang Mai Area”. In: *2018 53rd International Universities Power Engineering Conference (UPEC)*. 2018, pp. 1–6. DOI: 10.1109/UPEC.2018.8541895.

[70] Romi Fadillah Rahmat et al. “The depth-first search column by column approach on the game of Babylon Tower”. In: *2017 Second International Conference on Informatics and Computing (ICIC)*. 2017, pp. 1–6. DOI: 10.1109/IAC.2017.8280613.

[71] Ahmad Syarif Hidayatullah, Agung Nugroho Jati, and Casi Setianingsih. “Realization of depth first search algorithm on line maze solver robot”. In: *2017 International Conference on Control, Electronics, Renewable Energy and Communications (ICCREC)*. 2017, pp. 247–251. DOI: 10.1109/ICCEREC.2017.8226690.

[72] Lijun Wu et al. “An I/O Efficient Approach for Detecting All Accepting Cycles”. In: *IEEE Transactions on Software Engineering* 41.8 (2015), pp. 730–744. DOI: 10.1109/TSE.2015.2411284.

[73] Jian Dang et al. “Fast Single-phase Fault Location Method Based on Community Graph Depth-first Traversal for Distribution Network”. In: *CSEE Journal of Power and Energy Systems* 9.2 (2023), pp. 612–622. DOI: 10.17775/CSEEJPES.2020.04650.

[74] Yan Du et al. “Fast Cascading Outage Screening Based on Deep Convolutional Neural Network and Depth-First Search”. In: *IEEE Transactions on Power Systems* 35.4 (2020), pp. 2704–2715. DOI: 10.1109/TPWRS.2020.2969956.

[75] Rômulo G. Bainy et al. “Dynamic Zone Selection for Busbar Protection Based on Graph Theory and Boolean Algebra”. In: *IEEE Transactions on Power Delivery* 35.4 (2020), pp. 1769–1778. DOI: 10.1109/TPWRD.2019.2953594.

[76] Ke Jia et al. “Ground Fault Distance Protection for Paralleled Transmission Lines”. In: *IEEE Transactions on Industry Applications* 51.6 (2015), pp. 5228–5236. DOI: 10.1109/TIA.2015.2416243.

[77] N. George and O.D. Naidu. “Distance protection issues with renewable power generators and possible solutions”. In: *16th International Conference on Developments in Power System Protection (DPSP 2022)*. Vol. 2022. 2022, pp. 373–378. DOI: 10.1049/icp.2022.0969.

[78] T.S. Sidhu et al. “Performance of distance relays on shunt-FACTS compensated transmission lines”. In: *IEEE Transactions on Power Delivery* 20.3 (2005), pp. 1837–1845. DOI: 10.1109/TPWRD.2005.848641.

[79] M. Kezunovic et al. "Distance relay application testing using a digital simulator". In: *IEEE Transactions on Power Delivery* 12.1 (1997), pp. 72–82. DOI: 10.1109/61.568227.

[80] Douglas C. Montgomery. *Design and Analysis of Experiments*. New York, NY, USA: John Wiley & Sons, Inc., 8th edn., 2012.

[81] Lauri Kumpulainen et al. "Benefits and performance of IEC 61850 Generic Object Oriented Substation Event-based communication in arc protection". In: *IET Generation, Transmission & Distribution* 11.2 (2017), pp. 456–463. DOI: https://doi.org/10.1049/iet-gtd.2016.1003. URL: https://ietresearch.onlinelibrary.wiley.com/doi/abs/10.1049/iet-gtd.2016.1003.

[82] Davide Della Giustina et al. "Smart Grid Automation Based on IEC 61850: An Experimental Characterization". In: *IEEE Transactions on Instrumentation and Measurement* 64.8 (2015), pp. 2055–2063. DOI: 10.1109/TIM.2015.2415131.

[83] Vinicius Ferrari and Yona Lopes. "Dynamic Adaptive Protection based on IEC 61850". In: *IEEE Latin America Transactions* 18.07 (2020), pp. 1302–1310. DOI: 10.1109/TLA.2020.9099773.

[84] Mahdi Ghotbi-Maleki et al. "Design of Setting Group-Based Overcurrent Protection Scheme for Active Distribution Networks Using MILP". In: *IEEE Transactions on Smart Grid* 12.2 (2021), pp. 1185–1193. DOI: 10.1109/TSG.2020.3027371.

[85] DIgSILENT GmbH. *DIgSILENT PowerFactory Technical Reference Documentation: Digsilent Programming Language (DPL)*. 2023.

[86] Schneider Electric. *Easergy MiCOM P44y Fast Multifunction Distance Protection, Technical manual*. Tech. rep. accessed Nov. 15, 2024. Schneider Electric, 2013. URL: chrome-extension://efaidnbmnnnibpcajpcglclefindmkaj/https://download.schneider-electric.com/files?p_Doc_Ref=P44y_EN_M_E63__VD0_M&p_enDocType=User+guide&p_File_Name=P44y_EN_M_E63__VD0_M.pdf.

[87] Thanakorn Penthong and Komsan Hongesombut. "An efficient method of automatic distance relay settings for transmission line protection". In: *2013 IEEE International Conference of IEEE Region 10 (TENCON 2013)*. 2013, pp. 1–4. DOI: 10.1109/TENCON.2013.6718905.

[88] CIGRE Report. *Evaluation of Characteristics and Performance of Power System Protection Relays and Protection System*. Tech. rep. SC 34 - WG04, CIGRE, Paris, France, 1985.

[89] Michael J. Thompson and Amit Somani. "A tutorial on calculating source impedance ratios for determining line length". In: *2015 68th Annual Conference for Protective Relay Engineers*. 2015, pp. 833–841. DOI: 10.1109/CPRE.2015.7102207.

[90] System Protection and Control Task Force of the North American Electric Reliability Council. *Switch-on-to-Fault Schemes in the Context of Line Relay Loadability*. Available: https://www.nerc.com. June 2006.

[91] A. L. P. De Oliveira and P. M. Da Silveira. "Evaluation of Distance Protection Performance applied on Series Compensated Transmission Lines using Real Time Digital Simulation". In: *Proc. IEEE/PES Transmission & Distribution Conference and Exposition: Latin America*. 2006, pp. 1–6. DOI: 10.1109/TDCLA.2006.311637.

[92] Elmer Sorrentino and Virgilio De Andrade. "Optimal-Probabilistic Method to Compute the Reach Settings of Distance Relays". In: *IEEE Transactions on Power Delivery* 26.3 (2011), pp. 1522–1529. DOI: 10.1109/TPWRD.2010.2091724.

[93] SAS Institute Inc. *JMP® Version 17*. Cary, NC, USA. 1989–2023.

[94] P.F. de Aguiar et al. "D-optimal designs". In: *Chemometrics and Intelligent Laboratory Systems* 30.2 (1995), pp. 199–210. ISSN: 0169-7439. DOI: https://doi.org/10.1016/0169-7439(94)00076-X. URL: https://www.sciencedirect.com/science/article/pii/016974399400076X.

[95] International Electrotechnical Commission. *Communication networks and systems for power utility automation – Part 10: Conformance testing, International Standard, Edition 2.0, 2012*. 2011.

[96] SEL. *Instruction manual, SEL-751 Feeder Protection Relay*. Tech. rep. accessed Jan. 13, 2025. SEL, 2017. URL: https://sertecrelays.net/wp-content/uploads/2019/02/751_IM_20170927.pdf.

[97] ABB. *Technical manual, 615 series*. Tech. rep. accessed Jan. 13, 2023. ABB, 2013. URL: https://library.e.abb.com/public/389adf763fb4f46ac1257c7b00438810/RE_615_tech_756887_ENg.pdf.

[98] International Electrotechnical Commission. *Communication networks and systems for power utility automation – Part 7-4: Basic communication structure – Compatible logical node classes and data object classes, Edition 2.0, 2010*. 2010.

[99] International Electrotechnical Commission. *Communication networks and systems for power utility automation – Part 7-3: Basic communication structure – Common data classes, Edition 2.0, 2010*. 2010.

[100] Yubo Yuan and Yi Yang. *IEC61850-Based Smart Substations, Principle, Testing, Operation and Maintenance*. ELSEVIER Inc., 2019. ISBN: 978-0-12-815158-7.

[101] *Communication networks and systems for power utility automation – Part 6: Configuration description language for communication in electrical substations related to IEDs, International Standard, 2009*. 2009.

[102] Omicron. *Voltage and Current Amplifier, CMS356 Brochure*. accessed Feb. 27, 2023. 2022. URL: https://www.omicronenergy.com/en/products/cms-356/.

E.ON ERC Band 1
Streblow, R.
Thermal Sensation and Comfort Model for Inhomogeneous Indoor Environments
1. Auflage 2011
ISBN 978-3-942789-00-4

E.ON ERC Band 2
Naderi, A.
Multi-phase, multi-species reactive transport modeling as a tool for system analysis in geological carbon dioxide storage
1. Auflage 2011
ISBN 978-3-942789-01-1

E.ON ERC Band 3
Westner, G.
Four Essays related to Energy Economic Aspects of Combined Heat and Power Generation
1. Auflage 2012
ISBN 978-3-942789-02-8

E.ON ERC Band 4
Lohwasser, R.
Impact of Carbon Capture and Storage (CCS) on the European Electricity Market
1. Auflage 2012
ISBN 978-3-942789-03-5

E.ON ERC Band 5
Dick, C.
Multi-Resonant Converters as Photovoltaic Module-Integrated Maximum Power Point Tracker
1. Auflage 2012
ISBN 978-3-942789-04-2

E.ON ERC Band 6
Lenke, R.
A Contribution to the Design of Isolated DC-DC Converters for Utility Applications
1. Auflage 2012
ISBN 978-3-942789-05-9

E.ON ERC Band 7
Brännström, F.
Einsatz hybrider RANS-LES-Turbulenzmodelle in der Fahrzeugklimatisierung
1. Auflage 2012
ISBN 978-3-942789-06-6

E.ON ERC Band 8
Bragard, M.
The Integrated Emitter Turn-Off Thyristor - An Innovative MOS-Gated High-Power Device
1. Auflage 2012
ISBN 978-3-942789-07-3

E.ON ERC Band 9
Hoh, A.
Exergiebasierte Bewertung gebäudetechnischer Anlagen
1. Auflage 2013
ISBN 978-3-942789-08-0

E.ON ERC Band 10
Köllensperger, P.
The Internally Commutated Thyristor - Concept, Design and Application
1. Auflage 2013
ISBN 978-3-942789-09-7

E.ON ERC Band 11
Achtnicht, M.
Essays on Consumer Choices Relevant to Climate Change: Stated Preference Evidence from Germany
1. Auflage 2013
ISBN 978-3-942789-10-3

E.ON ERC Band 12
Panašková, J.
Olfaktorische Bewertung von Emissionen aus Bauprodukten
1. Auflage 2013
ISBN 978-3-942789-11-0

E.ON ERC Band 13
Vogt, C.
Optimization of Geothermal Energy Reservoir Modeling using Advanced Numerical Tools for Stochastic Parameter Estimation and Quantifying Uncertainties
1. Auflage 2013
ISBN 978-3-942789-12-7

E.ON ERC Band 14
Benigni, A.
Latency exploitation for parallelization of power systems simulation
1. Auflage 2013
ISBN 978-3-942789-13-4

E.ON ERC Band 15
Butschen, T.
Dual-ICT – A Clever Way to Unite Conduction and Switching Optimized Properties in a Single Wafer
1. Auflage 2013
ISBN 978-3-942789-14-1

E.ON ERC Band 16
Li, W.
Fault Detection and Protection inMedium Voltage DC Shipboard Power Systems
1. Auflage 2013
ISBN 978-3-942789-15-8

E.ON ERC Band 17
Shen, J.
Modeling Methodologies for Analysis and Synthesis of Controls and Modulation Schemes for High-Power Converters with Low Pulse Ratios
1. Auflage 2014
ISBN 978-3-942789-16-5

E.ON ERC Band 18
Flieger, B.
Innenraummodellierung einer Fahrzeugkabine in der Programmiersprache Modelica
1. Auflage 2014
ISBN 978-3-942789-17-2

E.ON ERC Band 19
Liu, J.
Measurement System and Technique for Future Active Distribution Grids
1. Auflage 2014
ISBN 978-3-942789-18-9

E.ON ERC Band 20
Kandzia, C.
Experimentelle Untersuchung der Strömungsstrukturen in einer Mischlüftung
1. Auflage 2014
ISBN 978-3-942789-19-6

E.ON ERC Band 21
Thomas, S.
A Medium-Voltage Multi-Level DC/DC Converter with High Voltage Transformation Ratio
1. Auflage 2014
ISBN 978-3-942789-20-2

E.ON ERC Band 22
Tang, J.
Probabilistic Analysis and Stability Assessment for Power Systems with Integration of Wind Generation and Synchrophasor Measurement
1. Auflage 2014
ISBN 978-3-942789-21-9

E.ON ERC Band 23
Sorda, G.
The Diffusion of Selected Renewable Energy Technologies: Modeling, Economic Impacts, and Policy Implications
1. Auflage 2014
ISBN 978-3-942789-22-6

E.ON ERC Band 24
Rosen, C.
Design considerations and functional analysis of local reserve energy markets for distributed generation
1. Auflage 2014
ISBN 978-3-942789-23-3

E.ON ERC Band 25
Ni, F.
Applications of Arbitrary Polynomial Chaos in Electrical Systems
1. Auflage 2015
ISBN 978-3-942789-24-0

E.ON ERC Band 26
Michelsen, C. C.
The *Energiewende* in the German Residential Sector: Empirical Essays on Homeowners' Choices of Space Heating Technologies
1. Auflage 2015
ISBN 978-3-942789-25-7

E.ON ERC Band 27
Rohlfs, W.
Decision-Making under Multi-Dimensional Price Uncertainty for Long-Lived Energy Investments
1. Auflage 2015
ISBN 978-3-942789-26-4

E.ON ERC Band 28
Wang, J.
Design of Novel Control algorithms of Power Converters for Distributed Generation
1. Auflage 2015
ISBN 978-3-942789-27-1

E.ON ERC Band 29
Helmedag, A.
System-Level Multi-Physics Power Hardware in the Loop Testing for Wind Energy Converters
1. Auflage 2015
ISBN 978-3-942789-28-8

E.ON ERC Band 30
Togawa, K.
Stochastics-based Methods Enabling Testing of Grid-related Algorithms through Simulation
1. Auflage 2015
ISBN 978-3-942789-29-5

E.ON ERC Band 31
Huchtemann, K.
Supply Temperature Control Concepts in Heat Pump Heating Systems
1. Auflage 2015
ISBN 978-3-942789-30-1

E.ON ERC Band 32
Molitor, C.
Residential City Districts as Flexibility Resource: Analysis, Simulation, and Decentralized Coordination Algorithms
1. Auflage 2015
ISBN 978-3-942789-31-8

E.ON ERC Band 33
Sunak, Y.
Spatial Perspectives on the Economics of Renewable Energy Technologies
1. Auflage 2015
ISBN 978-3-942789-32-5

E.ON ERC Band 34
Cupelli, M.
Advanced Control Methods for Robust Stability of MVDC Systems
1. Auflage 2015
ISBN 978-3-942789-33-2

E.ON ERC Band 35
Chen, K.
Active Thermal Management for Residential Air Source Heat Pump Systems
1. Auflage 2015
ISBN 978-3-942789-34-9

E.ON ERC Band 36
Pâques, G.
Development of SiC GTO Thyristors with Etched Junction Termination
1. Auflage 2016
ISBN 978-3-942789-35-6

E.ON ERC Band 37
Garnier, E.
Distributed Energy Resources and Virtual Power Plants: Economics of Investment and Operation
1. Auflage 2016
ISBN 978-3-942789-37-0

E.ON ERC Band 38
Calì, D.
Occupants' Behavior and its Impact upon the Energy Performance of Buildings
1. Auflage 2016
ISBN 978-3-942789-36-3

E.ON ERC Band 39
Isermann, T.
A Multi-Agent-based Component Control and Energy Management System for Electric Vehicles
1. Auflage 2016
ISBN 978-3-942789-38-7

E.ON ERC Band 40
Wu, X.
New Approaches to Dynamic Equivalent of Active Distribution Network for Transient Analysis
1. Auflage 2016
ISBN 978-3-942789-39-4

E.ON ERC Band 41
Garbuzova-Schiftler, M.
The Growing ESCO Market for Energy Efficiency in Russia: A Business and Risk Analysis
1. Auflage 2016
ISBN 978-3-942789-40-0

E.ON ERC Band 42
Huber, M.
Agentenbasierte Gebäudeautomation für raumlufttechnische Anlagen
1. Auflage 2016
ISBN 978-3-942789-41-7

E.ON ERC Band 43
Soltau, N.
High-Power Medium-Voltage DC-DC Converters: Design, Control and Demonstration
1. Auflage 2017
ISBN 978-3-942789-42-4

E.ON ERC Band 44
Stieneker, M.
Analysis of Medium-Voltage Direct-Current Collector Grids in Offshore Wind Parks
1. Auflage 2017
ISBN 978-3-942789-43-1

E.ON ERC Band 45
Bader, A.
Entwicklung eines Verfahrens zur Strompreisvorhersage im kurzfristigen Intraday-Handelszeitraum
1. Auflage 2017
ISBN 978-3-942789-44-8

E.ON ERC Band 46
Chen, T.
Upscaling Permeability for Fractured Porous Rocks and Modeling Anisotropic Flow and Heat Transport
1. Auflage 2017
ISBN 978-3-942789-45-5

E.ON ERC Band 47
Ferdowsi, M.
Data-Driven Approaches for Monitoring of Distribution Grids
1. Auflage 2017
ISBN 978-3-942789-46-2

E.ON ERC Band 48
Kopmann, N.
Betriebsverhalten freier Heizflächen unter zeitlich variablen Randbedingungen
1. Auflage 2017
ISBN 978-3-942789-47-9

E.ON ERC Band 49
Fütterer, J.
Tuning of PID Controllers within Building Energy Systems
1. Auflage 2017
ISBN 978-3-942789-48-6

E.ON ERC Band 50
Adler, F.
A Digital Hardware Platform for Distributed Real-Time Simulation of Power Electronic Systems
1. Auflage 2017
ISBN 978-3-942789-49-3

E.ON ERC Band 51
Harb, H.
Predictive Demand Side Management Strategies for Residential Building Energy Systems
1. Auflage 2017
ISBN 978-3-942789-50-9

E.ON ERC Band 52
Jahangiri, P.
Applications of Paraffin-Water Dispersions in Energy Distribution Systems
1. Auflage 2017
ISBN 978-3-942789-51-6

E.ON ERC Band 53
Adolph, M.
Identification of Characteristic User Behavior with a Simple User Interface in the Context of Space Heating
1. Auflage 2018
ISBN 978-3-942789-52-3

E.ON ERC Band 54
Galassi, V.
Experimental evidence of private energy consumer and prosumer preferences in the sustainable energy transition
1. Auflage 2017
ISBN 978-3-942789-53-0

E.ON ERC Band 55
Sangi, R.
Development of Exergy-based Control Strategies for Building Energy Systems
1. Auflage 2018
ISBN 978-3-942789-54-7

E.ON ERC Band 56
Stinner, S.
Quantifying and Aggregating the Flexibility of Building Energy Systems
1. Auflage 2018
ISBN 978-3-942789-55-4

E.ON ERC Band 57
Fuchs, M.
Graph Framework for Automated Urban Energy System Modeling
1. Auflage 2018
ISBN 978-3-942789-56-1

E.ON ERC Band 58
Osterhage, T.
Messdatengestützte Analyse und Interpretation sanierungsbedingter Effizienzsteigerungen im Wohnungsbau
1. Auflage 2018
ISBN 978-3-942789-57-8

E.ON ERC Band 59
Frieling, J.
Quantifying the Role of Energy in Aggregate Production Functions for Industrialized Countries
1. Auflage 2018
ISBN 978-3-942789-58-5

E.ON ERC Band 60
Lauster, M.
Parametrierbare Gebäudemodelle für dynamische Energiebedarfsrechnungen von Stadtquartieren
1. Auflage 2018
ISBN 978-3-942789-59-2

E.ON ERC Band 61
Zhu, L.
Modeling, Control and Hardware in the Loop in Medium Voltage DC Shipboard Power Systems
1. Auflage 2018
ISBN 978-3-942789-60-8

E.ON ERC Band 62
Feron, B.
An optimality assessment methodology for Home Energy Management System approaches based on uncertainty analysis
1. Auflage 2018
ISBN 978-3-942789-61-5

E.ON ERC Band 63
Diekerhof, M.
Distributed Optimization for the Exploitation of Multi-Energy Flexibility under Uncertainty in City Districts
1. Auflage 2018
ISBN 978-3-942789-62-2

E.ON ERC Band 64
Wolisz, H.
Transient Thermal Comfort Constraints for Model Predictive Heating Control
1. Auflage 2018
ISBN 978-3-942789-63-9

E.ON ERC Band 65
Pickartz, S.
Virtualization as an Enabler for Dynamic Resource Allocation in HPC
1. Auflage 2019
ISBN 978-3-942789-64-6

E.ON ERC Band 66
Khayyamim, S.
Centralized-decentralized Energy Management in Railway System
1. Auflage 2019
ISBN 978-3-942789-65-3

E.ON ERC Band 67
Schlösser, T.
Methodology for Holistic Evaluation of Building Energy Systems under Dynamic Boundary Conditions
1. Auflage 2019
ISBN 978-3-942789-66-0

E.ON ERC Band 68
Cui, S.
Modular Multilevel DC-DC Converters Interconnecting High-Voltage and Medium-Voltage DC Grids
1. Auflage 2019
ISBN 978-3-942789-67-7

E.ON ERC Band 69
Hu, J.
Modulation and Dynamic Control of Intelligent Dual-Active-Bridge Converter Based Substations for Flexible DC Grids
1. Auflage 2019
ISBN 978-3-942789-68-4

E.ON ERC Band 70
Schiefelbein, J.
Optimized Placement of Thermo-Electric Energy Systems in City Districts under Uncertainty
1. Auflage 2019
ISBN 978-3-942789-69-1

E.ON ERC Band 71
Ferdinand, R.
Grid Operation of HVDC-Connected Offshore Wind Farms: Power Quality and Switching Strategies
1. Auflage 2019
ISBN 978-3-942789-70-7

E.ON ERC Band 72
Musa, A.
Advanced Control Strategies for Stability Enhancement of Future Hybrid AC/DC Networks
1. Auflage 2019
ISBN 978-3-942789-71-4

E.ON ERC Band 73
Angioni, A.
Uncertainty modeling for analysis and design of monitoring systems for dynamic electrical distribution grids
1. Auflage 2019
ISBN 978-3-942789-72-1

E.ON ERC Band 74
Möhlenkamp, M.
Thermischer Komfort bei Quellluftströmungen
1. Auflage 2019
ISBN 978-3-942789-73-8

E.ON ERC Band 75
Voss, J.
Multi-Megawatt Three-Phase Dual-Active Bridge DC-DC Converter
1. Auflage 2019
ISBN 978-3-942789-74-5

E.ON ERC Band 76
Siddique, H.
The Three-Phase Dual-Active Bridge Converter Family: Modeling, Analysis, Optimization and Comparison of Two-Level and Three-Level Converter Variants
1. Auflage 2019
ISBN 978-3-942789-75-2

E.ON ERC Band 77
Heesen, F.
An Interdisciplinary Analysis of Heat Energy Consumption in Energy-Efficient Homes: Essays on Economic, Technical and Behavioral Aspects
1. Auflage 2019
ISBN 978-3-942789-76-9

E.ON ERC Band 78
Möller, R.
Untersuchung der Durchschlagspannung von Mineral-, Silikonölen und synthetischen Estern bei mittelfrequenten Spannungen
1. Auflage 2020
ISBN 978-3-942789-77-6

E.ON ERC Band 79
Höfer, T.
Transition Towards a Renewable Energy Infrastructure: Spatial Interdependencies and Stakeholder Preferences
1. Auflage 2020
ISBN 978-3-942789-78-3

E.ON ERC Band 80
Freitag, H.
Investigation of the Internal Flow Behavior in Active Chilled Beams
1. Auflage 2020
ISBN 978-3-942789-79-0

E.ON ERC Band 81
Razik, L.
High-Performance Computing Methods in Large-Scale Power System Simulation
1. Auflage 2020
ISBN 978-3-942789-80-6

E.ON ERC Band 82
Mirz, M.
A Dynamic Phasor Real-Time Simulation Based Digital Twin for Power Systems
1. Auflage 2020
ISBN 978-3-942789-81-3

E.ON ERC Band 83
Schmitz, H.
Energy Consumption Behavior of Private Households: Heterogeneity, Prosuming, and Rebound
1. Auflage 2020
ISBN 978-3-942789-82-0

E.ON ERC Band 84
Cupelli, L.
Data-driven Methods for Voltage Control in Distribution Networks: A Bottom-Up Approach
1. Auflage 2020
ISBN 978-3-942789-83-7

E.ON ERC Band 85
Happ, S.
A Scalable Simulation Method for Cyber-Physical Power Systems
1. Auflage 2020
ISBN 978-3-942789-84-4

E.ON ERC Band 86
Rewitz, K.
Modellierung des thermischen Komforts in Kabinen-innenräumen
1. Auflage 2021
ISBN 978-3-948234-00-3

E.ON ERC Band 87
Wesseling, M.
Probabilistische Bewertung von Entrauchungsanlagen
1. Auflage 2021
ISBN 978-3-948234-01-0

E.ON ERC Band 88
Stoyanova, I.
Cooperative Energy Management and Cross-Domain Optimization for Electro-Thermal Devices at City-District and City-Level
1. Auflage 2021
ISBN 978-3-948234-02-7

E.ON ERC Band 89
Tran, T.
Advanced hierarchical control structure for Virtual Oscillator-based distributed generation in multi-bus microgrids under different grid dynamics and disturbances
1. Auflage 2021
ISBN 978-3-948234-03-4

E.ON ERC Band 90
Yang, Z.
On the Stability of Three-Phase Grid-Tied Photovoltaic Inverter Systems
1. Auflage 2021
ISBN 978-3-948234-04-1

E.ON ERC Band 91
Wang, T.
Fault Detection and Isolation in DC Distribution Grids
1. Auflage 2021
ISBN 978-3-948234-05-8

E.ON ERC Band 92
Beushausen, S.
A GaN-Based Switched-Mode Gate-Drive Unit for Medium-Voltage IGBTs
1. Auflage 2021
ISBN 978-3-948234-06-5

E.ON ERC Band 93
Schumacher, M.
Design and Assessment of Grid-driven Distributed Cogeneration
1. Auflage 2021
ISBN 978-3-948234-07-2

E.ON ERC Band 94
Joebges, P.
Distributed Real-Time Simulation of Modular Bidirectional DC-DC Converters for Control-Hardware-in-the-Loop
1. Auflage 2021
ISBN 978-3-948234-08-9

E.ON ERC Band 95
Averous, R.
Analysis of the Application of a Grid Emulator to Conduct Grid Compliance Tests for Multi-Megawatt Wind Turbines A Contribution towards Ground Testing of Wind Turbines
1. Auflage 2021
ISBN 978-3-948234-09-6

E.ON ERC Band 96
Virdag, A.
Design, Implementation and Analysis of DC Circuit-breaker for Low-Voltage DC Grids with Counter-current Injection Principle
1. Auflage 2021
ISBN 978-3-948234-10-2

E.ON ERC Band 97
Dähling, S.
Cloud-based Multi-Agent Systems for Flexibility Management in Future Distribution Grids
1. Auflage 2021
ISBN 978-3-948234-11-9

E.ON ERC Band 98
Qawasmi, A.
Fault Current Interruption Analysis and Development of a Power Semiconductor Switch for a Medium-Voltage DC Hybrid Circuit Breaker
1. Auflage 2021
ISBN 978-3-948234-12-6

E.ON ERC Band 99
Nolting, L.
Die Versorgungssicherheit mit Elektrizität im Kontext von Liberalisierung und Energiewende
1. Auflage 2021
ISBN 978-3-948234-13-3

E.ON ERC Band 100
Mathis, P.
Heat Transfer Enhancement in Natural Convective Channel Flows by Vortex Streets
1. Auflage 2022
ISBN 978-3-948234-14-0

E.ON ERC Band 101
Wolff, S.
Stated Preferences Concerning Private Passenger and Light-Duty Electric Vehicles in Germany
1. Auflage 2022
ISBN 978-3-948234-15-7

E.ON ERC Band 102
Hackbarth, A.
Private Households' Preferences for Alternative Fuel Vehicles in Germany – An Empirically Founded Analysis of Adoption Decisions, Willingness-to-Pay, and Policy Scenarios
1. Auflage 2022
ISBN 978-3-948234-16-4

E.ON ERC Band 103
Ge, L.
Performance Enhancement of Switched Reluctance Machines for High-speed Backup Generators: Design, Measurement and Control
1. Auflage 2022
ISBN 978-3-948234-17-1

E.ON ERC Band 104
Atasoy, T.
Strategic and Behavioral Responses of Consumers and Producers to Energy and Environmental Policies
1. Auflage 2022
ISBN 978-3-948234-18-8

E.ON ERC Band 105
Remmen, P.
Automated Calibration of Non-Residential Urban Building Energy Modeling
1. Auflage 2022
ISBN 978-3-948234-19-5

E.ON ERC Band 106
Schild, T.
Systematische Entwicklung strukturierter Steuerungs-algorithmen für die Gebäude- und Anlagentechnik
1. Auflage 2022
ISBN 978-3-948234-20-1

E.ON ERC Band 107
Sidik, Y.
Modeling, Control, and Dynamic Stability Analysis of Two-Stage DC Collector Grids in Offshore Wind Park Clusters
1. Auflage 2022
ISBN 978-3-948234-21-8

E.ON ERC Band 108
Sadu, A.
Towards resilient design of distribution grid automation system: An evaluation of its reliability against random failures and susceptibility to targeted attacks
1. Auflage 2022
ISBN 978-3-948234-22-5

E.ON ERC Band 109
Hinz, A.
Electrical Propulsion Systems for Civil Transportation Aircraft
1. Auflage 2022
ISBN 978-3-948234-23-2

E.ON ERC Band 110
Mehrfeld, P.
Evaluation of Heat Pump Systems Under Dynamic Operating Conditions
1. Auflage 2022
ISBN 978-3-948234-24-9

E.ON ERC Band 111
Teichrib, J.
A Hybrid Semiconductor Device for Medium-Voltage DC-DC Converters - The Combination of Thyris-tor and Transistor Technologies
1. Auflage 2022
ISBN 978-3-948234-25-6

E.ON ERC Band 112
Frehn, A.
Under voltage ride through tests on nacelle test benches equipped with a power hardware in the loop setup
1. Auflage 2023
ISBN 978-3-948234-26-3

E.ON ERC Band 113
Bode, G.
Generation of Training Data for Fault Detection and Diagnosis Algorithms Using Fault Simulation and Parameter Uncertainty
1. Auflage 2023
ISBN 978-3-948234-27-0

E.ON ERC Band 114
Vering, C.
Optimale Auslegung von Wärmepumpensystemen für Bestandsgebäude
1. Auflage 2023
ISBN 978-3-948234-28-7

E.ON ERC Band 115
Bogdanović, M.
Towards model partitioning automation of distributed real-time power systems simulations of distribution networks
1. Auflage 2023
ISBN 978-3-948234-29-4

E.ON ERC Band 116
Hering, D.
Optimization of district heating networks using mixed integer quadratically constrained programs
1. Auflage 2023
ISBN 978-3-948234-30-0

E.ON ERC Band 117
De Din, E.
Multi-Timescale Framework for the Voltage Control of Active Distribution Grids
1. Auflage 2023
ISBN 978-3-948234-31-7

E.ON ERC Band 118
Specht, J.
The Energy Supplier 2.0 – Activating Private Households' Flexibility Potential for Value Creation and Services Supply
1. Auflage 2023
ISBN 978-3-948234-32-4

E.ON ERC Band 119
Teichmann, J.
Auswirkungen der Hydraulik auf das Betriebsverhalten von raumlufttechnischen Anlagen
1. Auflage 2023
ISBN 978-3-948234-33-1

E.ON ERC Band 120
Haghgoo, M.
Semantic Interoperability as a Service for the Smart Energy System
1. Auflage 2023
ISBN 978-3-948234-34-8

E.ON ERC Band 121
Roy, G.
Automation Architectures for hybrid ac-dc grid
1. Auflage 2023
ISBN 978-3-948234-35-5

E.ON ERC Band 122
Mork, M.
Model Predictive Control of Building Energy Systems
1. Auflage 2023
ISBN 978-3-948234-36-2

E.ON ERC Band 123
Zargar, B.
Data-Driven Distribution System State Estimation Using Synchrophasor Measurements
1. Auflage 2023
ISBN 978-3-948234-37-9

E.ON ERC Band 124
Rohn, M.
Einseitiges Induktionsverhalten von multiplen Luftstrahlen unterschiedlicher Düsengeometrien
1. Auflage 2024
ISBN 978-3-948234-38-6

E.ON ERC Band 125
Sheykhha, S.
Four essays on the sustainable energy transition: Model-based analyses of regional energy market structures and regulations
1. Auflage 2024
ISBN 978-3-948234-39-3

E.ON ERC Band 126
Warmuz, J.
Current Interruption Capability and Feasibility Assessment for a Medium-Voltage Direct Current Hybrid Circuit Breaker Application
1. Auflage 2024
ISBN 978-3-948234-40-9

E.ON ERC Band 127
Gürses, G.
Machine learning techniques for time series forecasting in power systems operation
1. Auflage 2024
ISBN 978-3-948234-41-6

E.ON ERC Band 128
Baranski, M.
Design of Distributed Model-based Control Agents for Building Automation Systems
1. Auflage 2024
ISBN 978-3-948234-42-3

E.ON ERC Band 129
Karami, M.
Driving Sustainability Through Business Model Innovation in the Energy Industry and Related Sectors
1. Auflage 2024
ISBN 978-3-948234-43-0

E.ON ERC Band 130
Hoffmann, M.
Entwicklung eines Simulationsmodells zur Vorhersage und Optimierung eines Luftwäschers mittels 3-dimensionaler Mehrphasen-Strömungssimulation
1. Auflage 2024
ISBN 978-3-948234-44-7

E.ON ERC Band 131
Stoffel, P.
Learning Strategies for Data-Driven Model Predictive Control of Building Energy Systems
1. Auflage 2024
ISBN 978-3-948234-45-4

E.ON ERC Band 132
Dognini, A.
Multi-criteria service restoration methods for AC and AC/DC distribution grids
1. Auflage 2024
ISBN 978-3-948234-46-1

E.ON ERC Band 133
Schreiner, L.
International Public-Private Strategies in Sustainable Investment and Finance
1. Auflage 2024
ISBN 978-3-948234-47-8

E.ON ERC Band 134
Priesmann, J.
Verteilungseffekte im Kontext der Energiewende: Herausforderungen und regulatorische Lösungsansätze
1. Auflage 2024
ISBN 978-3-948234-48-5

E.ON ERC Band 135
Mortimer, B.
Horizontal Network Coupling for Charging Infrastructure Based on Three-Phase Solid-State Transformers
1. Auflage 2024
ISBN 978-3-948234-49-2

E.ON ERC Band 136
Gümrükcü, E.
A Versatile Strategy for Optimizing Electric Vehicles' Charging Spot Selections in Distribution Grids
1. Auflage 2024
ISBN 978-3-948234-50-8

E.ON ERC Band 137
Pan, Z.
Large Language Model Based Semantic Interoperability Enhancement for Energy Data Management
1. Auflage 2025
ISBN 978-3-948234-51-5

E.ON ERC Band 138
Korompili, A.
Two-Level Control for Multi-Terminal DC Distribution Grids
1. Auflage 2025
ISBN 978-3-948234-52-2

E.ON ERC Band 139
Dinkelbach, J.
Enabling the Real-Time Simulation of Low-Inertia Power Systems by Dynamic Phasor Modelling and Efficient Computing Methods
1. Auflage 2025
ISBN 978-3-948234-53-9

E.ON ERC Band 140
Kümpel, A.
Adaptive agentenbasierte modellprädiktive Regelung für Gebäudeenergiesysteme
1. Auflage 2025
ISBN 978-3-948234-54-6

E.ON ERC Band 141
Gurumurthy, S.
Advanced Harmonic Stability Monitoring and Control of Power-Electronics Dominated Grids
1. Auflage 2025
ISBN 978-3-948234-55-3

E.ON ERC Band 142
Sowa, I.
Distributed Consensus Control Supported by High Reporting Rate Meters in Cyber-Physical Microgrids
1. Auflage 2025
ISBN 978-3-948234-56-0

E.ON ERC Band 143
Klingebiel, J.
Bedarfsgesteuerte Abtauung von Luft-Wärmepumpen durch Reinforcement Learning
1. Auflage 2025
ISBN 978-3-948234-57-7

E.ON ERC Band 144
Ginocchi, M.
Sensitivity Analysis for Power System Applications
1. Auflage 2025
ISBN 978-3-948234-58-4

E.ON ERC Band 145
Ahmadifar, A.
Resilient Microgrid Management in Active Distribution Systems for Normal and Contingency Operations
1. Auflage 2025
ISBN 978-3-948234-59-1

E.ON ERC Band 146
Höges, C.
Kältemittelkreislaufkonfigurationen von Wärmepumpen für die Gebäudebeheizung
1. Auflage 2025
ISBN 978-3-948234-60-7

E.ON ERC Band 147
Stock, J.
Separation of Existing District Heating Networks for Optimal Utilisation of Sustainable Heat Sources
1. Auflage 2025
ISBN 978-3-948234-61-4

This dissertation proposes to solve problems of distance relay (DR) settings and DRs coordination validation, methodologies for DR testing, and interoperability (IOP) testing for digital substations.

In the context of DR settings and DRs coordination validation, novel and more broadly applicable algorithms are developed for automatizing the path determination, DR settings and DRs coordination validation, which can be applicable regardless of the network topology, can handle apparent impedance with/without multiple currents fed by generation units, without under- and over-reach issues of the protection zones, have better accuracy and lesser computational time than manual and Depth-First Search algorithm-based techniques.

In the context of DR testing, testing methodologies are proposed to allow testing a broader spectrum of functions and enable the optimal choice of the tests while maintaining efficacy, objectivity, and generalization of testing activity.

In the context of IOP testing, a proposal for functional testing of protection schemes for digital substations is proposed to enable IOP testing of multi-vendor bay-level relays for assessing the performance of the protection scheme.

ISBN 978-3-948234-62-1

Thinking the Future
Zukunft denken